UNIVERSITÀ DEGLI STUDI DI MILANO

DIPARTIMENTO DI
SCIENZE FARMACEUTICHE

PhD Course in Chemical Sciences, XXVIII Cycle

Chiral transition metal complexes: synthesis, characterization, applications.

Ph.D. Thesis

Marco Fusè

R10255

Tutor: Prof. Edoardo Cesarotti

Co-Tutor: Dr. Isabella Rimoldi

Coordinator: Prof. Emanuela Licandro

November 24, 2015

Abstract

The main target of this thesis was the investigation of different aspects of the chirality at the metal centre. In particular we studied stereo-specific synthesis of octahedral transition metallic complexes or their resolution in enantiomeric pure form, in order to evaluate the influence of the chirality at the metal centre in different fields such as: catalysis, emission or interaction with chiral environment.

The use of chiral-at-metal complexes in catalysis is somewhat less common than that of other chiral organometallic architectures. Via stereospecific reaction, we were able to obtain ruthenium(II) complexes of general formula [Ru(NN)(PP)Cl_2] in optically pure form, where NN was a chiral diamine and PP was a chelating or two mono phosphines. These complexes, after the activation into the hydride species, were active catalysts for the reduction of ketones via asymmetric transfer hydrogenation. We observed that, in complexes where two chiral ligands were simultaneously present, the third chirality that located at the metal centre was prevalent in the definition of the configuration of the products.

In order to introduce the planar chirality, we synthesised different complexes of the types [η^6-arene-Ru(NN)Cl], however in the most cases intractable complex mixture of stereoisomers were obtained. This results prompted us to explore different techniques able to describe complex mixtures of complexes with several type of chirality involved.

VCD in tandem with DFT calculation is powerful technique for the determination of the absolute configuration and conformational analysis; despite new results concerning transition metal complexes are coming out, their application in the study of metallorganic compounds are not common. The strength of IR and VCD spectroscopy lies in the fact that the spectra of a chiral molecule contain sufficient stereochemical details to be consistent with only a single absolute configuration and an unique solution-state conformation, or distribution of conformations, of the molecule; moreover compared with ECD the DFT calculation is more reliable.

For our purpose we selected three common motifs in organometallic chemistry never investigated by VCD spectroscopy.

We decided to investigate the carbon monoxide as the first chromophore; carbon monoxide is one on the most common ligand for transition metal complexes; the carbonyl complexes found application as catalysts, precatalysts or stoichiometric reagents in many different reactions. Therefore we synthesised and resolved a series of of heteroleptic ruthenium (II) cyclopentadienyl complexes.

The second chromophore was a metal-hydride, which has important role in catalytic reduction. We were able to synthesis one Ru(II) hydride complex as single enantiomer that was completely and whose metal chirality was highlighted by VCD.

The third class of compounds was the cyclometallated iridium(III) complexes that due to their photophysical properties have been extensively studied in the last years, founding application in several fields. Here the chromophore was constituted by two orthometalled phenylpyridine coordinated at the metal in helical shape.

In this latter case, our interest was also adressed to study the photophysical properties of the different diastereomers and in order to verify if the emission could be influenced by the diastereomeric nature of the complexes. In spite of that in solution no differences were highlighted, we found that the different packing of the enantiomers and stereoisomers produces aggregates with different emitting properties.

By VCD spectrometry integrated with DFT calculation we were able to identify the characteristic features of the different stereogenic centre present in the complexes. In the CO and Ir(III) complexes we also investigated the origin of the VCD sign. VCD spectroscopy proved to be a valuable and powerful technique when applied to metallorganic chromophores, moreover the results of these investigations appear in the literature and here for the first time.

Contents

Chapter 1

Introduction

1.1 Chirality

1.1.1 Concepts of chirality

In chemistry, the definition of chirality is codified by International Union of Pure and Applied Chemistry (IUPAC) in the gold book as:

> 'The geometric property of a rigid object (or spatial arrangement of points or atoms) of being non-superposable on its mirror image; such an object has no symmetry elements of the second kind (a mirror plane, $\sigma = S_1$, a centre of inversion, i = S_2, a rotation-reflection axis, S_2n). If the object is superposable on its mirror image the object is described as being achiral.'

This definition does not state compulsory the absence of symmetry at all.

The word derived from the Greek '$\chi\varepsilon\iota\rho$' (cheir) that means hand and it could be translated as handness; indeed the hands are one of the most recognized example of chirality: there is no way of wearing the right hand with the left glove.

Two molecules, related by mirror image operation, are defined as enantiomers; if more than one chiral features are present and not all of them are related by mirror image operations the molecules are defined as diastereomers. Enantiomers interact in achiral environment in the same way, differently in chiral environment and with opposite sign in racemic one; whereas a system is defined chiral if contain molecules of opposite chirality in ratio different than 50:50, in this latter case the system is called racemic. As a consequence two enantiomers can be distinguished by their interaction with linear polarized light that is indeed a racemic mixture of right and left handed circularly polarized light.

We are surrounded by chirality, our body has the hands and feet and every objects with an helical shape, such a screws, is indeed chiral. Actually the life on earth, with really few exception, has developed with a preferred chirality, the (L) amino-acids and the (D) sugar are the building blocks of the life; also at the higher level, the DNA-helix or the α-helix of the proteins, the preponderance of one chirality is present. This phenomenon is called homochirality of life and it is still debated in its origin.

The unbalance between the two enantiomers is usually described as 'symmetry breaking' and it is measured in enantiomeric excess (e.e.). Until 1956 it was accepted the principle of conservation of parity, formulated by Wigner, that stated that a world built like the mirror images of ours will behave exactly in the same way with only the inversion of the spatial coordinates; the experiment of Wu [1, 2], prompted by the works of Lee and Yang [3], proved a violation in the β-decay of the cobalt-60 atoms concerning the weak interaction.

Nowadays the CPT theorem, where C is the charge conjugation, P the parity operation and T the time reversal, states the exact symmetry for the four fundamental forces, defining the relation between two objects of opposed chirality even if inside it the single symmetry could be broken. Weak interaction plays a role even at molecular level, as in the interaction between electrons ad nuclei, so that an asymmetry in the energy of two enantiomers ground states is predicted. Although it actually define two

enantiomers as diastereomers, the energy difference can be estimated in the tiny value of 10^{-11} J mol^{-1} [4, 5], it was never unambiguous observed at molecular level to date and its relevance in the origin of the homochirality in nature is still unclear.

Of course an absolute asymmetric synthesis in the absence of a chemical or physical chiral directing force could occur stochastically, for example an odd number of chiral molecules brakes the symmetry.

Whatever is the origin of the imbalance between the enantiomers and its amplification processes the net result is a chiral environment in which the chirality of one object (a molecule) plays a fundamental role.

The enantiomers show different interactions with the chiral receptor of human body; often enantiomers exhibit diverse smell, in the pharmacology: only the molecule with the proper absolute configuration correctly interacts and give rise to a desired respond, in the best case the other one is less active or inactive but often unwanted reaction could be obtained.

After some tragic cases happened in the last century, nowadays a complete physical-chemical and pharmacological characterization of both enantiomers must be taken into account.

At the end of '90, FDA (Food and Drug Administration) and EMA (European Medicines Agency) have issued guidelines concerning the chiral active substances: if the active substance is administered, it is necessary provided the full characterization of the physico-chemical, pharmacological and clinical properties of both the enantiomers. This has great stimulated the research and development of stereoselective reactions able to provide the single enantiomer.

In this wide field a pivotal role is played by transition metal complexes used as stoichiometric reagents or, mainly, as catalyst. The discovery of rhodium phosphine complexes and their use as catalysts for the synthesis of L-DOPA opened the way to an extremely fruitful field of academic and industrial researches [6, 7].

The most common way of introducing the chirality in the metal complexes is based on the use of chiral ligands, therefore the chiral information is located on the coordination sphere of the metal. This approach, mainly in catalysis, was able to deal with several processes providing enantiomeric pure forms of the products. Unfortunatly this is not true for a great number of other interesting and useful reactions characterised by unacceptable low stereocontrol.

Referring to these catalytic reaction which are still non optimized to satisfactory stereocontrol, a different approach could be to transfer the chiral information located on the ligands to the metal centre itself, in a stable form. This approach is based on the fact that closer is the chiral chiral information to the reacting substrate, better should be the the stereochemical control. Indeed, the chirality at the metal centre can be also but not only seen as a description of the spatial arrangement of the involved molecules in the reaction environment. Perhaps this statements could be considered rather simplistic, but it was the kick start of this thesis.

Actually, complexes chiral at the metal could be not sufficient to achieve high enantiomeric excess; generally catalytic reactions have multi-step mechanism that often implies the change of the metal oxidation state and its coordination number. The consequence is that several intermediates of the catalyst in the catalityc cycle can be chiral or achiral, thus the metal can retain its configuration, the optical purity could change during the reaction but it could also be loose along the mechanism. Therefore the comprehension of the catalytic cycle plays an important role.

An outstanding example of successful catalytic system is the Noyori catalyst for the asymmetric reduction of prochiral ketones. Although the metal is not directly interacting with the substrate, it is the metal centre configuration that establishes the configuration of the product. In scheme 1.1 is reported the catalytic cycle: at the right it can be seen that the chirality of the metal is the key of the stereoselection in the six member concerted transition state [8], on the left, when the catalyst is restored, the stereoselection is instead provided by the chirality of the ligand's 5-

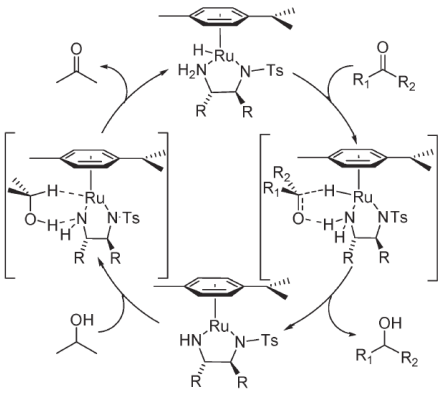

Scheme 1.1: Catalytic cycle of Noyori catalyst for the reduction of ketones via six member concerted transition state

member chelated cycle.

1.1.2 Chirality in coordination compounds

In coordination compounds the higher possible coordination number (CN) and coordination geometries (CG) allow a great number of isomers; for example an hexa-heteroleptic octahedral complex, the most common geometry in organometallic chemistry, can exist in 15 couples of enantiomers. The importance of the coordination geometry is evident in the disclosure of the structure of the two possible compounds, with the same formula, $PtCl_2(NH_3)_2$. Alfred Werner [9] proposed a square planar geometry, instead of a tetrahedral one, for the platinum atom that allowed two different isomers, both not chiral.

The coordination geometry of transition metals is guided by the ligand field stabilization, however this is not the only factor. Other factors, such as the Jahn-Teller effect or the steric hindrance, could be important; referring only to the metal studied in this thesis, a d^6 central metal as Ru(II) or Ir(III) preferentially adopts an octahedral geometry (OC-6) whereas a

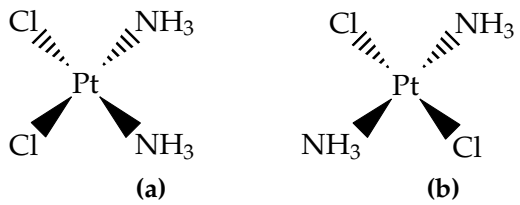

Figure 1.1: (a) cis platin, (b) trans platin

d^8 as Ir(I),Rh(I) or Pt(II) a square planar (SP-4) one. Nevertheless these preferred geometries should be considered as a rough guide, since they give only the most common coordination number and coordination geometries.

Historically the organic stereochemistry was focused on asymmetric centre chirality, usually in the shape of tetrahedral carbon atom with four different substituents. Although the tetrahedral carbon has played a crucial role in the chemistry of the chiral compounds, the presence of an asymmetric tetra-substituted carbon atom is sufficient condition but not necessary. Even in organic chemistry, since the synthesis of spiro compounds in 1955, the concept of chirality without asymmetry was introduced. In 1966 Cahn, Ingold and Prelog unified the terminology in a milestone paper where also the axial and planar chirality were defined [10]. A modern view considers chirality as a property of the all system and uses the stereogenic centre to point out the moiety of the molecule responsible of it [11].

The possibility of chiral coordination compound was first theorized, once again, by Werner in 1899 with the term 'Spiegelbildisomer' [12], literally mirror image isomerism. In that work was clarified the difference between asymmetric carbon atom and chirality induced by chelated ligands. He correctly predicted the existence of two enantiomers in coordination compounds, whose experimental evidence was then obtained by the resolution in enantiomers of the cobalt complexes such as $[Co(en)_2(NH_3)Br]Br_2$ [13]. Thanks to this last example the Werner's coordination theory was

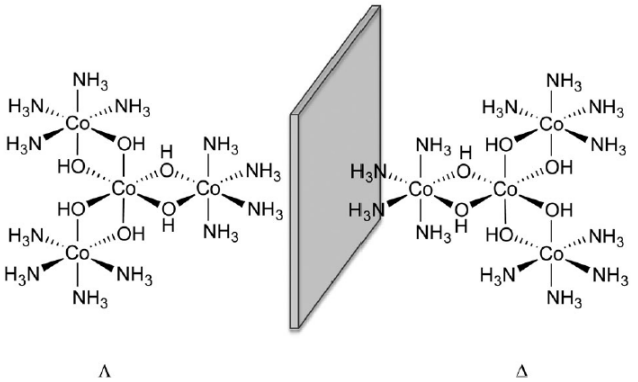

Figure 1.2: The two enantiomers of $[\{cis-(H_3N)_4Co(OH)_2\}_3Co]_6^+$. Charge omitted for clarity [11]

completely proved and he won the Nobel prize in 1913. Two years later he was also able to demonstrate that also inorganic salts can be resolved in enantiomers [14] (figure 1.2).

In coordination chemistry is common the absence of chiral centre whereas helix chirality is present. Carbon atom can be seen itself as coordination centre with a tetrahedral geometry particularly inert to substitution; this behaviour allows to isolate in the most cases the isomers.

The chirality in coordination compounds has been originated in different moiety of the complex:

I by the different nature of the substituents, as for the stereogenic carbon atom;

II by the production of helica structure upon coordination of chelated ligands, as in Werner's complexes;

III by chiral conformation of the chelated ring;

IV by coordination of chiral ligands themselves;

V by breakage of improper symmetry ligand elements so that the ligand became chiral, as in case of nitrogen bearing three different substituents;

VI by mutually broken of the improper rotation elements of two coordinated ligands.

Though the comprehensive review of the stereochemistry nomenclature of the coordination and metallorganic compounds is outside of the scope of this theses, in appendix A a brief outlook will be given for the geometry of our interest.

One important issue is the stability of these complexes due to the lability of the ligands that allows the interconversion of the chirality, so the racemization in solution could be a problem via cleavage followed by bond re-formation. As remembered before, carbon with its relative substitution and configuration stabilities allows the isolation of the enantiomers in most cases. Use of chelating ligands mainly stabilized the complex towards substitution and labilization (chelation effect), moreover organometallic complexes are kinetically inert, because the ligands are strongly bound to the metal atoms by the combination of σ-donor and π-acceptor bonds.

In the field of metal complexes chiral at the metal centre, due to their higher stability [15, 16], two kind of complexes are the most investigated: the three legged piano stool half-sandwich complexes that are octahedral complexes with the substituents forced in *fac*-arrangement (figure 1.3), thus these complexes can be approximated to a tetrahedron and exist in two enantiomeric forms.

The others are the complexes bearing chelating ligands, the metal results the stereocentre since the ligands arrange around it in helical shape. The two configurations are called as Λ or Δ according to the helix orientation (see appendix A).

Others geometries than the octahedral one could be chiral due to the helical arrangement of their bidentate substituents with different geome-

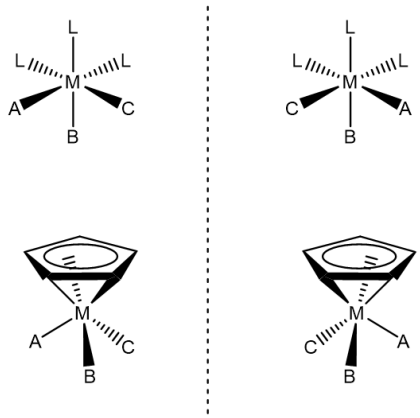

Figure 1.3: Octahedral ML_3ABC and half-sandwich chiral complexes

tries or coordination number; for a comprehensive treatise of the stereochemestry of coordination compounds see reference [17].

1.2 Synthesis of metal complexes chiral at the metal centre

The synthetic control of coordination compounds and metallorganic molecules is still under an intense development. However, as for the classic organic compounds, two principal ways to obtain enantiopure complexes exist: the resolution of a racemic mixture or a proper asymmetric synthesis, both methods have been used in this thesis.

1.2.1 Racemate resolution

The first possible strategy to obtain enantiopure metal complexes, that is also barely attended, consists in the resolution of a racemic mixture. In all his works, Werner never used chiral auxiliaries thus all the complexes were obtained as racemate and then resolved.

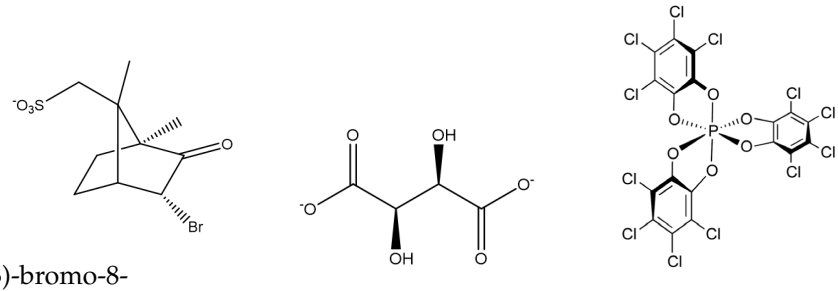

Figure 1.4: Examples of chiral aion used in resolution.

Enantiopure counter-ion This kind of resolution is based on the fact that many metal complexes are positively charged. Using a chiral counter ion it is possible to produce a couple of diasteromeric salts with different solubility. Usually the counter ions are organic products available from the chiral pool as (3)-bromo-8-camphorsulfonate (Werner) or the tartrate used to resolve complexes such as $[Co(en)_3]^{3+}$]. More recently the chiral TRISPHAT counter anion was used to resolve ruthenium(II) complexes [18]. Trisphat anion is configurationally stable at room temperature and it can be isolated in the two Λ/Δ enantiomeric forms: its helical shape allows selective interaction with the Λ/Δ possible forms of an octahedral complex. The counter ion could be subsequently removed by ion exchange to afford the metal complex in enantiopure form.

Chiral ligands Deals with diastereomers is somewhat easier than the enantiomers, because their sterochemical purity can be readily assessed by NMR spectroscopy (vide infra) and their different physico-chemical properties allow their separation via fractional crystallization or chromatography [1].

[1] Although a resolution of enantiomer by chiral-HPLC was recently reported [19],it is not common.

A first approach consist in the treatment of the racemic mixture with an enantiopure reactant that is able to covalently link a ligand giving rise to a couple of diastereomers, different only at the metal configuration. After the resolution this auxiliary-ligand can generally be removed providing the complex in the two enantiomeric pure forms. Examples are the synthesis of Manganese complex reported by Brunner [20] or the Rhenium complex reported by Gladysz [21]. Another approach could be the introduction of a chiral ligand on a preformed chiral metal complex, in order to obtain diastereomeric mixture and, once separated, removing them by metathesis reaction or changing the coordination properties of the ligands. For the first one, an example is the synthesis of enantiopure molybdenum complexes proposed by Faller at al. [22] while for the latter one, a recent example is the synthesis of optically pure Ir(III) complexes proposed by Meggers: the diastereomers are separated by simple silica-gel chromatography, after that the two enantiomers are obtained upon protonation of the amino alcohol chiral auxiliary ligand and substitution by two acetonitrile ligands [23].

1.2.2 Asymmetric synthesis

The first synthesis of metal complex in presence of a chiral ligand was reported by Smirnoff in 1920, a Werner's co-worker [24]. The author reported the reaction of the propilendiamine with H_2PtCl_6 and based on the polarimetric data claimed the steroselectivity of the reaction. Eighty-five years later A. von Zelewsky [25] reinvestigated the reaction with the modern NMR techniques; even if with low diasteroselectivity, the reaction leads to the formation of a preferred diastereomer. This study could be considered the first asymmetric synthesis of a metal complex since the chirality of the ligands induced the chirality at the metal centre. The transmission of chiral information from one or several enantiopure ligands to a metal center remains the most efficient and rational way to achieve asymmetric synthesis within a complex and within an assembly [26].

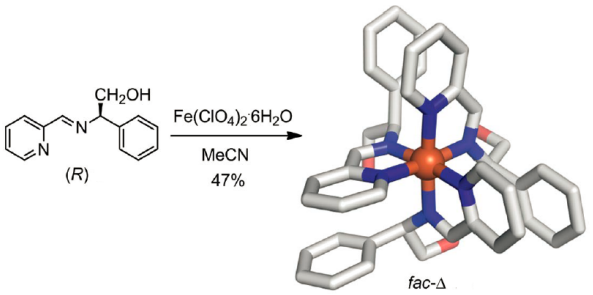

Scheme 1.2: Single diastereomer complex formation guided by π-stacking of the ligands

Chiral ligands When a new stereocentre is formed in presence of a chiral ligand, a mixture of diastereomers is obtained, usually with a diastereomeric excess that can be increased by precipitation or chromatography. Therefore an accurate design of the ligands can efficiently control the stereochemestry of the coordination complexes. As usual, Nature provided examples: due to the conformational restrains of the ligands the structure of Fe(III)-enterobactin, which belongs to a class of iron chelators that eases the absorbition and the transport of iron, is homochiral with a Δ configuration.

In recent years enantiopure octahedral complexes have growing interest for they possible application in several fields such as catalysis [27, 28, 29], materials [11, 30] and life science [31, 32]. Thus in literature are present several examples of tailored chiral ligands able to control the stereoselection based on steric and electronic interaction. The one-pot distereoselective synthesis of *fac*-Δ-$[Fe(A\text{-}B)_3]^{2+}$ from chiral iminopyridine ligands is just one example; in that case, the aromatic π-stacking is responsible for the control at the metal centre configuration (scheme 1.2)[33].

In order to obtain complexes in enantiomeric relation, ligands containing a chiral cleavable linker were designed; after the chiral induction, the linker can be removed leaving only achiral ligands [34].

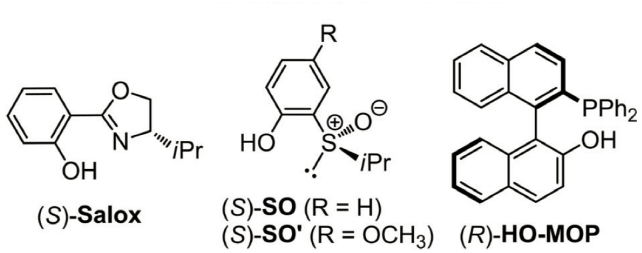

Figure 1.5: Chelating ligands with switchable properties, all present the phenolic groups.

Chiral anion mediated In labile metal complexes the asymmetric synthesis is the result of a thermodynamically controlled process in which the distereomers are in equilibrium. A perturbation of this equilibrium allows to shift the equilibrium toward one of the configurations. The interaction with a chiral environment can give rise to distereomeric interaction - such as electrostatic interactions, formation of hydrogen bonds, aromatic or van der Waals interaction - able to induce a stereoselection. This effect was also known as Pfeiffer effect, from a Werner's student. He observed the formation of non-racemic zinc complexes when chinchonine hydrocloride was added at the achiral zinc sulfate and 1,10-phenantroline [35]. As remembered before the metal complexes are frequently charged, Lacour et al. using a chiral anion and the ion pair interaction were able to separate diastereomers chiral at metal centre [36] up to gram scale.

Chiral auxiliary mediated A different approach consists in the use of a chiral compounds as a transient ligands during the metal synthesis. After the formation of the strereogenic centre this auxiliary ligand can be removed in order to achieve enantiomerically pure compounds. The first example of this strategy is dated 1948 by Bailar Jr., who demonstrated that tartrate can be used as chiral transient ligand in the synthesis of chiral $[Co(en)_3]^{3+}$ complexes. The auxiliary ligands can be mono or multidentate, however, the general idea is that the auxiliary ligands are co-

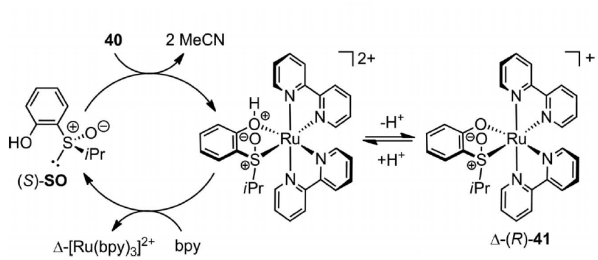

Figure 1.6: Proposed catalytic cycle for the synthesis of Δ-$[Ru(bpy)]_3^{2+}$ with chiral 2-(Isopropylsulfinyl)phenol as auxiliary ligand and catalyst.

ordinated weaker than the final ligands so that they could be easily subsequently exchanged with retention of configuration [37, 38]. A slightly different approach is using auxiliary which coordination properties can be easily tuned weakening the binding strength after the chiral induction. The key aspect is the strength interaction with the metal, able to high asymmetric induction that nevertheless can be reverted without loss of the absolute metal-centre configuration. Three types of these ligands are synthesised so far and are reported in figure 1.6. Despite the different nature, all these ligands present a common scaffold: a phenolic group linked with a moiety responsible of the chiral induction. A base in the reaction medium deprotonates the ligand allowing the chelate coordination sphere, subsequently released using an acid [39, 40, 41, 42, 43].

Catalytic asymmetric synthesis Based on one of the ligands presented in the preview section, recently a catalytic asymmetric synthesis of a coordination compounds were reported [39]. Albeit catalysis plays a crucial role in the asymmetric synthesis of organic compounds, this is so far the only case where an organic molecule "catalyzed" the enantioselective synthesis of a coordination compounds. In that case seems that a fundamental role is played by the solvent: the starting complexes showed only a small solubility thus the catalyst is in excess to the substrate during all the reaction.

1.3 Spectroscopic characterization of chiral metal complexes

1.3.1 Outline of the techniques

Until 1951 it did not existed a methodology able to directly determinate the absolute configuration of a molecule; the chirality was distinguished on the base of the optical activity emboded by the optical rotation that is the measure of the angle of rotation of a linear polarized light beam (at a certain concentration and fixed wavelength). It is the oldest technique however it was not able to correlate the absolute configuration and the optical activity, at least until it was not developed the modern quantum mechanic methodologies.

After that the anomalous x-ray dispersion (XRD) technique appeared, it was possible to determine the absolute configuration of the molecules. Diffraction methods are the only that actually give direct information on the atoms position and XRD is their most common method. The measurements require a single crystal of the sample of sufficient size and quality that it is not always easy to obtain and it represents only a small amount of the total substance that, in addiction, is passed trough a phase transition process.

Concerning the metal complexes, increasing attention is pointed on the dynamic nature in solution that may adopt very different structures compared to that in solid. NMR is a common technique for these porpoises; it is usually and successfully applied on several compounds, even in this thesis, but it is not a chiral methodology and it required distereomeric interactions.

The only spectroscopic technique capable of directly probing molecular chirality are those that use the mirror relationship between left and right circular polarized states of the electromagnetic radiation. During the last decades, some spectroscopic techniques able to determine the absolute configuration af a chiral molecule have been developed.

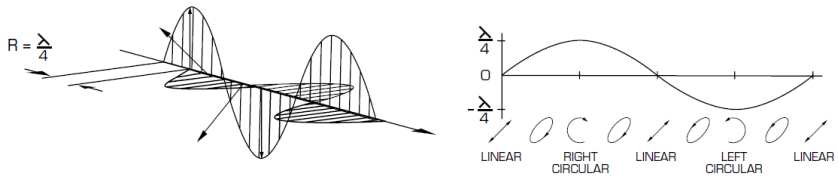

Figure 1.7: Left circularly polarized (LCP) and right circularly polarized (RCP) radiation, with intermediate states of linear and elliptic polarization, generated by a photoelastic modulator.

Among these spectroscopic technique, vibrational and electronic circular dichroism (VCD and ECD) have been applied to the field of coordination chemistry. Such a trend was allowed by the significant advance in the theoretical and computational methodologies, moreover for VCD it was also possible due to the development of commercial available spectrometers. While ECD is well known and widespread, VCD is surely less common up to now.

Although both of them are able to predict the conformation in solution and ECD has signals of higher intensity, VCD has some advantages that allow to obtain more detailed stereochemical information [44, 45].

VCD spectrum has an enhanced stereochemical sensitivity that relies on the set of the 3N-6 normal modes in a molecule; this allow a great number of transition that often are well resolved. The relation between the normal modes and the molecular stereochemistry is more clear if we think that the set of the 3N-6 degree of freedom are defined in the same space that defines the stereochemistry. In contrast, in ECD spectra the details provided are limited by the broad nature of the bands.

Another advantage is that the VCD simulations relay on the ground state electronic structure, which is considered reliable. For these reason VCD together with the DFT calculation is a powerful technique to determine the absolute configuration of a molecule.

1.3.2 Vibrational circular dichroism

VCD, as the name states, can be consider as the extension of electronic circular dichroism in the infrared vibrational region of the spectrum. Thus:

'VCD is defined as the difference in the absorbance of left minus right circularly polarized light for a molecule undergoing a vibrational transition.' [46]

For a molecule undergoing a transition between two vibrational levels of the ground electronic state the IR absorbition (namely Vibrational Absorbance) is given by

$$VA \quad A = \frac{1}{2}(A_L + A_R) \tag{1.1}$$

thus VCD can be express as

$$VCD \quad \Delta A = A_L - A_R \tag{1.2}$$

where A_L is the absorbance for left circularly polarized light and A_R is the absorbance for right circularly polarized light.

If the Lambert-Beer law is valid, experimentally VA intensity at a certain wave-number (ν) is defined by the relationship

$$A(\nu) = \varepsilon(\nu) bC \tag{1.3}$$

where b is the path length, C the sample concentration (we assume here a measure in solution) and $\varepsilon(\nu)$ the molar absorptivity of the sample. This leads us to a definitions of the VCD intensity avoided of the sampling variables

$$\varepsilon(\nu) = \frac{\Delta A(\nu)}{bC(e.e.)} \tag{1.4}$$

where e.e. is the enantiomeric excess.

A deeper insight of the VCD theory will be provid later in text (see section 2.2).

Chapter 2

Results and Discussion

2.1 Synthesis of 8^{th} group complexes chiral at metal

One of the most important application of metal complexes is as catalyst in synthesis of fine chemicals.

> 'The employment of chiral-at-metal complexes in catalysis is somewhat less common than that of other chiral organometallic architectures, where the chiral information is located at the ligand. However, chiral-at-metal complexes can provide a unique electronic or steric environment about the metal center, which is crucial for the production of enantiomeric excesses in catalyzed organic transformations' [47].

Recalling a concept presented in the introduction and taking due precautions (see 1.1.1), chirality at the metal centre can provide a solution for stereocontrolled catalytic reactions.

Among the several catalytic process in which transition metal catalyst are involved, the reduction of polarized and un-polarized double bond were extensively studied in our laboratory, in particular employing chelating diphosphine ligands. The cooperation of the metal−hydrogen and

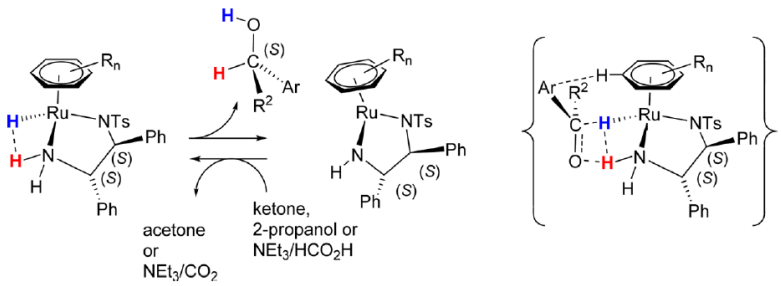

Figure 2.1: Mechanism of the ATH of Aryl Ketones Catalyzed by Noyori's Catalysts and proposed transition state. [50]

the amine nitrogen−hydrogen functions in the asymmetric transfer hydrogenation (ATH) of ketones and imines with 2-propanol or triethylammonium formate as the hydrogen source was a key discovery of the Noyori group [48, 49] and one outstanding example of stereoselection leaded by the metal chirality.

In order to obtain new complexes chiral at that metal the can be use in catalysis and evaluate the role played by the chirality at the metal centre, we synthesised different type of ruthenium and iron complexes.

2.1.1 Ruthenium(II) diamine-diphosphine complexes

If the Noyori's type catalyst have been extensively employed in ATH, on the other hand the very active catalysts generated by the addition of diamines to $RuCl_2$Phosphines in 2-propanol in presence of a base have been studied essentially as hydrogenation catalyst (AH) but they received less attention as catalyst for AHT [51].

Both the mechanisms of action of these catalysts, ATH and AH, have been studied in detail and almost completely elucidated by several research groups [52, 53, 50, 54, 55]; in figure 2.1 and 2.2 the proposed catalytic cycles of both the catalytic systems are showed.

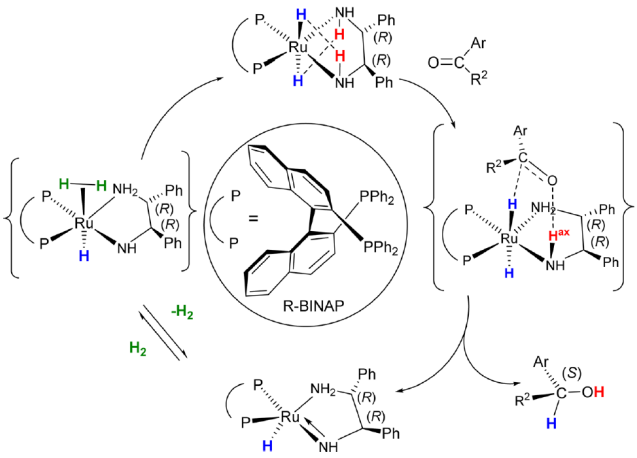

Figure 2.2: Proposed mechanism for AH of Ketones Catalyzed by Noyori-type Catalysts. [50]

In literature is present a series of active ATH catalysts of the type $[RuH_2(NN)(PP)]$ where PP was a chiral diphosphine and NN was the 2-picolylamine (figure 2.3a). However, the crucial role of the metal chirality was not highlighted, pointing essentially the attention on the chiral ligands [51].

With the aim of developing new catalysts and elucidating the role played by the spatial arrangement around the metal we synthesised a series of complexes of the type $[RuH_2(NN)(PP)]$, where PP is a chelating or two mono phosphine and NN is the 8-amino-5,6,7,8-tetrahydroquinoline (H-Campy), that was known for its chemokine receptor ligand properties [56] but never used as ligand in coordination chemistry.

This C_1 chiral di-nitrogen ligand has a pyridine connected to a primary amino group which is crucial for the catalytic activity and the two nitrogen donors are fused in a rigid cyclohexane ring. Upon coordination the NH_2 group is forced into an equatorial position; moreover the dihedral angle between the axial hydrogen of the amine and the *cis* substituent

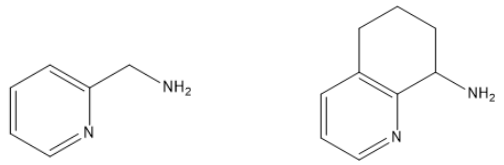

(a) **(b)**

Figure 2.3: (a) 2-picolylamine; (b) 8-amino-5,6,7,8-tetrahydroquinoline (H-Campy).

orthogonal to the Campy plane is small, these are the optimal condition based on the proposed reaction mechanism (in an octahedral Ir(III) complexes that angle is $\approx 2.5°$ see section 2.2.3).

(*S*)-Campy reacts rapidly with $[RuCl_2(PPh_3)_3]$ **1-Ru**$_{ATH}$ in CH_2Cl_2 at room temperature to give the kinetic favoured OC-6-14, **2-Ru**$_{ATH}$, *t,c*-$[RuCl_2$((*S*)-Campy)$(PPh_3)_2]$ which in turn evolves to the chiral-at-metal optically pure OC-6-42-C, **(S)-3-Ru**$_{ATH}$ *c,c*-$[RuCl_2$((S)-Campy)$(PPh_3)_2]$.

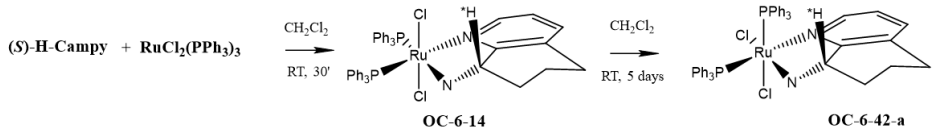

Scheme 2.1

2-Ru$_{ATH}$ reacts with the chelating diphosphine providing the complexes with the two chloride in *trans*, that then isomerized to the thermodinamically stable *cis* form (scheme 2.1). The substitution and subsequent isomerization process is completly sterereoselective as stated by the presence of only two couple of doublets in the ^{31}P-NMR spectra. Even in the presence of chiral diphosphines the isomerization is stereoselective.

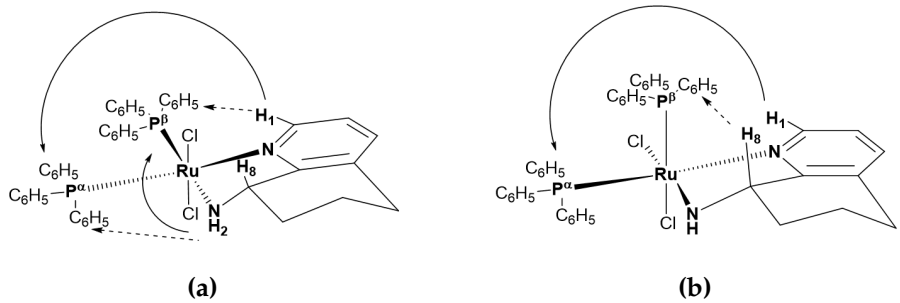

Figure 2.4: Significative correlation of (a) **(*R*)-2-Ru**$_{ATH}$ (b) **(*R*)-3-Ru**$_{ATH}$; NOE correlation dashed line; COSY correlation solid line

Stereochemical characterization

Unfortunately crystals suitable for the X-Ray diffractometry were not obtained, the stereochemical characterizations were made by 2D-NMR experiments and corroborated by ECD spectra.

A complete set of mono-dimensional and bi-dimensional NMR experiments allowed to define the absolute configuration at the metal centre for the complexes. In particular the ^{1}H, ^{13}C-NMR and the ^{13}C-^{1}H HSQC were used to unequivocally assign the signals related to the ancillary diamine ligands, whereas ^{1}H-^{31}P HMBC evidenced cross peaks between the phenyl protons and the phosphorous to which phenyls are bonded. Once defined the characteristic peaks of the two moieties the cross peaks between them in the ^{1}H-^{31}P HMBC and NOESY experiments allowed to define of the stereochemistry of the complexes.

Thus the kinetic complexes **(*S*)-2-Ru**$_{ATH}$ was recognised as OC-6-14 with the two chlorine atoms in *trans* grounding on the following correlation (figure 2.4a):

- ^{1}H-^{31}P HMBC evidenced a $^{4}J_{PH}$ coupling between the pyridine α-proton (H_1) with the phosphorus signal labelled as P^{α} ppm and between NH_2 protons and P^{β}, that indicate that P^{α} and pyridine

nitrogen and NH_2 and P^{β} are mutually *trans*;

- NOESY experiment highlighted the cross peaks between H_1 and the phenyl protons on P^{β}, while NH_2 protons show cross peaks with the P^{α} fraction, these ones were confirmed by ^{1}H-^{31}P HMBC observation. It is worth noting that the proton on the stereogenic carbon of the diamine (H_8) does not show cross peaks with the phosphine.

Trans complex **(*S*)-2-Ru**$_{ATH}$ spontaneously evolved in solution at room temperature to the thermodynamically stable *cis* isomer **(*S*)-3-Ru**$_{ATH}$ in 5 days (scheme 2.1). The strereselective isomerization can be easily followed by ^{31}P-NMR, the two doublets of the *trans* isomers evolved in only two doublets.

Among the four possible isomers only one was obtained and always by 2D-NMR experiments was possible to determinate its absolute configuration. The main features consisted of:

- the $^{4}J_{PH}$ coupling between H_1 and P^{α} in ^{1}H-^{31}P HMBC, while the one between NH_2 and P^{β} was absent;
- in NOESY the most important correlation was that one between H_8 and the phenyl protons on P^{β}

These correlations implicate that the complex stereochemistry can be univocally related to a OC-6-42-C configuration (figure 2.4b).

The isomerization from **(*S*)-2-Ru**$_{ATH}$ to **(*S*)-3-Ru**$_{ATH}$ was followed by ECD spectroscopy, in figure 2.5 is shown the CD evolution of the kinetically favoured **(*S*)-2-Ru**$_{ATH}$ into the thermodynamically more stable **(*S*)-3-Ru**$_{ATH}$; the direct stereoselective transformation was supported by the presence of two isodichroic [57] points at 358 nm and 478 nm and it confirmed previous NMR observations that the reaction proceeds completely stereoselective.

These specific patterns of correlations were then used to define the absolute configuration of the complexes that bear also a chelating diphosphine.

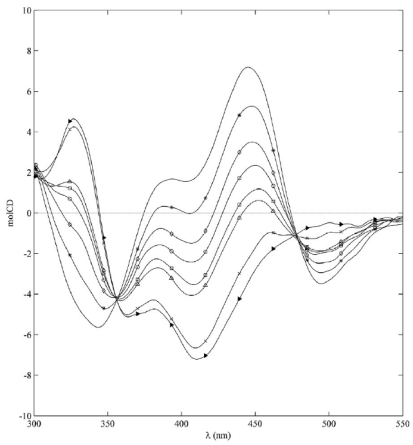

Figure 2.5: Isomerisation of complex 2(—) to complex 3(-► -) followed via CD spectroscopy: 1h (∗),2h (⋄), 3h(∘), 4h(□), 5h(△) and 3 days(×)

The results are reported in [58, 59] and it is clear how the absolute configuration at the metal centre defines the configuration of the products in the ATH catalytic reduction of ketones, however is also evident that an enantiopure metal alone did not guarantee a complete stereocontrol of the reaction, the complete stereocontrol was only obtained when the metal chirality was correctly matched with the chirality carried on the diphosphine ligands.

We have described the stereochemistry of the pre-catalysts, the di-chloride complexes, that must be converted in the hydride catalytic active species, they proved to be extremely reactive species and thus we were not able to directly observe them. In order to better understand the stereochemistry of the conversion from Ru-Cl bond to Ru-H, we decided to try different synthetic strategies to achieve ruthenium hydride complexes that should represent the catalytic active species of the reaction.

It is worth mentioning that in this period we were not involved in VCD spectroscopy yet.

We found that (*S*)-Campy (or the opposite enantiomer) reacted with [RuH Cl(PPh_3)$_3$] to give [RuHCl((*S*)-Campy)(PPh_3)$_2$] almost quantitatively in 30 minutes. The monohydride was fully characterized by a complete set of 2D-NMR experiments; the hydride complex had hydrogen and chlorine mutually trans and the hydridic proton resonated at -16.62 ppm as a doublet of doublets (J_{PH}= 29.57, 23.12 Hz). There was also a second doublet of doublets at -16.21ppm (J_{PH} = 26.8, 21.9 Hz) less than 1 % of the major one. The ^{31}P-NMR showed an intense AB system at 74.30 and 69.65 ppm (J=36.9 Hz) and a second AB system, less than 1% of the former, at 67.01 ppm being the second doublet hidden by the doublet at 69.65 ppm.

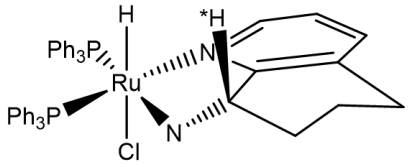

OC-6-54-A

Figure 2.6: Structure of S-RuH major product with configuration OC-6-54-A, determined by NMR. see text.

The absolute configuration was based on the NMR experiments:

- the unambiguous identification of the phosphorous *trans* to the pyridine nitrogen by the J^4 coupling in the COSY experiment;
- the two coupling constant J_{HP} defines both the PPh_3 in *cis* position with the hydride;
- the strong NOE between NH_2 and the phenyl protons on phosphorus *trans* to the pyridine, the strong NOE between the H^8 on the stereogenic carbon and the Ru hydride.

These correlation indicated that (*t,c,c*-[RuHCl((*S*)-Campy)(PPh_3)$_2$]) (***S*-Ru H**) is the diastereoisomer OC-6-54-A, 99% optically pure at the metal cen-

tre 2.6.

The complexes showed to be stable and the isomerisation did not be detected even after refluxing in toluene solution and, in the same way, further attempts to substitute the PPh_3 with a chelating phosphine failed. If dissolved in chlorinated solvents (CH_2Cl_2 or $CHCl_3$), (***S*-RuH**) gives the optically pure OC-6-42-C **(*S*)-3-Ru**$_{ATH}$ complex (section 2.1.1). Used as catalyst showed the same enantiomeric excess of **(*S*)-2-Ru**$_{ATH}$ in the ATH of acetophenone, consistent with a conversion in the same catalytic active species. However in absence of base and in stoichiometric amount complex ***S*-RuH** was not able to reduce acetophenone; this confirms the hypotesis that only one of the hydride is catalytically active, the one with small dihedral angle with respect to the axial NH, consistent with the outersphere mechanism and on the main role played by the metal configuration.

These non-racemic hydride metal complex gave us the unique opportunity to investigate the M-H bond via VCD spectroscopy (*vide infra* section 2.2.2).

2.1.2 η^6-arene ruthenium complexes

The Noyori's type ATH catalyst is indeed a η^6-paracymene ruthenium complexes, where the chiral information determining the absolute configuration at the metal centre is located on the diamine ligand. These complexes were synthesised starting from [η^6-p-cymene-Ru(II)Cl_2]$_2$ that is the ubiquitous starting material for active AH and ATH catalyst, easily prepared from $RuCl_3 \cdot nH_2O$ and α-phellandrene. Our aim was to prepare new η^6-arene ruthenium complexes chiral at the metal that could be used in ATH, characterized by the presence of chiral prompting group on the arene instead of the diamine ligand and the study of the substitution of the coordinated arene-ring able to influenced the catalytic activities.

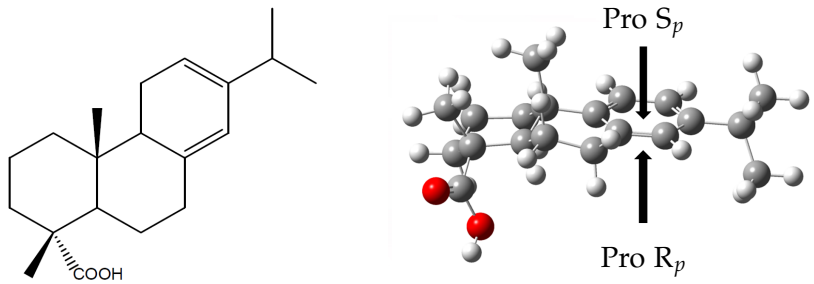

Figure 2.7: (a) Levopimaric acid (LPA) (b) The two possible face of the dehydroabietic acid coordination are shown, with respect to the planar chirality: the pro S_p top and the pro R_p bottom.

Levopimar acid

First we focus our attention on the α-phellandrene motif, thus we searched in the chiral pool molecules with six member ring characterized conjugated diene that should be able to reacts with $RuCl_3 \cdot nH_2O$ (scheme 2.2). The best candidate was Levopimaric acid (LPA) that is a constituent of conifer oleoresin and is its major component with conjugated *cis* double bond, that could be extracted from the waste of the logging industry.

Diterpene resin acids play important roles in the tree defence against insects and microbial pathogens. The major constituents are tricyclic carboxylic acids which are divided in two mainly groups: abietanes and pimaranes. Levopimaric, abietic, neoabietic, palustric and dehydroabietic acids are the constituents of the abietanes. The dehydro and tetrahydroresin acids are usually present only after acid or heat treatments.

This compound allowed us to introduce two new chiralities in the complex: the planar chirality (figure 2.7b) and the sp^3 chirality of the stereogenic carbons.

In reactions involving the double bond LPA is more reactive than abi-

etic, neoabietic and palustric acids but it is also the most sensitive to autoxidation [60]. The thermodynamic composition of heated abietanes is: abietic acid 81%, palustric acid 14%, neoabietic acid 5% [61]. The most available derivatives on market are the rosins (wood, gum, tall), however all these oils have suffered heating or acid/base treatments that caused the isomerization of LPA to abietic acid [60]. Thus we used crude oleoresins, which contains from 23% to 40% of LPA. The elevated presence of one of the abietanes could be detected qualitatively by the presence of crystals, that appear when one component is present more than about 30%.

We studied two different types of resin: one from Megara (Greece) and one from China. The concentrations of these phytochemicals are highly variable, due to both environmental and genetic differences. The resin acids are usually analysed using GC-chromatography as methyl-esters with FID as detector [62], other methods were developed, as reversed-phase HPLC [63]. We chose to use the GC-methodology as reported in literature. The GC signals were assigned by GC-mass investigation considering the NIST fragmentation database. The resins analysis showed that the Chinese one was richer in LPA than the Greek one: 38.4% of LPA against only 13.55%. The acid was isolated in 11% yield [64]; the molecule has been fully characterized by NMR-spectroscopy (H-NMR, ^{13}C-NMR,COSY,NOESY, TOCSY, HSQC); furthermore the specific rotation was the same reported in literature ($[\alpha]_d$= -265°, 2% methanolic solution) and the absolute configuration was confirmed by single-crystal X-Ray diffraction. The obtained white crystals had to be stored protected from light and in freezer in order to avoid the oxidation and isomerization.

We attempted to synthetize the dimeric complex [Ru(η^6-arene)Cl_2]$_2$ from the reaction of levopimarc acid (or its mentoxy derivatives)with $RuCl_3 \cdot nH_2O$ [65, 66] (Scheme 2.2).

The reaction did not proceed: the initial dark red solution became blue/ green without further evolution. Prolonging the reflux overnight

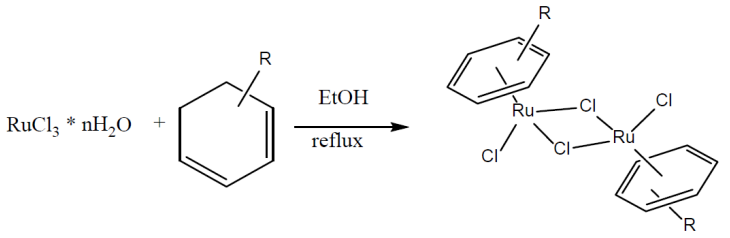

Scheme 2.2

we observed the formation of black precipitate and the solution turned to green/ brown. We varied the conditions, (temperature, concentration, sequence of addition, inert atmosphere, microwaves), but the result obtained was always the same.

The analysis of the solution evidenced the presence of abietic acid (AA) as major product, originated by thermal isomerization, and also the presence of dehydroabietic acid (DHAA). The presence of this latter product means that the oxidation of the ring took place, confirmed by the strong acidity of the solution. However the conversion was not complete, the reaction was probably stopped by the isomerization of LPA. Moreover the aromatic ring was not coordinate to the metal centre, otherwise its characteristics ^{1}H-NMR peaks should be shifted at higher fields.

The black solid was soluble only in boiling DMSO and DMF, the elementary analysis showed the presence of organic material; the % composition showed an hydrogen/carbon ratio 7:5, compatible with the structure of DHAA ($C_{20}H_{28}O_2$). The NMR experiments were not conclusive due to the presence of paramagnetic materials. This black solid was problably composed by a ruthenium (III) cluster that trapped organic ligands.

Even if we were not able to obtain pure compounds of definite structure and composition we used the black precipitate as catalyst in ATH and in asymmetric hydrogenation (AH) of acetophenone. First of all we tried to activate the complex refluxing the black precipitate with N-Tosyl-ethylendiamine (Ts-en) for 2 hours. The reaction led to an heteroge-

neous dispersion which, after filtration, gave a pale yellow solution able to enantioselectively reduced acetophenone in ATH. In addition this solution showed an active ECD around 400nm, a region of the spectra avoided of signal in pure DHAA that confirmed an interaction between the chiral ligand and the metal. Although the conversion was disappointing low, the 50% e.e. confirmed the presence of a chiral induction; however it was not possible to relate such effect with the structure of catalytic species, especially to the chirality at the metal.

For what concerned the reaction between the LPA and $RuCl_3 \cdot nH_2O$, we hypothesised that the blue solution of ruthenium [67, 68] was composed by a cluster of Ru(II) anions. In order to confirm the nature of the solution obtained with LPA, we prepared a pure blue solution following the procedures reported in literature and then we tested the reactivity of both in the studied reaction with: LPA, DHAA, α-phellandrene and p-cymene. Both the blue solutions presented the same reactivity: we observed reaction only with α-phellandrene, obtaining in both cases the same ruthenium complex $[\eta^6(p\text{-cymene})Ru(Cl_2]_2$. The explanation is probably that LPA acts as reducing agent but, due to its steric hindrance, it was not coordinated in high yield and the non-coordinating Ruthenium (II) species rearrange in cluster.

We tried different synthetic path was study involving arene substitution. It is reported that high hindrance arene complex [69, 66] (as Ruthenium hexamethylbenzene dichloride dimer) can be obtained by exchanges of coordinate ring (scheme 2.3).

The reaction was carried out in neat at 205°C in a sealed tube; we obtained a brown precipitate, slightly soluble in chloroform and soluble in methanol. The NMR spectrum showed the presence of two doubles and one singlet between 5.40 and 5.85 ppm that could belong to the coordination of DHAA. Interesting, the IR-Spectra of this precipitate showed one carbonyl band at 1952.14 cm^{-1}. Probably it was originated from the decarboxylation of the DHAA, in fact DHAA in high temperature conditions [70] realise one molecule of carbon monoxide that could be coordinated

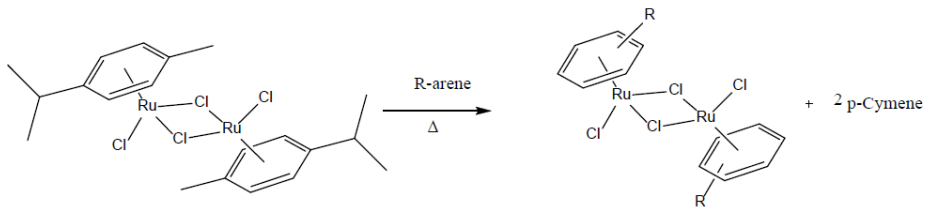

Scheme 2.3

to the ruthenium(II); this hypothesis was supported by the absence of the carboxylic band. It is worth mentioning that the exchange reaction, described to occur with $C_{12}H_{18}$, does not proceeds with m-methyl-anisole and even with anisole.

The last synthetic strategies tested was the reaction with the [Ru(0)(COD)(COT)] complex [71, 72] under H_2 atmosphere, or the exchange of a before coordinated naphthalene [Ru(naphthalene)(COD)], and subsequent oxidation with HCl 6M (scheme 2.4).

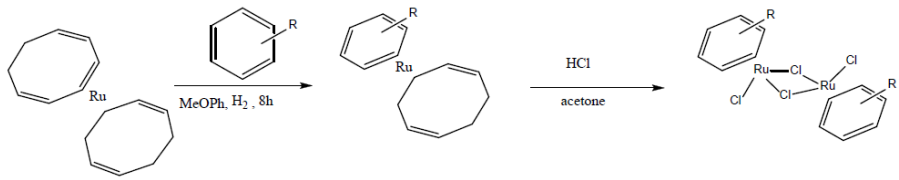

Scheme 2.4

The reaction was tested with *m*-methyl-anisole where we obtained in good yields the dimeric complexes. The ^{1}H-NMR spectrum revealed the presence of the two possible planar chirality, it was highlighted by the broaden or double signals of the phenyl protons in $CHCl_3$, whereas in deuterated DMSO the four peaks were well defined due to the bridge splitting. However even in this case the results of the reaction was a mixture of products difficult to characterise.

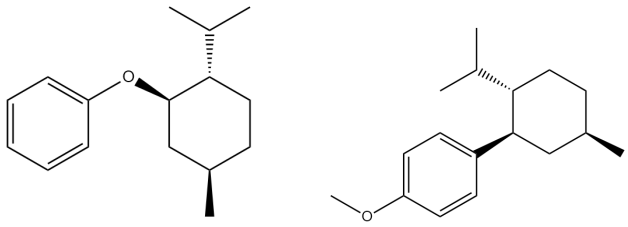

(a) menthyloxybenzene **(b)** 4-menthylanisole

Substituted benzenes

Persuaded that the steric hindrance around the aromatic ring was the reason of our failure we decided to simplify the substituent, so we synthesized benzenes with chiral substituents.

The first attempt was with menthyloxybenzene (figure 2.8a) that we synthesized starting from 4-nitroclhorobenzene. The corresponding Ru(II) complexes was synthesized in 30% yields with the synthetic strategy reported in scheme 2.4, the coordination of the arene was confirmed by the chemical shift of its protons. In order to obtain complexes suitable for the ATH and to confirm the chiral induction of the menthyloxy group, the dimeric complex was reacted with the disymmetric diamine Ts-en. Although with a partial decomposition of the starting complexes, the diastereomeric complexes were obtained. Stated that the substituend was too far, the d.e. was low (16 %) and in ATH the mixture was able to reduce acetophenone with a poor e.e.

The next step was to bring closer the chiral group to the metal, for this porpoise we synthesized the 4-menthylanisole by coupling reaction [73] (figure 2.8b). Following the reaction scheme reported in 2.4, the dimeric complexes were achieved in 60% overall yields, however the ^{1}H-NMR spectra highlighted the presence of two systems of multiplets between 6.2 ppm and 5.3 ppm, that was compatible with the presence of two complexes with coordinated arene. Our possible explanation of the different

complexes was the presence of rotamers due to hinder rotation around the carbon-carbon bond between phenyl and menthyl moiety; the rotation barrier was evaluated by DFT calculation[1] over the 10 kcal/mol.

The subsequent reaction whit Ts-en diamine was not stereselective and the obtained mixture of complexes were able to reduce acetophenone only as racemate.

2.1.3 η^5-cyclopentadienyl-Iron(II) hydride complex

In the previous sections we synthesised optically pure diamine diphosphine ruthenium complexes and we reported our attempts to obtain the stereoselctive synthesis of η^6-arene ruthenium complexes, both the types of complexes can be used as catalyst in ATH reaction. The most part of the catalytic reactions deal in the presence of noble transition metals essentially of the eight groups such as palladium, iridium, rhodium, ruthenium. These are characterized by low availability, high price and considerable renal toxicity. For these reasons interest is growing into the first-raw transition metal, in particular iron which is the second most abundant metal on the Earth's crust and it is better life-compatible [74]. Recently iron(II) complexes active in the reduction of the polarized double bonds were reported [50, 75].

In order to have a deeper insight of the chemistry of the chiral metal hydride complexes that could be active in the reduction of polarized double bond, we synthesized an η^5-C_5H_5Fe hydride complex.

Cyclopentadyenyl iron complexes chiral at the metal centre have given outstanding results in the stereselctive alkylation reaction, where however the iron complexes acted as stoichiometric reagent [76, 77].

Due to the labilizing effect of the hydride [78], we chose to replace the ligands present in a preformed iron-hydride complexes. [$FeCpH(CO)_2$] was a possible starting complexes, however it is a pale-yellow oil unstable

[1] G09, B3LYP/3-21G in gas phase.

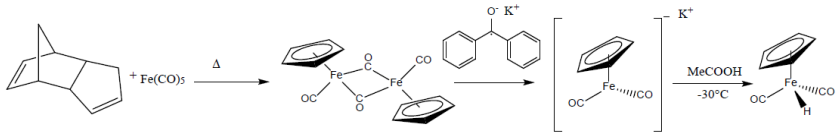

Scheme 2.5

over -20°C [79, 80]. Conversely, the potassium salt of the unsaturated iron complex is a orange solid, extremely air sensitive but it can be stored in inert atmosphere for several months [81]. The hydride complex can then be easily generated in situ by addition of a weak acid at low temperature (scheme 2.5).

Our purpose was to obtain hydride complex chiral at the metal, thus we used the optically active disimmetric chelating ligand (*S*)-Prolophos that was first synthesized in our laboratories. This ligand is easily synthesized in enantiomeric pure form from the natural product (*S*)-prolinol [82] and it has the advantage to present two really different phosphorus atoms (free $P^N \approx 47$ ppm, $P^O \approx 114$ ppm) that makes easy distinguish between them (upon coordination P^N and P^O shifted to $\approx 110 \pm 15$ ppm and $\approx 180 \pm 15$ ppm respectively).

The chelating ligand was added at -20 °C for ten minutes after the addiction of CH_3COOH and the reaction was followed by NMR and IR spectroscopy. Unlike the $[RuCpH(CO)_2]$, where the presence of the hydride allows the substitution of both the carbonyls, we found that the monosubstituted hydride complexes was the major products (scheme 2.6).

The coordination took place by the phosphite moiety and this complex was partially converted to the cationic carbonyl complexes of formula $[CpFe(PP)(CO)]^+$ with a 43% d.e. stereoselection, based on the ^{31}P-NMR integration of the diastereomers. $[CpFe(\eta^1\text{-PP})(CO)H]$ complexes are known to give rise to disproportionation reactions [83] giving several products amongst which is the prevailing specie is the cation $[CpFe(PP)(CO)]^+$ complexes. The reaction never reached full conversion,

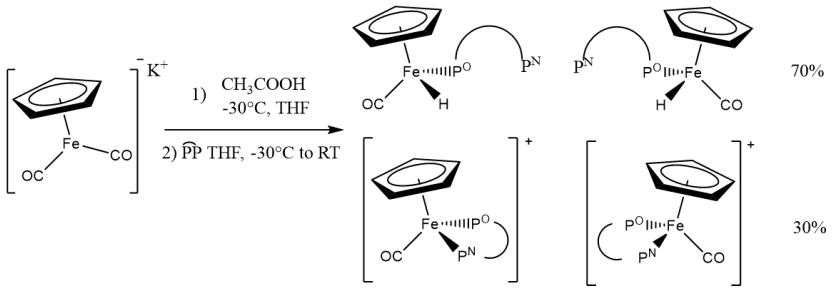

Scheme 2.6

even at refluxing THF; however an increase of the d.e.% was observed; this effect must be due essentially to the preferential decomposition of the minor diastereomers. When $CHCl_3$ was added to the reaction mixture, it gave $[CpFe(PP)(CO)]^+$ Cl^- quantitatively in 87% d.e., a result similar to that obtained in the reaction of prolophos with $[CpFe(CO)_2Cl]$ [84].

In order to obtain the chelate hydride complex we decided to perform the reaction in presence of UV source (scheme 2.7). After 4 hours of irradiation the major products were represented by two couple of doublets in the 31P-NMR spectrum up to the 56% of the products, whereas the rest was still the monocoordinate specie. We identified to different hydridic species; they were described by two doublets at $\approx$ -13 ppm (the monocoordinated specie) and two doublet of doublets at $\approx$ -14.5 ppm. The two double doublets showed the coupling constants of J_{PH}=72Hz,68Hz and J_{PH}=72Hz,72Hz leaving no doubts on the presence of the chelating diphosphine.

The two diastereomers showed an d.e. of 55%, based on ^{1}H-NMR hydride integration, and they were separated from the cationic complexes by extraction in pentane, however further attempts to resolve the diastereomers failed.

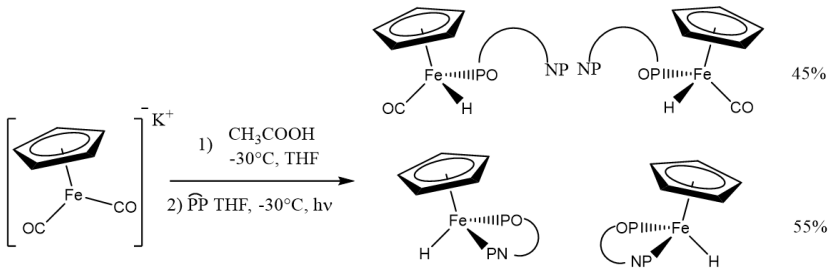

Scheme 2.7

Due to the low d.e.% and the difficult to separate the diasteromers into an optically pure form, we decided to postpone further investigations.

2.2 Vibrational circular dichroism

The chirality of the metal centre is determined exactly by X-ray structure determination, provided that suitable crystal will be obtained. In diastereomeric couple NMR represent another technique of choice but not always it is possible to obtain meaningful informations. The results obtained in the synthesis of η^6-arene ruthenium complexes and η^5-cyclopentadienyl iron complexes prompted us to explore different techniques able to describe complex mixtures of regioisomers.

VCD in tandem with DFT calculation is powerful technique for the determination of the absolute configuration and conformational analysis; despite new results concerning transition metal coordination compounds are coming out [85, 86, 87], their application in the study of metallorganic compounds are not common. The strength of IR and VCD spectroscopy lies in the fact that the spectra of a chiral molecule contain sufficient stereochemical details to be consistent with only a single absolute configuration and an unique solution-state conformation, or distribution of conforma-

tions, of the molecule [46].

The main drawback of VCD spectroscopy concern the low intesity of its signals, therefore we decided to apply VCD spectroscopy to some metallorganic complexes containing widespread vibrational chromophore in order to found relationship between spectra and structure that could be used as probe to define the chirality of metal centre.

In this section we report our results in the application of Vibration Circular Dichroism to chiral transition metal complexes.

2.2.1 Carbonyl Chromophore

The first chromophore we decided to investigate was the carbon monoxide; carbon monoxide is one on the most common ligand for transition metals; the metal carbonyl complexes found application as catalyst, precatalyst or stoichiometric reagent [76] in different kind of reactions.

What make carbon monoxide attractive is its infra-red stretching frequency that, in mononuclear carbonyl complexes, lies in the range 2125-1850 cm^{-1}, a region of the IR spectrum devoid of other signals. The stretching frequency value originates from a thigh interaction between the metal orbitals and the carbonyl ones and it is highly affected by the nature of metals and their substituents (see A); infra-red spectroscopy is known to be a well established technique to study carbonyl complexes and their electronic properties; therefore our intent was to demonstrate that also VCD could be a probe of the metal centre chirality.

A number of chiral carbonyl complexes of Mn, Fe, Mo, W, Ru, Re are known (see [47],[88] and reference therein), a consistent part of them is characterized by the presence of an η^5-cyclopentadienyl ring; we focused our attention on a series of heteroleptic ruthenium(II) complexes of general formula [η^5-((1*R*,2*S*,5*R*)-menthyl)-$C_5H_4Ru(CO)(P(C_6H_5)_3)X$],[2] where X could be Cl,Br,I, and the related cation complex [η^5-(menthyl)-$C_5H_4Ru(CO)$

[2](1*R*,2*S*,5*R*-menthyl here after defined menthyl

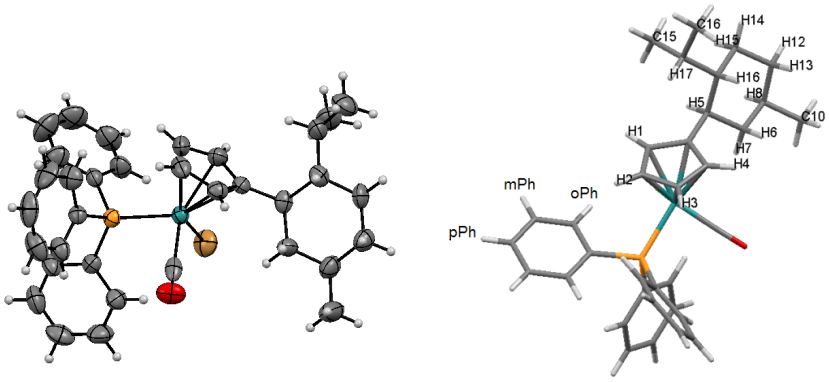

(a) **(b)**

Figure 2.9: (a) Crystallographic structure of $(R)_{Ru}$RuBr; (b)Crystallographic structure of $(S)_{Ru}$RuCl) with labels required in the text. It should be noted that the structures have the same spatial arrangement.

$(P(C_6H_5)_3)(NCMe)]BF_4$ here after defined RuCl, RuBr, RuI and $RuBF_4$) and to the analogue diastereoisomeric complexes [η^5-((1*S*,2*S*,5*R*)-neomenthyl)-C_5H_4Ru (CO)$(P(C_6H_5)_3)$Br].[3]

Due to the three *fac* positions occupied by the η^5-cp ring, the diastereomers can be defined according to the extended CIP sequence[17] (see appendix B): the presence of the η^5-cyclopentadienyl ring introduces an higher chemical stability and an obvious simplification in the stereochemical treatment because it can be considered a sort of fourth substituent connected to the metal by a ghost atom at the centre of the Cp ring.

The synthesis of these kind of menthyl- and neomenthyl- cyclopentadienyl complexes was first attended in our laboratory [89, 90, 91], these ruthenium complexes can be easily synthesized and resolved in single diastereomers; they are stable half sandwich, three-legged piano stool cyclopentadienyl complex in which the ruthenium atom is in a slightly

[3](1*S*,2*S*,5*R*)-neomenthyl here after defined neomenthyl

distorted octahedral geometry. The complexes were prepared following a modified procedure of that reported in literature (refluxing heptane instead of xylene) and obtained as pure diastereomers by preparative TLC or flash chromatography: $Ru_3(CO)_{12}$ reacts with the substituted cyclopentadienyl in refluxing heptane; if the reaction is performed in inert atmosphere hydride monomer $Ru(\eta^5-C_5H_4R)(CO)_2H$ is obtained, otherwise the $[Ru(\eta^5-C_5H_4R)(CO)_2]_2$ dimer. The hydride dissolved in chloroform gives the dicarbonyl [Ru (η^5-C_5H_4R)$(CO)_2Cl$] complex that for subsequent reaction with PPh_3 provides the desired products as an almost racemic mixture of diastereomers. Conversely the bromide and iodide complexes were synthesised starting from the dimer with the corresponding molecular halogen. Instead the cationic complexes was synthesised by reaction with $AgBF_4$ in acetonitrile solution.

Attempts to obtain the bromide and iodide complexes by stereoselective metathesis reaction with KBr and KI in acetone and the diastereosimeric pure RuCl complexes failed due to partial racemization. The process was followed by ^{31}P-NMR and provided information on the relative stability of the complexes. The metathesis reaction was stereospecific; the reactions started with complete retention on configuration in the early stages but was flanked by partial racemization of the products. The lower configurational stability of the Br and I derivateves was confirmed by the slow racemization in solution of the optically pure diastereomer. In table 2.1 are listed the data for the reaction in acetone; two observation can be made: the configuration stability decreases in the group and among the couple of diastereomers the *R* configuration (S in the due to the change in priority order) is the more stable. The complexes left in $CDCl_3$ solution confirmed the trends: RuCl complexes are stable for at least two weeks in solution the RuI complexes racemize in a couple of days.

For sake of clarity before discussing the results we think is helpfull to introduce a simplification in the sterochemical notation. As remembered above, for these complexes CIP notation should be used; we are perfectly aware that η^5 has an higher priority on Cl (A.M. 35 amu) and a lower one than Br (A.M. 80 amu) and I (A.M. 127 amu). The consequence is

that complexes with the same spatial disposition of the ligands can be defined *S* with iodine and bromine and *R* if the halogen is the chlorine. This could make the discussion rather difficult and misleading, for these reasons further in the text an arbitrary notation will be introduced, we do apologize for this over simplification.

Table 2.1: Metathesis reaction of RuCl in enantiopure for with KBr and KI and racemization; the reaction were performed in acetone solution with 6 eq. of the respective salts.

	$(R)_{Ru}$RuBr		$(S)_{Ru}$RuBr			$(R)_{Ru}$RuI		$(S)_{Ru}$RuI	
t(h)	C	d.e.	C	d.e.	t(h)	C	d.e.	C	d.e.
6	100	100	42	90	3	13	100	22	100
14	100	100	82	83	8	34	73	33	100
22	100	94	93	80	14	76	89	61	85
					22	83	68	78	9

We started developing the method on the well established RuCl complexes and then we verified the correlation between the carbonyl VCD sign and the chirality at the metal centre with the other complexes.

Methods of investigation

NMR Characterization

The complexes were fully characterized by NMR spectroscopy: ^{1}H-NMR spectrum of the complexes presents three well defined region: over 7 ppm are present the aromatic signals of the $P(Ph)_3$, between 5.5 ppm and 3.5 ppm the signals of the coordinated Cp ring while below 2.5 ppm the peaks of the alifatic menthyl and neomenthyl protons, moreover the four signals of the Cp ring do not overlap with other signals and are well apart (figure 2.10). All these features allow the investigation via NOESY experiments and in particular the relative position of the menthyl moiety with respect to the $P(Ph)_3$ and the angle between the Cp plane and the

menthyl.

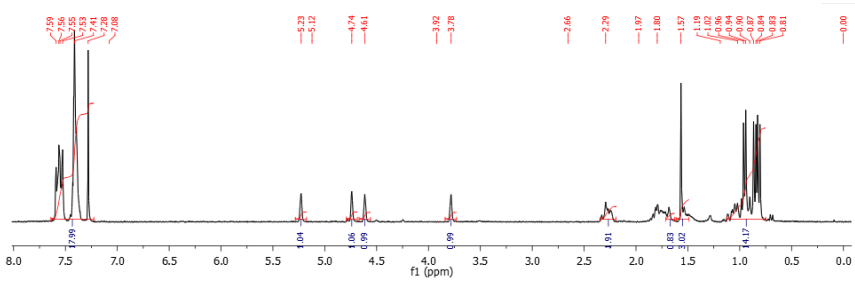

Figure 2.10: ^{1}H-NMR spectra of $(S)_{Ru}$RuBr, it is clear the split of the different kind of signals.

The NOESY spectra of the complexes revealed a very specific pattern: the hindered menthyl and $P(Ph)_3$ moieties occupy an antipodal position. Moreover, the presence of cross-peaks of each proximal hydrogens on the Cp ring (H_1 e H_4) with a different portion of the menthyl moiety implies a severe restriction of menthyl rotation or puckering, with the isopropyl fragment oriented farther from the metal, as highlighted by the presence of only one cross-peak between the aryl proton of $P(Ph)_3$ and H_7. In solution at 300 K it is remarkable that both diastereomers adopt a conformation with the bulky menthyl and $P(Ph)_3$ groups as far away as possible from each other quite similarly as observed in the solid by X-ray spectroscopy on the reported $(S)_{Ru}$RuCl and of the obtained $(R)_{Ru}$RuBr (see figure 2.9a).

We remind that NOEs are common used in semi-quantitative way in the structure determination of biomolecules, where the calculated internuclear distances are used as restraints for MD calculations. Recently several works reported high accurate and precise NOE-based distances determination for small organic molecule [92] and quantitative evaluation on organometallic complexes are also reported [93]. Therefore we decided to estimate quantitatively some key internuclear distances of complexes

RuCl in order to obtain a set of parameters useful for the conformer analysis (vide infra). The RuCl complex was choose because the structure of the (*S*) distereomer was the only available at the beginning of the work [89].

As first step the spin-lattice relaxation times (T_1) for some atoms in different molecule moieties were measured at 300 K; the recycle delay (d_1) should be set between 3-5 times the longest T_1 but to lied in the allowed walltime the value was set at 3 s [93]. Next, was the choice of the more suitable mixing time: the NOE build-up curves for some relevant cross-peaks were built recording several spectra varying the mixing time (τm) from 0.7s to 2.2s. As result (τm) was choose at 1.3s the mean value between the aliphatic and the aromatic moieties and sufficiently apart of the NOE maximum enhancement. For a first order multispin system the peak intensities are given by

$$I = M^0 \exp(\frac{-R}{\tau_m}) \tag{2.1}$$

where I is the matrix of peak intensities, M^0 is the matrix of equilibrium magnetization (the intensity of diagonal peaks at τ_m = 0), and R is the relaxation matrix [94]. Assuming that no exchange occurs between two nuclei, i and j, the off-diagonal elements of the relaxation matrix could be approximated to the cross-correlation rate between the two nuclei, σ_{ij}. Using the matrix method equation (2.1) could be solved as

$$R = -\tau_m^{-1} \ln(A) = -\tau_m^{-1} X(\ln \Lambda) X^{-1} \tag{2.2}$$

Where A is a matrix which elements are given by $I_{ij} \div M_j^0$, X is the matrix of eigenvectors of A and Λ = diag(λ_i) and λ is the *i*th eigenvalue of A [93]. It was reported that when this exponential expansion is used the dependency of the averaged integral intensity on the mixing time could be consider linear, with high degree of accuracy, above the normal range considered in the initial rate approximation. So, in the fast tumbling regime, $\sigma_{ij} = k r_{ij}^{-6}$ and k is $k = (\frac{\mu_0}{4\pi})^2 (\frac{\hbar^2 \gamma^4}{10} \frac{6\tau_c}{1+4\omega^2\tau_c^2} - \tau_c)$. Assuming τ_c

comparable for each spin pair, k is related to parameters fixed for a given experiment thus the internuclear distance r_{ij} could be estimated using a reference known distance (r_{ref}) as

$$r_{ij} = r_{ref} \sqrt[6]{\frac{\sigma_{ref}}{\sigma_{ij}}} \tag{2.3}$$

The intensity of the cross-peaks were measured using the included integration tool of MNova software while M^0 were defined running an experiment with τ_m = 1ms. As reference distance were used the reported distance of geminal proton (1.68Å) considering the cross-peak between the two geminal H_6 and H_7 proton on menthyl (see experimental section for labels) and for what concerned the distances between different moieties all the $\langle r_{ij} \rangle$ were increased by 10% in order to correct for overestimation of the short distances [95]. The results are listed in table 2.2, the obtained values are in good agreement with those of crystallographic data. This result allowed us to consider reliable the distances for others complexes of this type for which the crystallographic structure were not obtained.

VCD measurement

In Figure 2.11a we superimpose the experimental IR and VCD spectra of $(R)_{Ru}$RuCl and $(S)_{Ru}$RuCl: the monosignated VCD feature associated with the CO stretching observed at 1955 cm^{-1} in correspondence of the strong IR band, inverts its sign in going from $(R)_{Ru}$RuCl, to $(S)_{Ru}$RuCl. Interestingly the sign of the CO-stretching VCD band is the same as for OR and for the lowest energy ECD band [96]. On the contrary, the region 1700-850 cm^{-1} exhibits several weaker VCD bands with the same sign for the two diastereomers, $(R)_{Ru}$RuCl and $(S)_{Ru}$RuCl, with just two little exceptions: the couplet at 1420 cm^{-1} and the weak monosignated band at ca. 1000 cm^{-1}. Based on this, we may attribute the VCD bands in the latter region to normal modes localized mainly in the menthyl moiety (and, to a lesser extent, in the cyclopentadienyl and phenyl moieties). Thus the sign of the corresponding VCD bands depends only on the configuration

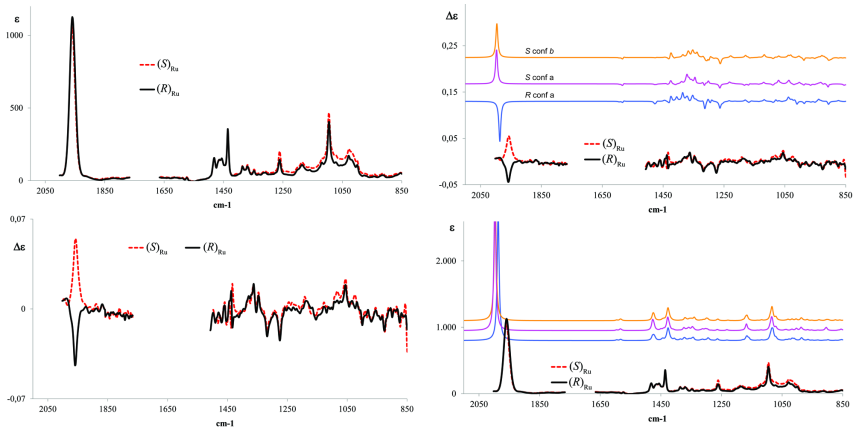

(a) **(b)**

Figure 2.11: (a) IR absorption and VCD spectra $(R)_{Ru}$RuCl and $(S)_{Ru}$RuCl complexes; (b) Comparison of experimental VCD (top) and IR (bottom) spectra of $(R)_{Ru}$Ru and $(S)_{Ru}$Ru with corresponding calculated spectra for the conformers a and b of $(S)_{Ru}$RuCl and conformer a of $(R)_{Ru}$RuCl

of the three asymmetric carbons in the menthyl, which does not change in going from $(R)_{Ru}$RuCl to $(S)_{Ru}$RuCl and bear good resemblance to the VCD spectra of menthone and menthol [97].

Instead the 1955 cm^{-1} band, associated to the CO stretching, is directly related in sign to the Ru chirality. About the intensities of VCD bands the dissymmetry factor $g(\nu) = (\Delta\varepsilon/\varepsilon)$ of the strongest VCD band, namely the CO stretching, is of the order of 10^4 (vide infra), which means that the intensity of the CO- stretching VCD band measured here is lower or comparable to other cases where coupled C=O stretching gives rise to an exciton chirality effect [98, 99], however it is quite intense if compared to the VCD of isolated C=O bond stretching in other molecules (e.g. for camphor [46]). As results the Ru-CO VCD signal is directly connected to the stereochemistry of the metal and it becomesprobe of the metal chirality.

This preliminary experimental results confirmed our intuition, some ligands can be promising probe for the chirality at the metal; particularly interesting if one thinks that IR is a technique widely used in the past to investigate the mechanism of catalytic activity, mainly in hydroformylation of course but also in hydrocarbonylation.

DFT

The relation between the chirality at the metal and the IR/VCD must be elucidated also from a theoretical and computational point of view; in particular DFT calculations allow to locate the normal modes at the origin of the VCD bands.

Table 2.2: Atom-atom distances in $(S)_{Ru}$RuCl and $(R)_{Ru}$RuCl as evaluated from NOE spectra; X-Ray diffraction data; calculated DFT data of the structures which are in the best agreement with X-ray and NOE data.

		(*S*)RuCl		(*R*)RuCl	
	XRD	NOE	DFT	NOE	DFT
H_1 - H_5	2.69	2.8	2.6	2.8	2.7
H_1 -$H_1$7	2.92	2.8	3.1	2.7	2.9
H_1 - $C_1$5	2.77	2.9	2.6	2.8	2.5
H_4 - H_6	2.41	2.5	2.4	2.4	2.3
H_4 - H_7	3.21	3.7	3.3	n.d.	3.1
H_1 - oPh[a]	3.18	3.1	2.4	2.9	2.6
H_4- oPh	5.85	4.0	4.4	3.7	4.2
H_2 - oPh	2.80	2.9	2.8	2.8	2.6
H_3 - oPh	2.78	3.0	3.1	2.9	3.1
H_7- oPh	4.30	4.6	4.3	4.2	4.5

[a] Hydrogen in ortho position in phenyl ring of the phosphine

DFT calculations were conducted with Gaussian09 [100]; for the choice of functional and basis functions, we followed the suggestions of a previous theoretical treatment of a Ru-complex [101]; the complex was treated

in vacuo. The conformational search was carried out starting from the X-ray conformer of $(S)_{Ru}$RuCl, introducing a pseudo atom PSu at the centre of the cyclopentadienyl and rotating the ring in five successive steps. For each one of the five positions thus reached, the menthyl moiety was allowed to rotate to avoid steric hindrance, the two orientation of the menthyl moiety (Ru-pentadienyl ring-menthyl- Isopropyl) and the ellepticity of the $P(Ph)_3$ have been tested.

Globally ten conformers were obtained in this way and optimized at B97D [102, 103]/SVP [104] level; analogously ten conformers were treated for $(R)_{Ru}$RuCl, whose initial conformation was obtained from the X-ray structure of $(S)_{Ru}$RuCl by mirror image at the metal atom. We considered only the first four conformers for both $(R)_{Ru}$RuCl and $(S)_{Ru}$RuCl, amounting to more than 95% of all possible conformers for each diastereomer. These complexes allow for large amplitude hindered rotational modes [105, 106]. The preferred conformation was then chose comparing the distances by calculated structures with the experimental distances determined by NOESY experiments for both $(R)_{Ru}$RuCl and $(S)_{Ru}$RuCl and that obtained by X-ray diffraction for $(S)_{Ru}$RuCl [89]. In Table 2.2 are listed the distances of the conformers that show the best compatibility between calculated and experimental distances (a complet version in presents in experimental section 4.4). For $(S)_{Ru}$RuCl is ensured by the conformers a, b while by conformer a for $(R)_{Ru}$RuCl.

In Figure 2.11b we compare the experimental IR (lower) and VCD (higher) spectra for $(R)_{Ru}$RuCl and $(S)_{Ru}$RuCl, with the calculated IR and VCD spectra of the conformers of the diastereomers $(R)_{Ru}$RuCl and $(S)_{Ru}$RuCl, chosen as described above. While the mid-IR region is predicted to be almost (*vide infra*) independent from the configuration of the metal atom and shows weak signals, on the opposite the CO stretching region inverts sign upon change of configuration at the metal. A very good correspondence is found not only for the sign of the VCD bands but also for the IR and VCD intensities.

The analysis of the normal modes allows to explain the origin of the cou-

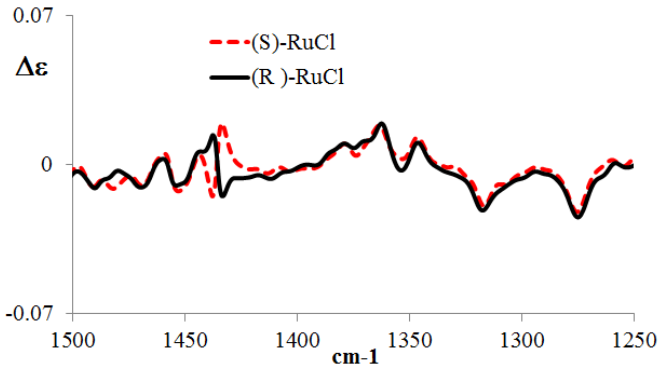

Figure 2.12: Expansion from 1250 cm^{-1} and 1500 cm^{-1}.

plet at 1420 cm^{-1} (figure 2.12: the two components of the doublet are the symmetric and anti-symmetric combinations of in plane CC-stretching modes located on the phenyl of the phosphine ligand, thus the signs inversion can be related with an inversion of the phosphine helix (M for $(R)_{Ru}$RuCl and P for $(S)_{Ru}$RuCl). In the crystallographic structure an H-bond is present between one of the phenyl and the chloride and it is probably because of it that one of the phosphine configuration is more stable and could be detected in solution, the chirality at the metal defines the chirality at the phosphine.

The strength of the method is well highlighted: with a single spectra we were able to individuate all the chirility involved in the molecule and to define their absolute configurations.

Application on the other complexes

Once tuned the method, we prepared and resolved other couple of diastereomers. The complexes were fully characterized by NMR and analysed by VCD spectrometry. We have before pointed out that for clarity it was necessary simplify the stereochemistry definition, more in detail it could be useful recall the nomenclature issue in the stereochemistry defi-

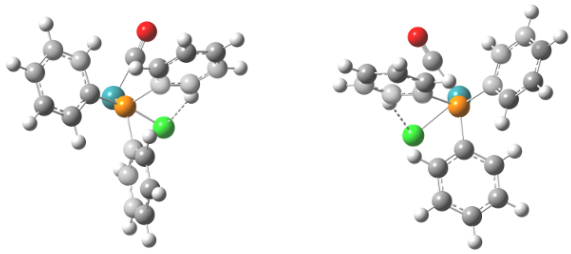

(a) $(S)_{Ru}$RuCl **(b)** $(R)_{Ru}$RuCl

Figure 2.13: Representation of the two induced helix chirality at the PPh_3 ligands. The H-bond between one proton of the PPh_3 and the halogen is also represented.

nition: if we consider the RuCl complex: η^5-((1*R*2*S*,5*R*)-menthyl)-C_5H_4 > Cl > P(C_6H_5)$_3$ > CO; since bromide and iodide exceed the CP substituent weight (60 amu), the substitution of the chlorine atom with heavier halogen caused an inversion of the absolute configuration even though the spatial arrangement of the substituents does not change. The same happen in the cation complexes $RuBF_4$, where acetonitrile has lower priority of the phosphine but higher than CO.

In order to prevail the spatial arrangement on the priority order, we decided to use, in addition to the correct nomenclature, two stereo-chemical descriptor $\bar{R}$ and $\bar{S}$ in which the priority sequence is always η^5-((1*R*2*S*,5*R*)-menthyl)-C_5H_4 > X > P(C_6H_5)$_3$ > CO where X is an halogen or the acetonitrile. Moreover it should be pointed out that all X ligands are double π donor.

As for RuCl, all the complexes presented a specific pattern of signal in the NMR spectra and allow to apply the same procedure described above to determine the structure in solution of the complexes; all presented the same conformation with the phosphine far apart of the menthyl moiety, exception made for the the two complex bearing the neomenthyl substituent on the CP ring, where the two groups are closer in conformity with the reported crystallographic structure [91].

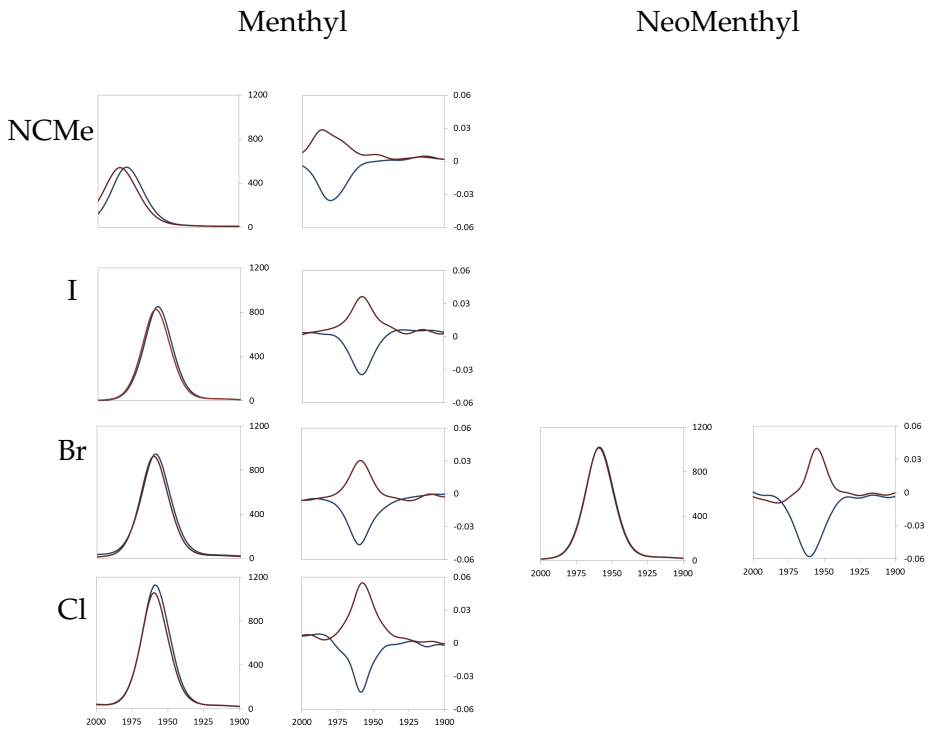

Figure 2.14: Experimental VCD spectra between 2000 and 1900 cm^{-1} of all the synthesised complexes; on the left spectra of the complexes bearing menthyl substituent on CP ring, while on the left neo-menthyl. (x axis: cm^{-1}; y axis: in IR spectra ε, in VCD spectra $\Delta\varepsilon$)

In figure 2.14 are showed the experimental spectra and in table 2.3 are reported the values of the spectroscopic parameters. The accordance between the metal spatial arrangement (chirality) and the sign of the VCD band is complete, to a $\bar{R}$ spatial arrangement coincide a negative dichroism sign, whereas a positive sign is related to a $\bar{S}$ configuration. Thus the carbon monoxide vibrational chromophore in a Ru(II)-heteroleptic carbonyl complex proved to be very sensitive to the chirality of the metal

Table 2.3: Experimental value of wavenumber frequency (ν), difference in molar absorptivity (circular dichroism) $\Delta\varepsilon$, molar absorptivity ε and dissymmetry factor (g=$\Delta\varepsilon/\varepsilon$)

		ν	$\Delta\varepsilon$	ε	g
RuCl	$\bar{R}$	1957	-0.0435	1113	-3.91E-05
	$\bar{S}$	1957	0.0547	1020	5.36E-05
RuBr	$\bar{R}$	1959	-0.0464	931	-4.98E-05
	$\bar{S}$	1957	0.0295	882	3.34E-05
RuI	$\bar{R}$	1957	-0.0343	849	-4.04E-05
	$\bar{S}$	1957	0.0363	808	4.49E-05
$RuBF_4$	$\bar{R}$	1981	-0.0353	544	-6.49E-05
	$\bar{S}$	1984	0.0283	542	5.22E-05
NMnRuBr[a]	$\bar{R}$	1959	-0.0577	966	-5.97E-05
	$\bar{S}$	1955	0.0397	966	4.11E-05

ν cm^{-1}, ε and $\Delta\varepsilon$ $M{\cdot}cm^{-1}$, [a] NMnRuBr = [(NMnCp)Ru(CO)(PPh_3)Br]

centre.

As expected, the cationic complexes present the carbonyl band shifted to higher frequencies than the other neutral complexes; it is well known that this is due to a reduced backdonation of the metal d-orbital. Excluded that, the frequencies of the bands does not seem sensitive to the nature of the halogen. Indeed the variations could be lower than the chosen resolution that was set at 8 cm^{-1}8. However an interest trend is showed in the intensity of the carbonylic band: the intensity decreases in going from neutral to cationic complexes, in the halogen series the intensity decreases down along the period. This can be easily seen in the experimental values of ε where: RuCl $>$ RuBr $>$ RuI $>$ $RuBF_4$, same trend is obtained in DFT calculations where a diminution of the dipole strength (D) is observed in the series. (table 2.7). Dipole strenght and rotational strenght can be related to molar absorptivity and difference in

Table 2.4: DFT calculation

		ν	D	R	g	ξ
RuCl	$\bar{R}$	1986.6	1089.1	-121.7	-4.47E-05	166.0
	$\bar{S}$	1997.4	1134.3	103.0	3.63E-05	76.8
RuBr	$\bar{R}$	1986.7	1074.8	-144.0	-5.36E-05	169.4
	$\bar{S}$	1997.7	1052.0	82.9	3.15E-05	73.9
RuI	$\bar{R}$	1986.9	1044.8	-137.5	-5.26E-05	131.8
	$\bar{S}$	1996.7	1028.0	72.9	2.84E-05	74.7
$RuBF_4$	$\bar{R}$	2024.7	900.4	-166.4	-7.39E-05	131.9

μ 10^{-40} esu·cm^2, m 10^{-44} esu·cm^2, ξ deg

molar absorptivity via:

$$\varepsilon = \frac{8\pi^3 N_A}{3 \cdot 2.302hc} \nu_i D(\nu) \tag{2.4}$$

$$\Delta\varepsilon = \frac{32\pi^3 N_A}{3 \cdot 2.303hc} \nu_i R(\nu) \tag{2.5}$$

Since XRD structures are similar, the DFT calculation of the complexes were performed starting from the conformers defined for RuCl complexes, and then checked by NMR analysis, as for the RuCl complexes. They are completely consistent with the experimental data.

So far we have used the DFT predicted VCD and IR spectra to assist and confirm the experimental data, therefore the definition of the reliability of the calculated VCD band is a crucial issue. The problem has been already evidenced and some authors have introduced the useful concept of robust normal mode [107]. They ranked the normal modes by the angle that stands between the electric and the magnetic dipole moment (ξ) which dot product determined the rotational strength of the mode. However due to the origin dependence of the imaginary magnetic dipole moment also the parameter ξ is dependent to the Cartesian system adopted during

the calculation. It was thus proposed the use of the dissymmetry factor as a criterion [108]. g(ν) has the undeniable vantage to evaluate either the calculated spectra either the experimental ones and allows a quick comparison between the two spectra.

$$g(\nu) = \frac{\Delta A}{A} = \frac{\Delta \varepsilon}{\varepsilon} = \frac{4R}{D} \tag{2.6}$$

Experimentally transition with $|g(\nu)| < 10^{-5}$ can not be routinely measured and considered reliable because of noise and because of the presence of possible artefacts, moreover in this situation the experimental condition has an high impact. For these reason a band can be defined as robust if $|g(\nu)|$ is higher than 10^{-5}. Concerning the calculated VCD it was proposed to use as threshold the value of $4 \cdot 10^{-5}$ for $|g(\nu)|$. Normal modes with lower values would not be reliable enough to be compared with the experiment [109]. However they also stated taht:'To provide some flexibility for individual situations, the limiting value of g(ν) can be set as a user defined parameter', leaving some degree of freedom.

Recently others authors [110] demonstrated on mathematical ground the relation between robustness angle and dissimmetry factor. They pointed out that every modes have a robust points where $\vec{\mu_{01}}$ and Im($\vec{m_{10}}$) are either symmetric or antisymmetric, increasing the distance from that cartesian coordinates origin cause a variation of the angle drawing the cups form reported [109]. They thus proposed the parameters κ

$$\kappa = \frac{4\pi\nu}{|g|} \tag{2.7}$$

that is the tangent of the cups at the robust point and describes the rapidity of which the robust angle change in the neighbourhood of the robust point. Therefore large g-value or small κ described the stability of the angle.

Keeping in mind these consideration, all the experimental value for the carbonylic band can be defined as reliable being over the threshold value. Concerning the DFT data a difference can be observed in the diastereomeric couple, if all the predicted VCD band of the $\bar{R}$ configuration can be considered unequivocally robust, the calculated band of the $\bar{S}$ configuration are borderline. However the g(ν) value are in good agreement with the experimental one and the sing are exactly predicted, thus we can considerer reliable the data and use it for further considerations, in any case consideration on the magnetic dipole moment should be taken carefully.

In order to better understand the phenomena related with the vibrational optical activity we must look at the theoretical background of VCD: the IR and VCD intensity of a vibrational transition could be defined as:

$$D = |\vec{\mu}_{01}|^2 \tag{2.8}$$

$$R = Im(\vec{\mu}_{01}) \cdot (\vec{m}_{10}) \tag{2.9}$$

where $\vec{\mu}_{01}$ and $\vec{m}_{10}$ represent the total electric and magnetic dipole transition moments respectively; they could be further decomposed in their atomic contributions (for simplicity only the electric component will be expressed):

$$\vec{\mu}_{01} = \sum_{N}^{\lambda=1} \vec{\mu}_{01}^{\lambda} \tag{2.10}$$

$\vec{\mu}_{01}^{\lambda}$ is the contribution of the atom λ to the dipole that, in turn, could be divided in nuclear and electronic contribution

$$\vec{\mu}_{01}^{\lambda} = \vec{\mu}_{01}^{\lambda nu} + \vec{\mu}_{01}^{\lambda el} \tag{2.11}$$

It should be pointed out that the nuclear component is defined by the motion of the atoms while the electronic component relapses on the electrons dragged by the nuclei, therefore they have opposite sign due the opposite charge.

Following the Stephens equation for VCD [111] the transition electric dipole moment of the i mode μ^i can be expressed as the derivatives of the

ground state dipole moments μ^G with respect of the normal coordinates Q_i as:

$$\mu_{01}^{i} = \left(\frac{\partial \mu^G}{\partial Q_i}\right)_o \left(\frac{\hbar}{4\pi\nu_i}\right)^{1/2} \tag{2.12}$$

and referred to Cartesian coordinates via

$$X_{\lambda\alpha} = \sum_i S_{\lambda\alpha,i} Q_i \tag{2.13}$$

so that (2.20) becomes

$$\mu_{01}^{i} = \left(\frac{\hbar}{4\pi\nu_i}\right)^{1/2} \sum_i S_{\lambda\alpha,i} P_{\alpha\beta}^{\lambda} \tag{2.14}$$

where

$$P_{\alpha\beta}^{\lambda} = \left(\frac{\partial(\mu^G)_\lambda}{\partial X_{\lambda\alpha}}\right)_o \tag{2.15}$$

$$P_{\alpha\beta}^{\lambda} = E_{\alpha\beta}^{\lambda} + N_{\alpha\beta}^{\lambda} \tag{2.16}$$

where $E_{\alpha\beta}^{\lambda}$ and $N_{\alpha\beta}^{\lambda}$ are respectively the electronic and nuclear component.

$\mathrm{P}_{\alpha\beta}^{\lambda}$ is a second-rank molecular tensor termed as atomic polar tensor (APT), that can be separated in the electronic and nuclear parts, in which the nuclear part affected only the in-diagonal elements being $N_{\alpha\beta}^{\lambda} = Z_\lambda e \delta_{\alpha\beta}$. The magnetic dipole moment can be as well expressed in term of molecular tensor, namely atomic axial tensor (AAT) for which treatise we refer to the literature [46].

$$m_{01}^{i} = \left(4\pi\hbar^3\nu_i\right)^{1/2} \sum_i S_{\lambda\alpha,i} M_{\alpha\beta}^{\lambda} \tag{2.17}$$

$$M_{\alpha\beta}^{\lambda} = I_{\alpha\beta}^{\lambda} + J_{\alpha\beta}^{\lambda} \tag{2.18}$$

In the rationalization of the results (the observed trend in ε and the orign of the VCD sign) we started assuming that carbon monoxide stretching is mainly located on itself and that the dipole moment of the transition are oriented along the CO major axis. The location of the mode was easily confirmed observing the displacing vector that are non zero almost only for the carbonyl ligand, while for the direction of the dipole moment and the role played by the single atom we looked into the APT and AAT. These data are produced by gaussian in the full DFT calculation of the VCD spectra and can be obtained in the formatted checkpoint file or running a calculation after VCD calculation with the following input line

```
# geom=allcheck freq=(readfc) iop(7/33=1)
```

The data are presented in in the following format

$$APT = \begin{matrix} \frac{\partial \mu_x}{\partial x} & \frac{\partial \mu_y}{\partial x} & \frac{\partial \mu_z}{\partial x} \\ \frac{\partial \mu_x}{\partial y} & \frac{\partial \mu_y}{\partial y} & \frac{\partial \mu_z}{\partial y} \\ \frac{\partial \mu_x}{\partial z} & \frac{\partial \mu_y}{\partial z} & \frac{\partial \mu_z}{\partial z} \end{matrix}$$

The system was reoriented so that the x axis coincided with the CO major axis and than translated to the carbonyl carbon in a new right handed Cartesian coordinate systems. As remembered before, $\vec{m}$ is origin dependent, if the origin is translated ($\vec{T}$) then $\vec{m}$ vary proportionally to $\vec{T} \times \vec{\mu}$, consequently AAT are also origin dependent. However we assumed that the gaussian standard orientation origin was close enough to the x axes (being near to the ruthenium atom that now lies close to it), which may be sufficient to allow some consideration in our systems. In table 2.5 are reported the APT and AAT of carbon and oxygen atoms for the $\bar{R}$ configured complexes.

As expected, the displacements revealed that the vibration takes place almost exclusively on the x axes, this allow us to reduced our analysis to the $\partial \mu_x$ column of the tensor APT_x and AAT_x. Thus the electric and the magnetic dipole moment can be estimated by the dot product with the

Table 2.5: APT and AAT in *a.u.* for the $\bar{R}$ configured complex.

	APT											
	$\bar{R}$-RuCl			$\bar{R}$-RuBr			$\bar{R}$-RuI			$\bar{R}$-RuBF$_4$		
	2.1132	0.0744	-0.3747	2.1012	0.0020	-0.4000	2.0741	-0.1033	-0.3778	1.9624	-0.1086	-0.4371
C	-0.0189	0.3744	-0.0626	-0.0265	0.4099	-0.0594	-0.0369	0.4570	-0.0506	-0.0350	0.3582	-0.0587
	0.0148	0.0102	0.6519	0.0126	0.0087	0.6670	0.0152	0.0083	0.6596	-0.0124	0.0459	0.7289
	-1.6833	-0.1612	-0.0039	-1.6679	-0.1140	0.0180	-1.6444	-0.0454	0.0117	-1.4952	-0.0916	0.0610
O	0.0411	-0.1907	0.0219	0.0358	-0.1970	0.0227	0.0356	-0.2057	0.0171	0.0433	-0.1638	0.0260
	0.0276	0.0003	-0.3096	0.0274	0.0014	-0.3202	0.0213	-0.0003	-0.3204	0.0278	-0.0199	-0.3075
	AAT											
	$\bar{R}$-RuCl			$\bar{R}$-RuBr			$\bar{R}$-RuI			$\bar{R}$-RuBF$_4$		
	-0.2190	-0.0072	-0.0587	-0.2287	-0.0017	0.0431	-0.1789	-0.1019	0.2239	-0.3497	-0.2604	-0.1558
C	0.0049	-0.2280	-0.2950	0.0130	-0.1724	-0.1696	0.0533	-0.1477	0.0761	-0.0414	-0.2230	0.0225
	0.1810	-0.4384	0.2257	0.1575	-0.4673	0.1921	0.0630	-0.4802	0.17271788	0.1711	-0.4524	0.2638
	0.0821	-0.0039	-0.0126	0.1134	-0.0080	-0.0662	0.1244	0.0757	-0.1768	0.1553	0.1564	0.0827
O	-0.0117	0.1369	-0.7544	-0.0111	0.1164	-0.7912	-0.0196	0.1116	-0.8620	0.0097	0.1153	-0.7939
	-0.0788	1.0880	-0.1295	-0.0743	1.1112	-0.1164	-0.0372	1.1348	-0.1103	-0.0715	0.9901	-0.1503

Table 2.6: Atomic displacements and dot products of APT and AAT with it.

	$\bar{R}$-RuCl		$\bar{R}$-RuBr		$\bar{R}$-RuI		$\bar{R}$-RuBF$_4$	
	C	O	C	O	C	O	C	O
				Displacements ($\vec{R}$)				
x	-0.8159	0.5674	-0.8194	0.5738	-0.8162	0.5679	-0.8160	0.5731
y	-0.0011	-0.0034	-0.0025	0.0006	-0.0005	-0.0041	-0.0036	0.0050
z	-0.0003	0.0016	-0.0043	0.0051	-0.0055	0.0013	0.0008	-0.0016
				APT$_x \cdot \vec{R}$				
x	-1.7241	-0.9545	-1.7200	-0.9570	-1.6907	-0.9336	-1.6013	-0.8575
y	0.0150	0.0240	0.0209	0.0206	0.0302	0.0211	0.0272	0.0240
z	-0.0123	0.0152	-0.0132	0.0141	-0.0160	0.0117	0.0105	0.0163
				AAT$_x \cdot \vec{R}$				
x	0.1787	0.0466	0.1872	0.0647	0.1449	0.0701	0.2862	0.0896
y	-0.0037	-0.0083	-0.0095	-0.0104	-0.0438	-0.0128	0.0346	0.0074
z	-0.1472	-0.0486	-0.1288	-0.0426	-0.0521	-0.0259	-0.1378	-0.0358

in *a.u.*

displacing vector (μ_{apx} and m$_{apx}$), so taking into account equation (2.14) and (2.17), in order to evaluate the trend D$_{apx}$ and R$_{apx}$ can be calculated as

$$\begin{aligned} D_{apx} &= \mu_{apx}^2 \\ R_{apx} &= \mu_{apx} \cdot m_{apx} \end{aligned} \tag{2.19}$$

Moreover in the approximated calculation of D$_{apx}$ and R$_{apx}$ resulted that, if included, the y and z components weight for less than 0.6% of the value (table 2.6), so in our evaluation we further simplify to only $\partial\mu_x/\partial x$ (APT$_x$) and $\partial\mu_x/\partial x$ (AAT$_x$) components.

In figure 2.15 are plotted the approximated value of R and D together with the full DFT results; the two series shows the same trend, therefore we can make the following observation:

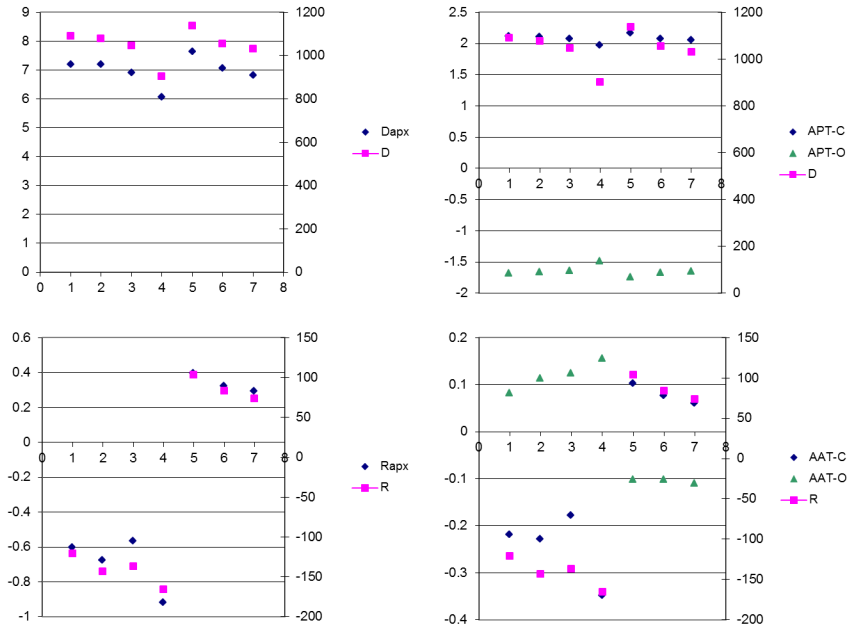

Figure 2.15: Plot of: approximated value of D_{apx} (top-left) and the approximated valued of R_{apx} (down-left) referred to the full DFT value; value of APT_{xx} and AAT_{xx} related to the D and R. (1:$\bar{R}$-RuCl, 2:$\bar{R}$-RuCl, 3:$\bar{R}$-RuCl, 4:$\bar{R}$-RuCl, 5:$\bar{R}$-RuCl, 6:$\bar{R}$-RuCl, 7:$\bar{R}$-RuCl)

- APT_{xx} can be used as indication of D, whereas (AAT_x) define the sign of R;
- the carbon atom has greater impact on the dipole than the oxygen;
- carbon and oxygen (APT_{xx}) and (APT_{xx}) have opposite sign, therefore, once multiply for the displacement, their components to the dipole moments have same directions;
- the nuclear contribution to (APT_{xx}) have almost the same value for all the complexes, since it is constant, the difference in the complexes can be ascribed to the electronic contribution.

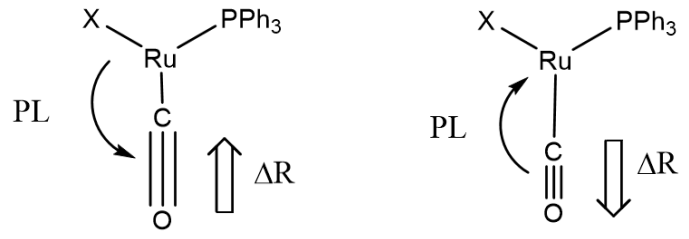

(a) **(b)**

Figure 2.16: Schematic representation of the complex, view from Cp substituent; Double arrow drawn the displacement while signe arrow the charge transfer.

Since in C atom (APT_{xx}) is positive we can argue that the nuclear component prevails, on the contrary the electronic term in higher on the O atom.

We are studying organometallic compounds where the electronic delocalization between the metal centre and the ligands is a crucial factor. In mononuclear complexes the CO strongly binds the transition metal via a σ bond matched with a synergic π bond formed by the overlap of the π^* of CO and the occupied d orbitals of the metal. Thus the π back-bond increased the electron density in the antibondig CO π^* orbital, whereas the σ bond decreased the electron density on C [112, 113].

To better understand the dynamic process the electronic contribution can be decomposed in a dragged $\vec{\mu}^{\lambda el}_{01,DG}$ term and in a polarization $\vec{\mu}^{\lambda el}_{01,PL}$ one, that takes in account the dynamic change during polarization

$$\vec{\mu}^{\lambda el}_{01} = \vec{\mu}^{\lambda el}_{01,DG} + \vec{\mu}^{\lambda el}_{01,PL} \tag{2.20}$$

We are aware that the following statement can be considered rather rough but a simple estimation of the change in electron density that takes place during the bond stretching can be obtained evaluating the Mulliken

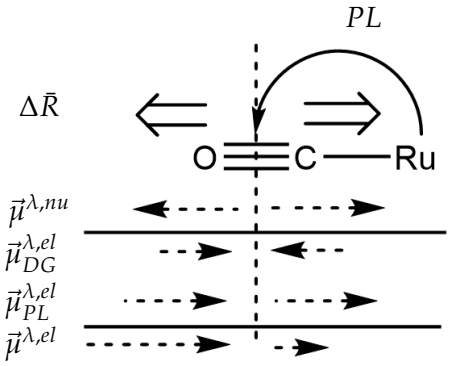

Figure 2.17: Schematic representation of the relative orientation of the atomic μ of C and O atoms.

charges at the equilibrium and at two displaced geometries $\pm$ 0.2 Å from the equilibrium geometries, in order to simulate the CO stretching motion. When the carbon gets closed to the metal (elongated position, figure 2.16a), a meaningful increase of the negative charge is observed on the oxygen atom while on the carbon and on the metal a decrease of the electron density is observed. On the contrary opposite trend takes place when the C moves apart from the metal (compressed position, figure 2.16b).

In figure 2.17, we reported a schematic representation of the relative orientation of the electronic dipole moment for atoms C and O in the carbonyl ligands in elongation. For our porpoise the displacement vector and the nuclear contribution along the CO axes were fixed with the same direction. Considering the oxygen atom the PL has the same direction of $\Delta\vec{R}$, this means that $\vec{\mu}^{\lambda el}_{01,DG}$ and $\vec{\mu}^{\lambda el}_{01,PL}$ have the same direction too; on the contrary carbon $\Delta\vec{R}$ and PL have opposite direction and so have $\vec{\mu}^{\lambda el}_{01,DG}$ and $\vec{\mu}^{\lambda el}_{01,PL}$. We can conclude that the amount of the polarization increased $\vec{\mu}^{\lambda,el}_{01}$ on oxygen atom whereas in carbon atom is reinforce $\vec{\mu}^{\lambda,nu}_{01}$, indeed $\vec{\mu}^{,el}_{01}$ and $\vec{\mu}^{C,nu}_{01}$ have the same direction such as the effect on the $\vec{\mu}_{01}$.

This model is consistent with the (APT_x) and the experimental trend: an increased electron density at the metal (see the neutral versus the cationic complexes) allows bigger π-backbondig, whereas a more electron negative halogen, bonded to the metal stronger, increases the inductive effect towards the σ-bond.

Table 2.7: ^{13}C-NMR chemical shifts (δ) in ppm of the carbonyl carbon atom (CO)

RuCl		RuBr		RuI		$RuBF_4$	
$\bar{S}$	$\bar{R}$	$\bar{S}$	$\bar{R}$	$\bar{S}$	$\bar{R}$	$\bar{S}$	$\bar{R}$
204.8	204.8	204.5	204.3	204.1	203.8	201.7	201.9

A possible experimental evidence of difference of the inductive effect in the complexes might be the ^{13}C-NMR chemical shift of the carbonyl carbon; in table 2.7 are reported the δ values, in order to be significant, this results must be confirmed by a careful determination of the chemical shifts. Experiments are not available yet due to the problems related to the instrument wall-time.

Nevertheless, the δ values decreases in going from the chloride to iodide and it has more lower value in the cationic species. Therefore, we can speculate that the chloride complex is the less shielded, whereas in $RuBF_4$ complexes it is the more electron rich, consistently with the results of ATPs [114]. Indeed the correlation between ε and δ seems to corroborate the results of a prevalence of the carbon atoms on the intensity origins, or at least of the mechanism that causes the electrodepletion on the carbon atoms.

The net result is an electric dipole moment parallel with the magnetic dipole moment in case of $\bar{S}$ configuration, it means a clockwise charge circulation, whereas an anti-parallel orientation with the $\bar{R}$ configuration means an anticlockwise charge circulation around the x axis.

Although a definitive theoretical interpretation lacks on the direction

of the charge circulation, the experimental values reveal a certain relationship between the stereochemistry of these compounds and the carbonyl VCD sign. If we observed figure 2.16 an $\bar{R}$ configuration is represented; the disposition of the partial charge on the substitution will be reverted in a $\bar{S}$ and with it the flow of the charge.

Nevertheless, an attempt to explain the origin of VCD sign can be done observing the molecular structures of the complex: both the structures present a weak interaction between the halogen and one proton on the PPh_3 phenyl ring, namely an hydrogen bond (HB) (figure 2.13). Halogens bonded to transition metals are known to be good HB acceptors. This property is based on the strongly polarised character of the MX bond resulting generally in an enhanced partial negative charge of the halogen. The phenomenon is known as metal-assisted HB [115]. In the examined structure the interatomic distances and angles are compatible with the presence of an hydrogen bond, moreover the existence of HB is confirmed by the topological analysis of electron density (AIM analysis) [116] performed on the DFT wavefunction, where a stable bond critical point (3,-1) and a bond bath are present. This HB closes a ring, it was confirmed by the presence of a ring critical point (3,+1), among metal, halogen and phosphine. Interestingly, even in the case of $RuBF_4$ complexes a CH/π hydrogen bond [117, 118] was highlighted between the methyl of the acetonitrile and one phenyl of the phosphine and, even in this case, the AIM analysis found a bond path between the methyl groups and the Csp^2 carbon in *para* position of phenyl with a stable bond critical point.

On pioneering work a ring current was proposed as major source of VCD intensity [119], it was then used to qualify the VCD sign in metal complexes [120, 121] and it was recently reproposed in coordination compounds [122]. The vibrational motion induces a current along an intramolecular loops and in particular when electrons are inserted into the ring a positive current flows preferentially toward the inducing oscillator along the bonded region with electron depletion. As current, it origins a magnetic dipole transition moment ($\vec{m}$), that could be qualitatively es-

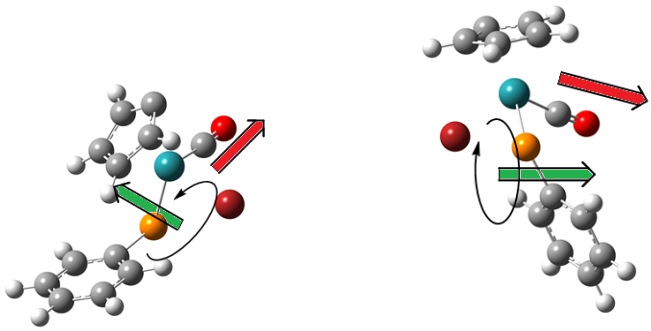

(a) $\bar{R}$-configuration **(b)** $\bar{S}$-configuration

Figure 2.18: Schematic representation of a generic [Ru(η^5 – C_5H_4R)(CO)(PPh_3)X] complex in the two configuration; $\vec{\mu}$, the positive charge flow and $\vec{m}$ of the compressed CO position are drawed (some atoms are omitted for clarity).

timated by the right hand rule. Thus, in system where $\vec{\mu}$ can be easily established, the ring current can be used to determine the sign of the VCD [122].

In the present systems we demonstrated that the carbonyl normal modes is almost localised on the carbonyl itself and according to the preview analysis the direction of $\vec{\mu}$ can be safely established. As depicted in figure 2.16b and considering the APT results, when the metal carbon bond is elongated electron density are partially left on the metal and $\vec{\mu}$ can be defined toward the oxygen. A positive current flow can be imagined going from phosphorus atom to the halogen crossing the hydrogen bond and back to the metal.

In figure 2.18 are illustrated the two configuration of a generic [Ru(η^5-C_5H_4R)(CO)(PPh_3)X] complexes: the inversion of the metal centre configuration causes the inversion of the ring current direction too. In a contracted geometries a $\bar{R}$-configuration is than associated with a anti-

clockwise rotation of the positive current that, according with right hand rule, generates a $\vec{m}$ pointing in the opposite direction of $\vec{\mu}$; as a consequence, in a $\bar{R}$-configuration the cosine between the two dipole is less than zero, therefore the VCD sign of normal mode associated with this transition will be negative.

The prediction on the VCD sign of the carbonylic band is in perfect agreement with the experimental data for all the complexes, confirming, at least for the examined geometries, the validity of the model.

2.2.2 Metal-Hydride Bond

The M-H bond plays a paramount role in the chemistry of the transition metal complexes. In fact the most part of the multi-step catalytic reactions involve the presence of a more or less stable and transient metal hydride. The importance in asymmetric catalysis was definitively established with the development of stereselective reduction of double bonds with Rh(I) phosphine complexes. For example in reduction of prochiral dehydroaminoacids by rhodium phosphine complexes, the origin of stereodifferentiation was dictated by the regiochemistry of insertion of a double bond into Rh-H bond [6, 7, 123, 124, 125]. The asymmetric transfer hydrogenation of the polar double bonds by a Ru-H diamine complex [52, 53, 54, 55] offers another evidence of the M-H bond pivotal role.

Metal hydrides are generally very reactive species, often characterized by pronounced kinetic and thermodynamic instabilities that make them difficult to handle and almost impossible to isolate and purify with standard procedures. Generally the hydrogen occupies one coordination site acting as a linearly coordinated ligand. The ν-M-H stretching vibration usually lies in the range 2200-1700 cm^{-1} with the corresponding absorption bands medium to weak in intensity, so in VCD spectroscopy it could be revealed as valuable probe as well as the carbonyl.

VCD was never used to investigate the linear coordinated hydride as a probe of chirality at the metal center and for these reasons VCD may sup-

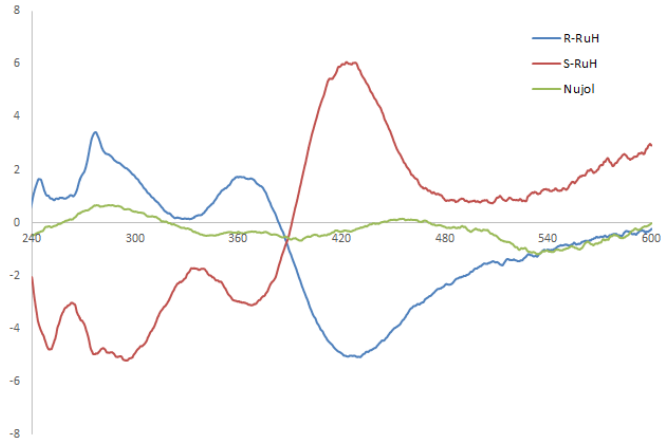

Figure 2.19: ECD spectra of ***S*-RuH** (red) and (***R*-RuH** (blue) recorded in nujol. The nujol is not subtracted but displayed apart. (x axis: cm^{-1}; y axis $\Delta\varepsilon$)

port the other techniques, essentially ^{1}H-NMR and neutron diffraction, to assign the configuration of chiral transition metals.

In section 2.1.1 we reported the synthesis of enantiomeric pure ATH precatalyst of general formula [Ru(NN)(PP)Cl_2] that are presumed to be the precursor the catalytic active hydride complexes. Unfortunately the hydride was not isolated and characterized; any attempt resulted in decomposition. However we synthesised the related mono-hydride complexes in optically pure form; this offered us the unusual opportunity to investigate the metal hydride chromophore by VCD spectroscopy.

Particularly attention should be taken in the sample preparation due to the high reactivity of the complexes; in particular these compounds proved to be stable for at least several weeks only in solid state under inert atmosphere, whereas decomposed in hours in solution under N_2. It should be considered that VCD spectra usually have intensity one thousand times lower than the related ECD spectra, thus to preserve the sample from decomposition is a priority.

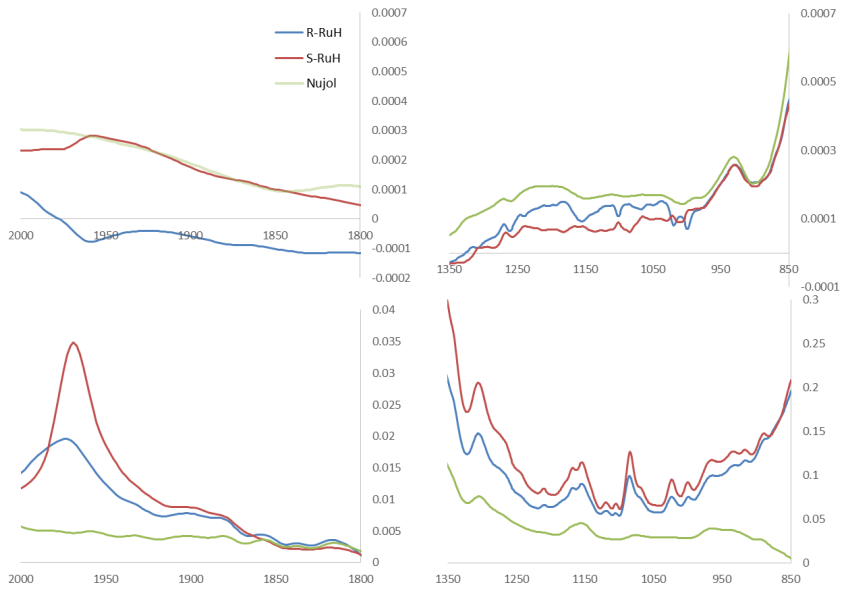

Figure 2.20: VCD and IR spectra of ***S*-RuH** (red) and (***R*-RuH** (blue) recorded in nujol. Hydride region and mid-infrared region. Considered the nature of nujol mulls, the nujol is not subtracted but displayed as well. (x axis: cm^{-1}; y axis: in IR spectra ε, in VCD spectra $\Delta\varepsilon$)

In order to avoid any possible decomposition in solution we "rediscovered" the nujol mulls technique.[126, 127, 128] The main drawbacks nujul measurements are reported to be the scattering and the absorption flattening due to the inhomogeneous particle distribution, however in the IR region the scattering is manifested less than in the UV [129].

We developed a protocol that allowed the preparation of the sample limiting the complex decomposition: in order to obtain sample as homogeneous as possible, the complexes were precipitated as fine powder by pentane addition to the toluene solution of the complexes. After that the powder was dispersed in nujol drops in order to avoid the presence of moisture and air and then gently mixed. The nujol mixture was placed

between two windows of CaF_2 with a 50 μm spacer. In these conditions the sample proved to be stable for at least a couple of day, the spectra recorded after 24 hours showed almost the same profile.

In order to restrict scattering and absorption flattening effect on the spectra, four spectra were recorded in different orientation (0°, 90°, 180°, 270°) of the cells. Moreover to be sure that the signals observed were related to the presence of chiral complexes, the VCD and the ECD spectra were subsequently recorded with the same samples.

The results are showed in figures 2.20 and 2.19. As can be seen, the ECD spectra are of good quality and the two eantiomers present specular spectra. In respect to the spectrum obtained in solution the band at lower energy has the same sign as well as the transition around 350 nm, although the relative intesity is inverted. It is interest to notice that below 350 nm the sign of the spectra in solution and in solid is reverted (see figure 4.1).

In any case this confirmed the goodness of the sample and it allowed us to consider the bands in the VCD spectra as actual. The region around 1900 cm^{-1} and the mid region are shown in figure 2.20; although the spectra presented signals with high noise, the spectra were one the mirror image of the other confirming the enantiomeric relation between the M-H stretching of the complexes.

Meaningful it is the g value of the M-H stretching band that could be estimated in 10^{-3}, a rather high value.

Preliminary DFT calculation were also done: the structure were build starting from the X-ray structure of the related complex $[RuClH(PPh_3)_2$ (tmen)] [4][130] and than optimized at B3LYP/6-31+g(d,p) level of theory with pseudopotential on the ruthenium atom in gas-phase.

Although the sign of the M-H band is coherent, a deeper conformational research must be done that taking in account the helical shape of

[4]tmen = 2,3-dimethylbutane-2,3-diamine

the phosphine and best fitting functional must be tried in order to better elucidate the origin of the bands.

However the M-H stretching band proved to be sensitive to the chirality at the metal centre and then to be used as probe in VCD spectroscopy.

It is worth notice that this is the first case reported in literature of VCD spectra of a chiral metal-hydride complex.

2.2.3 Iridium VCD

The third class of compounds that we investigated was that of the cyclometallated iridium(III) complexes. Due to their photophysical properties this complexes have been extensively studied in the last years, founding application in several fields [131, 132, 133]. The Ir(III) complexes studied here are characterized by an inert inner coordination sphere with a stereogenic metal centre that can be resolved in single enantiomers; by co-crystallization with a chiral counter anion [134], by HPLC with a chiral ligand [23, 135] or chiral stationary phase [136].

The applications of the enantiopure form of this family of compounds include several fields, such as asymmetric catalysts for enantioselective organic synthesis as well as in the biomacromolecules selective recognition [137, 138, 27, 139, 140, 141, 142, 140, 143]. Structurally sophisticated Ru(II) or Ir(III) compounds as selective inhibitors of protein kinases have been reported [29] and even a current study concerning enantiomers of octahedral Ir(III) complexes highlighted their chiral discrimination of enzyme active sites [144]. Furthermore, great efforts have been directed towards the exploration of other organometallic architectures, with a dual chiral information, at-ligand and at-metal center, expanding the stereochemical complexity, in order to obtain highly performing selective chiral chemical probes [31]. It is worthy to highlight that the presence in the same structure of two or more stereogenic centers combined with an efficient separation method, which affording to enantiomerically and diasteromerically pure species, provides the advantage of obtaining many isomers of one molecule possibly featuring different properties.

Our investigation started with the aim to verify if two diastereomers, in enantiomeric relation at the metal centre, could emit differently in an achiral or chiral environments and thus if they can be to be used as potential bio-markers.

Synthesis and Resolution

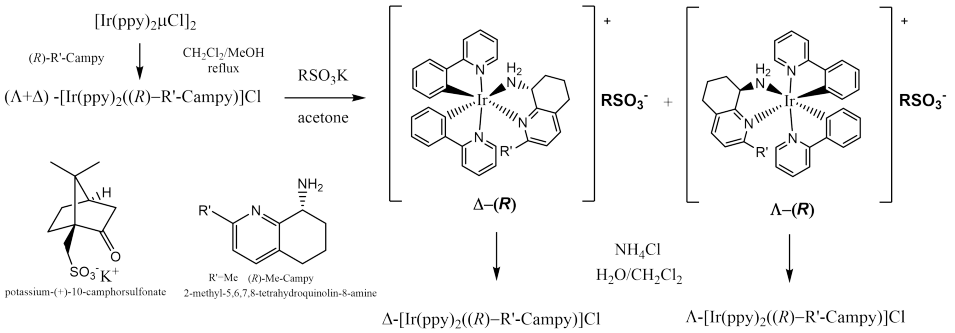

Scheme 2.8: Chose synthetic strategy to enantiopure Ir(III)complexes.

Our approach to achieve chiral Ir(III) complexes, enantiopure at the metal, was the introduction of a chiral diamine as ligand followed by co-crystallization with a common chiral counter anion. The complexes were synthesized starting from binuclear chloro-bridged Ir(III) complex $[Ir(ppy)_2(\mu-Cl)]_2$ [145]. The used chiral diamines were (*R*) or (*S*)-2-methyl-5,6,7,8-tetrahydroquinolin-8-amine (Me-campy) and (*R*) or H-Campy (figure 2.3b] [58]. The starting chloro-bridged dinuclear Ir(III) complex is a racemic $\Delta\Delta/\Lambda\Lambda$ mixture, thus the reaction with a stoichiometric amount of a chiral ligand give rise to a 50:50 diastereomeric mixture of complexes, as proven by the ^{1}H-NMR spectroscopy performed in deuterated $CDCl_3$. The ^{1}H-NMR spectra in $CDCl_3$ evidenced the different solubility of the diastereomeric couples, where an apparent percent diastereomeric excess (d.e.%) can be observed in saturated solution.

However this difference in solubility did not allow the complete sepa-

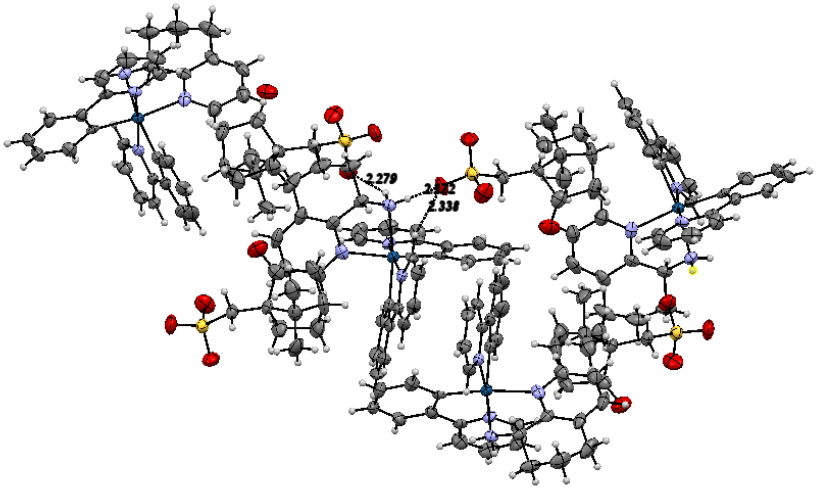

Figure 2.21: Packing structure of Λ-[Ir(ppy)$_2$((*S*)−H−Campy)]$^+$ camphorsulfonate$^-$, the interaction with two anion of the NH_2 groups is highlighted.

ration in diastereomers; it was achieved only after co-crystallization with a camphorsulfonate counter-anion in acetone after metathesis reaction (Figure 2.21). Finally the chloride complexes were restored with a large excess of ammonium chloride in water/CH_2Cl_2 biphasic medium. Ir(III) ortometallated complexes were found to be able of bimolecular recognition [31]; in these application the water solubility can be an important characteristic. We got this goal synthesizing the acetate derivatives of the complexes by metathetical reaction with silver acetate [146].

NMR characterization

The structure and the absolute configuration of the complexes were investigated and assigned by NMR spectroscopy and then confirmed by the x-ray structures. Due to the loss of symmetry, the spectra presented numerous peaks often superimposed, despite this we were able to assign all

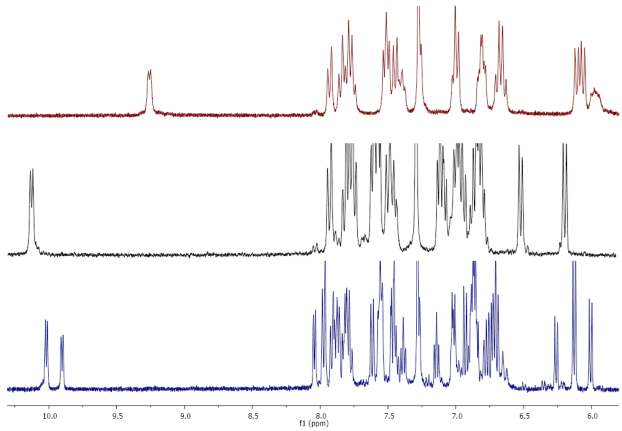

Figure 2.22: ^{1}H-NMR spectrum (300 MHz) from 5.8 to 10.5 ppm of: $\Delta,\Lambda S$-Ir-Me-Campy (blue, $CDCl_3$ bottom), ΔS-Ir-Me-Campy (black,$CDCl_3$ middle), ΛS-Ir-Me-Campy (red,CDCl3/CD3OD 3/1 top).

the signals by COSY, NOESY, HSQC, HMBC analysis. Compared to the starting binuclear complex, all compounds showed a considerable high frequencies chemical shift for the H^{a1} ($\approx$10 ppm) and for one H^{NH} proton (7 ppm) and the characteristic shielding of the proton next to the metal in the ortometallated phenyl-ring[147]. In the chloride diastereomers the chemical shifts are strongly affected by the polarity of the deuterated solvent. When CD_3OD was added to $CDCl_3$ (in the ratio 3:1 v/v) both protons H^{a1} and H^{NH} moved to lower frequencies of 0.97 and 1.08 ppm respectively, and the same behaviour was observed for all the remaining complexes (Figure 2.23). The switch to a more polar solvent increases the ion solvation, thus the high frequencies shift could be attributed to a strong interaction with the counter anion, which was confirmed by Density Functional Theory (DFT) calculation. All the diastereomeric structures were built on the base of the crystallographic structure of the related complex $[Ir(ppy)_2(pam)]Cl$ reported in [145] and optimized in presence and absence of the chloride counter anion in DFT calculation at B3LYP

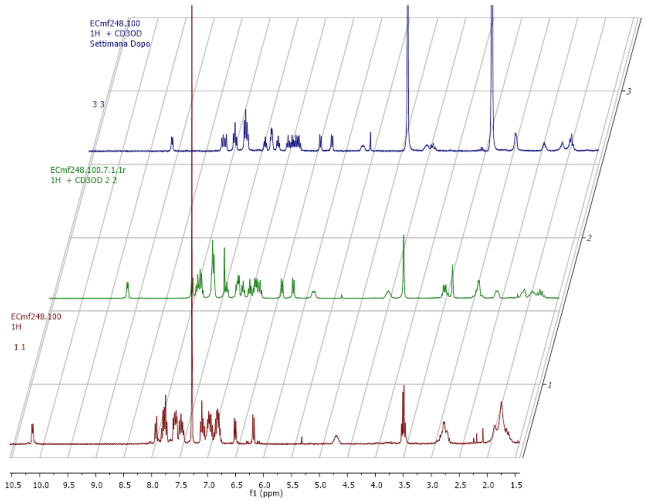

Figure 2.23: ^{1}H-NMR spectrum (300 MHz) of Δ*S*-Ir-H-Campy in different solvent : CD_3COD top; $CDCl_3/CD_3OD$ 3/1 in the middle; $CDCl_3$ bottom.

level with the implicit solvent model. The implicit model for the solvents was included because preliminary calculation indicated it as an appreciable improvement, whereas the B3LYP functional were choose because provided the best fitting results in ^{1}H-NMR prediction. Moreover the C6-ring of the tetrahydroquinoline moiety had an half-chair conformation on C(e7). Optimizations with different conformations for the tetrahydroquinoline ring suggest that boat or half-chair conformation on C(e6) structures exhibit negligible populations.

The reliability of the calculated structures and those obteined by NMR experiments were confirmed by the resolution of the structures of Δ*R*-Ir-Me-Campy and Λ*S*-Ir-H-Campy complexes. ^{1}H absolute shielding σ were computed and then converted in chemical shifts δ for better correlation with the experimental values. The result are reported in table 2.8, the values are in good agreement with the experimental ones. The impact of

the presence of the chloride counter-ion is evident, dramatic in the amine proton next to the chloride, confirming the hypothesis for the unusual chemical shifts and the great importance of the ion pair interaction.

Table 2.8: ^{1}H chemical shifts as obtained in NMR experiments and DFT calculation in presence and absence of the chloride counter anion.

	ΛS-Ir-H-Campy			ΔS-Ir-H-Campy		
	NMR	DFT Cl[a]	DFT[a]	NMR	DFT Cl	DFT
Ha6	10.13	10.19	8.51	10.20	10.35	8.54
NH	6.95	6.77	2.83	6.78	6.38	3.05
He8	4.65	4.59	4.74	3.92	4.17	4.19
	ΛS-Ir-Me-Campy			ΔS-Ir-Me-Campy		
	NMR	DFT Cl	DFT	NMR	DFT Cl	DFT
Ha6	9.77	9.83	8.25	9.91	9.93	8.31
NH	6.85	7.06	2.78	6.49	6.23	2.63
He8	4.75	4.41	4.57	3.77	3.91	3.84
CH3	1.87	1.93	2.15	1.71	1.83	1.94

[a] Counter anion Cl^- was taken in account, [b] Counter anion Cl^- was excluded

The signals of the asymmetric proton in the diamine ligand H^{e8} showed the greater differences in the NMR spectra of diastereomers, showing a chemical shift of ca. 0.9 ppm in Ir-Me-Campy and 0.7 ppm in the case of Ir-H-Campy complexes. The differences could be due to a greater influence exerted by the ring current of a neighbour pyridine ring on one of the diastereomers or to a different interaction with the chloride ion; however the small changes in the chemical shift in the (+)-10-camphorsulfonate or acetate complexes as well as the DFT results corroborate the first hypothesis. As confirmed by DFT calculation, the large difference between the two signal can not be attributed to the interaction with the counter-anion; indeed in table 2.8 is shown that the difference is retained with or without Cl^-. With an (*S*) amine configuration, an attribution to the $\Delta-$complex of

the low frequency shifted signal could be attributed observing the relative position of H^{e8} and pyridine ring in a molecular model. All complexes showed a specific pattern of NOE cross-peaks, in which the presence or the lack of cross-peak between H^{a1} and H^{e8} was particularly useful for an unambiguous identification.

The chiral ancillary ligand interacts in different ways with the chiral $[Ir(ppy)_2]^+$ moiety depending on its chirality; with (*S*) H-campy or (*S*) Me-campy a NOE between H^{a1} and H^{e8} can be observed only if the Ir(III) centre has Λ configuration; an opposite metal configuration would bear these two protons too far away from each other to give rise to a NOE effect. Thus if the diamine configuration is (*S*) the presence of cross-peak states the metal configuration as Λ, otherwise the configuration of the metal centre must be Δ. Furthermore, the H^{e8} chemical shifts were found as up frequencies and low frequencies shifted in Λ and Δ configurations respectively, as previously predicted by the DFT calculations.

Structural description from single crystal X-ray results

We obtained crystals suitable for x-ray structure determination of the diastereomer Δ-[Ir(ppy)$_2$((*R*)-Me-Campy)]Cl; as shown in figure 2.24 the iridium(III) metal centre in the cationic complex of *R*-Ir-Me-Campy is hexa-coordinated with achiral bidentate ligands, two cyclometalated ppy and the chiral Me-Campy ancillary ligand; the absolute configuration has been also determined, and corresponds to the Δ form. Several crystals of Ir-Me-Campy have been tested, but we never found racemic crystals, proving that the enantiomeric separation successfully occurred and the metathesis did not produce racemization [148].

Some consideration about the molecular structure: the asymmetric unit of Ir-Me-Campy is made up of a single cationic complex, exhibiting a distorted octahedral geometry around the Ir(III) metal centre, and one co-crystallized water molecule. [145, 149, 150] The Me-Campy ligand displays notably longer Ir-N distances, which can be attributed to the *trans*-influence of the strong Ir-C bonds of the ppy ligands. The five membered

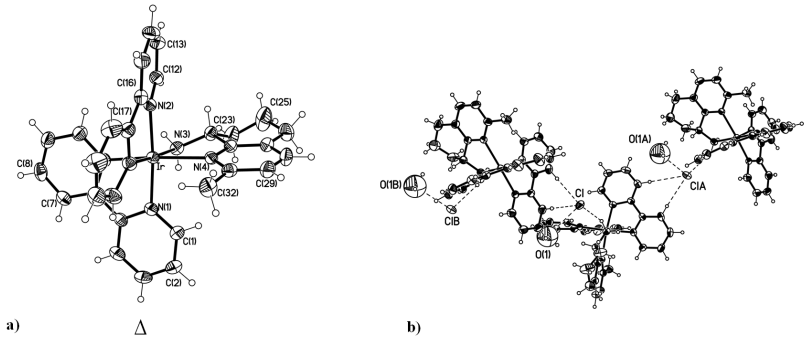

Figure 2.24: View of the Δ form in the metal cation of **Ir-Me-Campy** showing the atomic labelling scheme (a) and the perspective view of the 1D supramolecular motif of **Ir-Me-Campy** showing the anion intermolecular interactions (b).

chelate ring defined by the Me-Campy ligand at the Ir(III) metal centre is not planar. According to the ring puckering analysis of PLATON,[151] the metallacycle conformation is better described as an envelope form on N(3).[152] By using the same ring puckering parameters, the C6-ring of the tetrahydroquinoline moiety shows a conformation very close to an half-chair with the C(e7) atom about 0.7 Å out of the mean plane passing through the C(23), C(25), C(26), C(27) and C(31) carbon atoms. Thus the preferred conformation predicted by DFT calculation was confirmed.

In analogy with similar Ir(III) ppy derivatives containing the ethylendiamine and picolylamine as ancillary N,N chelated ligands, the supramolecular organization of Ir-Me-Campy is mainly built up through intermolecular interactions involving the NH_2 functionality of the Me-Campy ligand and the chloride anion. Indeed, the supramolecular building is sustained by N-H$\cdots$Cl interactions [N(3)$\bullet\bullet\bullet$Cl^i of 3.284(3) Å, N(3)-H(3b)$\bullet\bullet\bullet$Cl(1)^i distance and angle of 2.47 Å and 150°, respectively; i = x, y, z] and C-H$\cdots$Cl interactions with the ppy hydrogen atoms in meta position with respect to both the coordinated N and C atoms [C(4)-H(4)$\cdots$Cl$^i i$ distance of 2.80 Å and angle of 175°; C(7)-H(7)$\cdots$Cl(1)^{ii} distance of 2.88 Å and

Table 2.9: Selected distances (Å) and angles (°) in Δ*R*-Ir-Me-Campy

Ir-C(11)	2.021(4)	N(2)-Ir-N(4)	89.9(1)
Ir-C(22)	2.031(4)	N(3)-Ir-N(4)	76.6(1)
Ir(1)-N(1)	2.057(3)	C(11)-Ir-C(22)	86.0(1)
Ir(1)-N(2)	2.071(3)	C(11)-Ir-N(1)	80.5(1)
Ir(1)-N(3)	2.189(3)	C(11)-Ir-N(2)	95.8(1)
Ir(1)-N(4)	2.252(3)	C(11)-Ir-N(3)	95.7(1)
		C(11)-Ir-N(4)	170.9(1)
N(1)-Ir-N(2)	174.4(1)	C(22)-Ir-N(1)	95.5(1)
N(1)-Ir-N(3)	88.1(1)	C(22)-Ir-N(2)	80.0(1)
N(1)-Ir-N(4)	94.4(1)	C(22)-Ir-N(3)	176.3(1)
N(2)-Ir-N(3)	96.5(1)	C(22)-Ir-N(4)	102.1(1)

angle of 179°, with ii = 1/2-x+1, -y, z-1/2]. Moreover, the co-crystallized water molecule is anchored next to both the metal cation and the chloride counterion through an heteroatoms·halogen contact,[153] where chloride interacts noncovalently to the electronegative oxygen atom at a distance of 3.258(1) Å.

Table 2.10: Selected distances (Å) and angles (°) in Λ*S*-Ir-Me-Campy

Ir-C(11)	2.016(3)	N(2)-Ir-N(4)	95.8(1)
Ir-C(22)	2.022(3)	N(3)-Ir-N(4)	77.4(1)
Ir(1)-N(1)	2.070(2)	C(11)-Ir-C(22)	90.4(1)
Ir(1)-N(2)	2.052(2)	C(11)-Ir-N(1)	80.2(1)
Ir(1)-N(3)	2.195(2)	C(11)-Ir-N(2)	95.8(1)
Ir(1)-N(4)	2.163(2)	C(11)-Ir-N(3)	173.4(1)
		C(11)-Ir-N(4)	96.2(1)
N(1)-Ir-N(2)	173.7(1)	C(22)-Ir-N(1)	97.2(1)
N(1)-Ir-N(3)	98.1(1)	C(22)-Ir-N(2)	80.2(1)
N(1)-Ir-N(4)	87.4(1)	C(22)-Ir-N(3)	96.2(1)
N(2)-Ir-N(3)	88.0(1)	C(22)-Ir-N(4)	172.6(1)

We also resolved the structure of the diasteromer Λ-[Ir(ppy)$_2$((*S*)-H-Campy)]Cl (figure 2.25) ; even in this complex the structure has a distorted octahedral geometry, with almost the same puckering parameters in the five member chelate ring defined by the H-Campy ligand at the Ir(III) and in the C6-ring of the tetrahydroquinoline moiety. In this case, it was not observed water co-crystallization and in respect to the Me-Campy structure the Ir(1)-N(4) is significantly shorter due to the lack of the hindering methyl group.

Chiroptical properties: ECD and CPL results

The almost specular ECD proved the opposite configuration of the metal centre in the couple of diastereomers. The coherence of the configuration assigned by NMR was proved by the perfect mirror image shape of two complexes that should be in enantiomeric relation. Moreover, it was possible to observe a preponderance of the metal ellipticity role over the contribution of the ancillary ligand. Three regions of the spectrum could be recognised: below 300 nm, around 350 nm and over 400 nm in which the sign of the ECD inverts. If the metal chirality was kept constant (1/2)

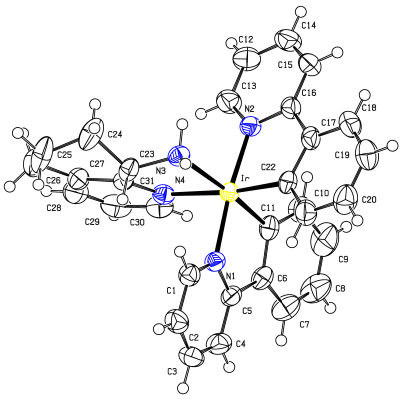

Figure 2.25: View of the Λ form in the metal cation of **Ir-H-Campy** showing the atomic labelling scheme.

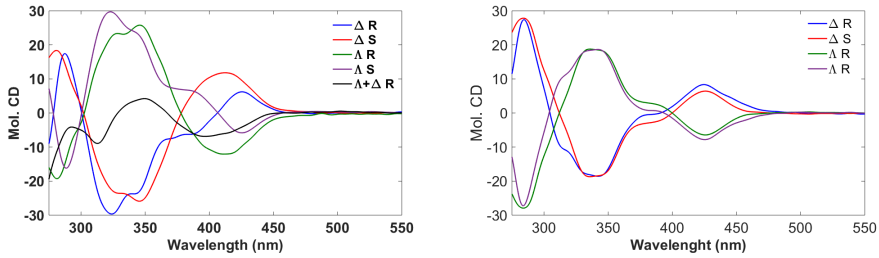

Figure 2.26: (a) Superimposed experimental Electronic Circular Dichroism (ECD) of Ir-H-Campy and (b) Superimposed experimental Electronic Circular Dichroism (ECD) of Ir-Me-Campy.

the sign of the ECD spectra remained the same in all the regions; on the contrary if the diamine configuration was kept constant the ECD sign inverted. This was also true when the Me-campy ligand was substituted by the H-campy ligand.

With the aim to isolate the different contributions of the chirality at the metal and that strictly related to the chiral ligand, the spectrum of the crude diasteromeric mixture product Δ,Λ (*S*)[$(ppy)_2$Ir (H-Campy)]Cl was recorded. Due to the racemic metal centre the ECD spectrum mainly represented the contribution of the optically pure diamine ligand. The spectra are showed in Figure 2.26. The ancillary ligand influences the overall ECD response[135] mainly in the regions below 300 nm and over 380 nm, where the intensity ratio is indeed higher (Figure 2.26a). Consequently the sign of the ECD spectrum at 350 nm could be taken as descriptor of the chirality at the metal centre.

According to related bis-cyclometalated Ir(III) complexes, for which the crystallographic structures are known [135, 23], the sequence of signs + ($<$ 300 nm), - (350 nm), + ($>$ 400 nm) can be related to a Δ configuration. These data are consistent with the configuration assigned by the NMR analysis and allow to unequivocally assign the absolute metal con-

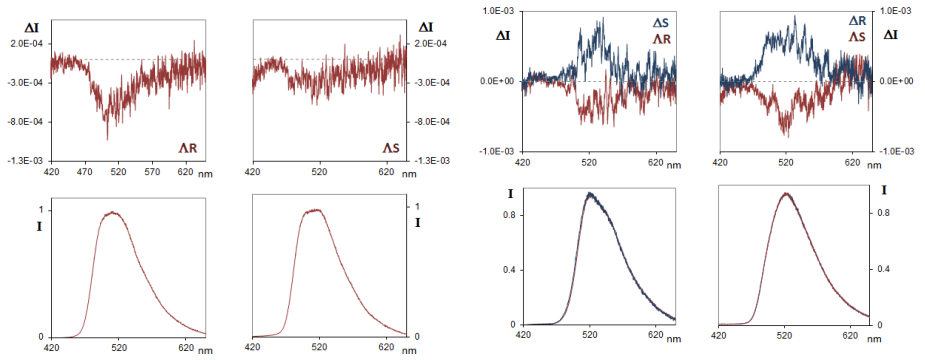

Figure 2.27: (a) Superimposed experimental CPL specra of Ir-H-Campy and (b) Superimposed experimental CPL spectra of Ir-Me-Campy, recorded at room temperature.

figuration. The counter anion change did not affect significantly the ECD spectrum. We are aware that further experimental data are necessary, the present statement are strictly related to the here studied systems.

Furthermore we registered the CPL spectra of the chlorinated complexes at room temperature. The CPL spectra are, within experimental error, mirror-image to each other and in particular the sign for the CPL band of each species, + for Δ and – for Λ, is the same of the lowest energy band in the ECD spectrum. The ancillary ligand slightly influences the most relevant features CPL data, consequently they are mainly originated in the Δ/Λ chirality of the metal. Finally we notice that the dissymmetry g_{lum} factors [g_{lum} = (I_L-I_R)/ 0.5(I_L+I_R)] for Ir-Me-Campy complexes are of the order of 10^{-3} [136, 154, 155].

In figure 2.24 are reported the crystallographic structure that confirmed the configuration assigned by ECD and NMR, it should be noted that they were obtained after the characterization with both the techniques.

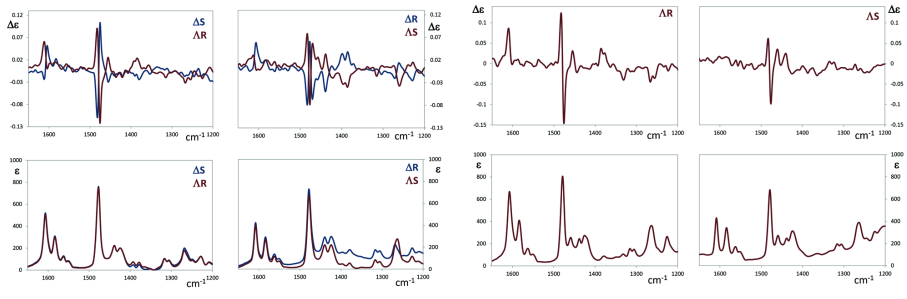

Figure 2.28: (a) Superimposed experimental Vibrational Circular Dichroism (VCD) (top panels) and IR (lower panels) spectra of Δ*S*-Ir-Me-Campy and of Λ*R*-Ir-Me-Campy (left) and superimposed experimental VCD and Δ*R*-Ir-Me-Campy and of Λ*S*-Ir-Me-Campy (right). (b) Experimental Vibrational Circular Dichroism (VCD) (top panels) and IR (lower panels) spectra of Λ*R*-Ir-Campy (left) and of Λ*S*-Ir-Campy (right). Notice the colour code for the spectra: blue for Δ-isomers and red for Λ-isomers.

Chiroptical properties: VCD results

The experimental IR and VCD spectra of the Ir-Me-Campy complexes are reported in figure 2.28a, the couple of enantiomer are superimposed, whereas in figure 2.28b we report the spectra of the Ir-H-Campy complexes. As expected the VCD spectra of the two couple of diastereomers in Figure 2.28. In figure 2.28a on the left we superimpose the experimental VCD (top) and IR absorption spectra of Δ*S*-Ir-Me-Campy and of Λ*R*-Ir-Me-Campy and on the right we superimpose the experimental VCD and IR spectra of Δ*R*-Ir-Me-Campy and Λ*S*-Ir-Me-Campy. In Figure 2.28b on the left we report the experimental VCD and IR spectra of Λ*R*-Ir-H-Campy, while on the right we report the experimental VCD and IR spectra of Λ*S*-Ir-H-Campy. Interestingly the VCD spectra of the enantiomeric couple of the left panel of Figure 2.28a are rather different from the VCD spectra of the diastereomerically related enantiomeric couple in the right panel of the same Figure, whereas the IR spectra show no appreciable

difference; in other cases an analogous situation with quite indistinguishable absorption spectra of diastereoisomers had already been observed, for example when planar and central chirality were co-present.[156] It is also interesting to notice a good correspondence of the VCD data of Ir-H-Campy (Figure 2.28b) with the VCD data of Ir-Me-Campy (Figure 2.28a) for cases endowed with the same chirality at the metal centre (once more the IR spectra of Figure 2.28b are quite similar to the spectra of Figure 2.28a).

A detailed analysis of the figure 2.28 let us to affirm that:

i Two doublets with alternating signs are observed in the VCD spectra of Ir-Me-Campy (Figure 2.28a) at ca. 1600 cm^{-1} and at 1475 cm^{-1} (the latter doublet is somewhat concealed by a nearby VCD band at ca. 1470 cm^{-1}): the two doublets have positive chirality for the Δ-diastereomers ((+,-) in order of increasing energy/wavenumber, as defined e.g. by Harada, Berova and Nakanishi for excitons[157]) and negative chirality for the Λ-diastereomers. The sign of the doublets is independent on the configuration of the stereogenic carbon. The second doublet is more intense and is observed also in the VCD spectra of ΛR-Ir-H-Campy and ΛS-Ir-H-Campy and it is negative in their spectra, since the absolute configuration at Ir is Λ. It can be recognized, at least for the doublets at 1475 cm^{-1}, the presence of *vibrational excitons*, even though the examples reported so far in literature are associated to C=O groups [158, 159, 87]. In any case the intensity of the corresponding IR absorption band is quite large, and is indeed the most intense in the whole IR spectrum. The discussion of the assignment of the 1475 cm^{-1} doublet to a vibrational exciton is given below, on the basis of DFT calculations.

ii On the other hand one may clearly notice at ca. 1380 cm^{-1} a medium-intensity monosignate structured VCD feature which is positive for *R* diastereomers and negative for *S* diastereomers, both for Ir-Me-Campy and Ir-Campy independently on the Δ/Λ chirality (cfr. Figures 2.28a and 2.28b). This is a clear proof of the powerfulness of the

VCD method, which is able to "see" both types of chiralities, even in the case of metal-dictated chirality. DFT calculations for Δ*S*-Ir-Me-Campy and for Λ*S*-Ir-Me-Campy help provide firmer ground to the above conclusions; the calculated VCD spectra are compared in Figure 2.29 with the experimental results.

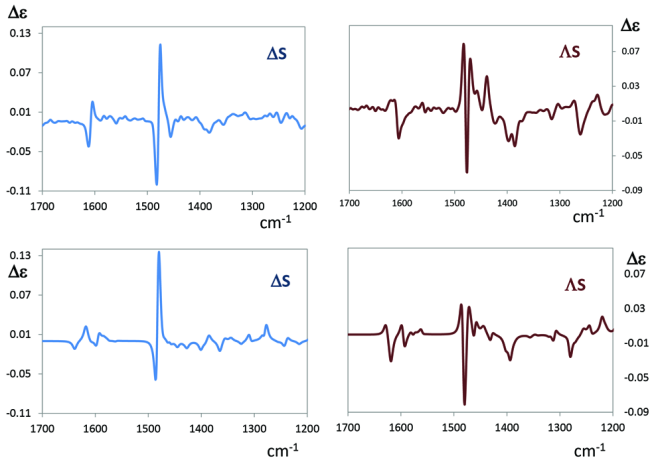

Figure 2.29: Comparison of calculated (top) and experimental (lower) VCD spectra of Δ*S*-Ir-Me-Campy (left in blue) and of Λ*S*-Ir-Me-Campy (right in red).

Calculated spectra are rather good in both signs and intensities. Also calculated IR spectra are in very good correspondence with the experimental ones (Figure 2.30). The calculated geometries for Δ*S*-Ir-Me-Campy and for Λ*S*-Ir-Me-Campy are provided in Figure 2.32 and are shown from an opportune perspective to better highlight the relation among the metal chirality (*vide infra*).

In particular can be notice that the intense doublet structure centred at ca. 1475 cm^{-1} is predicted by calculations in an excellent agreement with the experimental one: the our assignment[5] shows that the normal

[5]The tables of complete normal mode assignments is reported in experimental sec-

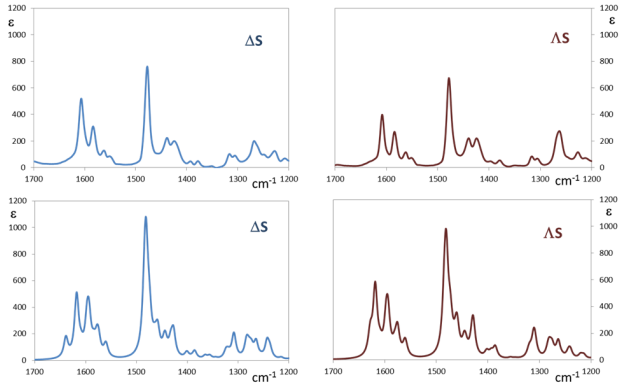

Figure 2.30: Comparison of calculated (top) and experimental (lower) IR spectra of Δ*S*-Ir-Me-Campy (left in blue) and of Λ*S*-Ir-Me-Campy (right in red).

modes underlying the two components of the doublet are the symmetric (at higher frequency) and anti-symmetric (at lower frequency) combinations of in plane CC-stretching modes located on the two ppy-moieties, whose electric dipole transition moments are strong and are oriented parallel to the major axis of the phenyl-pyridine groups. These are calculated at 1511 and 1514 cm^{-1} (no scaling factor applied to wavenumbers), with rotational strengths equal to +739x10^{-44} esu^2cm^2 (Δ*S* case)/-714 x10^{-44} esu^2cm^2 (Λ*S* case) and to -585x10^{-44} esu^2cm^2 (Δ*S*)/+572 x10^{-44} esu^2cm^2 (Λ*S* case). The experimental and calculated couplets are approximately conservative and show the typical values for vibrational excitons, like the ones introduced by Taniguchi and Monde [158] and discussed later for interacting C=O stretching vibrations: [159] recently a more similar case to the present has been reported, in that works two interacting phenoxy moieties were involved [160].

The vibrational exciton, also known as coupled oscillator model [161], described the through-space interaction of two harmonic oscillators. For

tion.

two degenerated oscillators **a** and **b** the coupling mixes their ground state function and the first vibrational exited state generates an in phase and an out of phase combination

$$\psi^{\pm} = (\psi_a^1 \psi_b^0 \pm \psi_a^0 \psi_b^1)/\sqrt{2} \tag{2.21}$$

The interaction between two oscillators is composed by dipole-dipole electrostatic term W_{ab} and by a term that sums up the van der Waal interaction contribution; however in system such that studied here the former term prevail[162] and can be expressed as

$$W_{ab} = (d)^{-3}[\boldsymbol{\mu}_a \cdot \boldsymbol{\mu}_b - 3(\mathbf{n} \cdot \boldsymbol{\mu}_a)(\mathbf{n} \cdot \boldsymbol{\mu}_b)] \tag{2.22}$$

where d is the distance between the two oscillators, $\boldsymbol{\mu}_a$ and $\boldsymbol{\mu}_b$ their electronic dipole moments and $n = d^{-1} \cdot \mathbf{R}_{ab}$, $\mathbf{R}_{ab}$ is the vector from **a** to **b**. Taking into account that the energy E of an uncoupled oscillator are related to the frequency to $E = \hbar c \nu$, the frequencies may be expressed as

$$\nu_{\pm} = (\hbar c)^{-1}[E \pm W_{ab}] = \nu \pm \frac{W_{ab}}{\hbar c} \tag{2.23}$$

where ν is the unperturbed frequency. We recall now that the rotational strength R of a transition is given by $R = Im(\boldsymbol{\mu}^{\pm} \cdot \mathbf{m}^{\pm})$ (2.9) thus if we define $\mathbf{m}_a$ and $\mathbf{m}_b$ as the magnetic dipole moments of **a** and **b**, $R_{\pm}$ is

$$\begin{aligned} R_{\pm} = \frac{1}{2} Im(\boldsymbol{\mu}_a \cdot \mathbf{m}_a + \boldsymbol{\mu}_b \cdot \mathbf{m}_b) \\ \pm \frac{1}{2}[Im(\boldsymbol{\mu}_a \cdot \mathbf{m}_b + \boldsymbol{\mu}_b \cdot \mathbf{m}_a) - \pi\nu \cdot \mathbf{R}_{ab} \cdot \boldsymbol{\mu}_a \times \boldsymbol{\mu}_b] \end{aligned} \tag{2.24}$$

where $\mathbf{R}_{ab}$ is vector between the centre of mass of the two oscillators and ν is the unperturbed frequency. In equation (2.24) the first term is the intrinsic rotation strength of the oscillators that is zero in case of achiral ones; the second term is the intrinsic moments contribution to the couple oscillator, while the third term depends on the geometric arrangements of the two electric dipole moments. The latter two give rise to a doublet

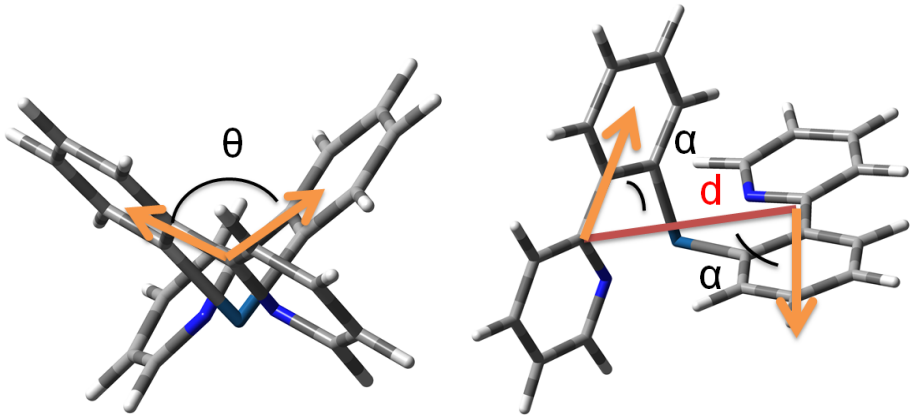

Figure 2.31: (a) Representation of the diedral angle, θ, between the two electric dipole moments (orange) (b) Representation of the angle (α) that the electric dipole moments (orange) form with respect to d (red). Only the iridium atoms and ppy ligands are shown.

signature in the VCD spectra. However, in this kind of system, the intrinsic magnetic moment of the oscillators could be consider negligible, so that the (2.24) could be approximated [6] to

$$R_{\pm} = \mp \frac{\pi\nu}{2} \cdot \mathbf{R}_{ab} \cdot \boldsymbol{\mu}_a \times \boldsymbol{\mu}_b \tag{2.25}$$

We assumed that both oscillators, with an almost C_2 symmetry, have the same transition dipole $\boldsymbol{\mu}$ so that the dependence from the spatial arrangement is even more clear if (2.25) is rewritten with respect to the angle notation introduced in figure 2.31:

$$R_{\pm} = \mp \frac{\pi\nu}{2} \cdot d\mu^2 \sin\alpha_a \sin\alpha_b \sin\theta \tag{2.26}$$

[6] The electric transition dipole of an oscillatory couple can be define as $\boldsymbol{\mu}^{\pm} = (\boldsymbol{\mu}_a) \pm \boldsymbol{\mu}_b)/\sqrt{2}$ while the magnetic dipole can be approximated to $\mathbf{m}^{\pm} = (i\pi\nu/2\sqrt{2})[\mathbf{R}_{ab} \times (\boldsymbol{\mu}_a \mp \boldsymbol{\mu}_b)]$ [163]

where α_a and α_b are the angle that they form with respect to d and θ is the dihedral angle between them. It is worth noting that with the applied approximation the result is the same obtained for the electronic case in related system[164]; although not so clear, if we observed figure 2.26 the transition at 300 nm exhibits the same sequence of CD sign (+,-) for Δ-diastereomers and (-,+) for Λ-diasteromers (in order of increasing energy) of the VCD spectra.

In the same way rotational strength $D_\pm$ and $\nu_\pm$ could be defined as

$$D_\pm = D \pm \boldsymbol{\mu}_a \cdot \boldsymbol{\mu}_b = D \pm D[\sin\alpha_a \sin\alpha_b \cos\theta - \cos\alpha_a \cos\alpha_b] \tag{2.27}$$

$$\nu_\pm = \nu \pm \frac{\mu^2}{\hbar c d^3}[\sin\alpha_a \sin\alpha_b \cos\theta + 2\cos\alpha_a \cos\alpha_b] \tag{2.28}$$

where D is the rotational strength of the uncoupled oscillator.

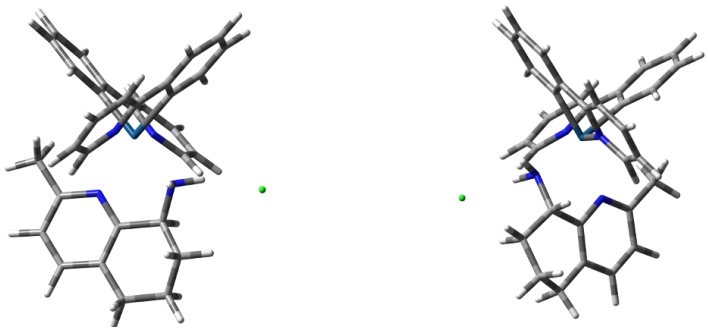

Figure 2.32: Calculated structures of Λ*S*-Ir-Me-Campy (left) Δ*S*-Ir-Me-Campy (right)

In figure 2.32 we show the two diastereomers Λ*S* and Δ*S*, both are reported with the carbon in position 2 of the pyridine ring aligned in order to underline the dihedral angle. Indeed in the Δ-case, in order to take the frontal ppy ligand to coincide with the rear one, a clockwise

rotation should be take this means positive chirality; in the Λ-case instead a counter clockwise rotation is needed to achieve the same result, and this means negative chirality. As pointed out in ref.[159], caution must be taken to apply the model.

In figure 2.33 are showed R_+ and ν_+ as function of α and θ (in C2 symmetry case), while R sign is dependent only on θ, the relative position of the symmetric and anti-symmetric band is also strictly affected by the value of α; the inversion of the two combination, related to the R sign, is more clear in the third panel where $R{\cdot}\nu$ is reported. Actually the geometry of the complexes as found in DFT calculation and confirmed by X-Ray structure (α_1, α_2 and dihedral angle) guarantee higher wavenumber for the symmetric normal mode; moreover the angle formed by the two electric dipole transition moments with respect to d is close to 90°, a situation in which the applicability of the vibrational exciton formulas to calculate rotational strengths is safe.

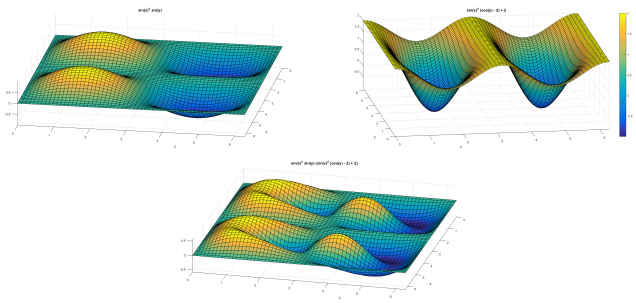

Figure 2.33: R (left), ν (right) and $R{\cdot}\nu$ (bottom) periodicity 0 - 2π for α and θ for the in-phase combination

Quantitative application of the expressed model [159] requires to know the electric dipole transition moment and frequency values for each one of the two isolated ppy-units: a DFT calculation was conducted on a ppy-group, which was opportunely coordinated to an isoelectronic Ir atom, which coordination sphere was completed with three NH_3-molecules and

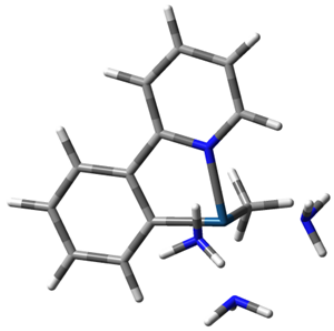

Figure 2.34: The simulated ppy-model.

a CH_3-group, as showed in Figure 2.34. For this model the relevant normal mode was found at 1512 cm^{-1}, with dipole strength equal to 496 x 10^{-40} esu^2cm^2. For Me-Campy the inter-ppy dihedral angle was assumed to be C(phe)-C(py)-C(py)-C(phe), and this turned out to be ca. $\pm 110°$; the distance d of the two ppy-units was taken as the C(py)-C(py)-distance and the angles α_1 and α_2 as C(phe)-C(py)-C(py). Results are given in table 2.11 and show excellent agreement between full DFT and model calculations for frequencies, dipole strengths and rotational strengths, leaving no doubt to the vibrational exciton interpretation of the doublets.

Following the DFT calculations, the origin of the VCD band at ca. 1380 cm^{-1} can be understand, which is negative for *S* and positive for *R* configuration of the stereogenic carbon atom, independently on the Δ/Λ chirality. Indeed, underneath that VCD band a couple of normal modes can be identify; their rotational strength is about -40$\times 10^{-44}$ esu^2cm^2 and they consist of the bending vibration of the C*H, where C* is the stereogenic carbon atom (the calculated frequencies for these modes are about 1430 cm^{-1}, prior to scaling factoring). The sensitiveness of C*H bending to carbon chirality had been noticed in similar circumstances in the VCD spectrum of two different molecules bearing an "external" C* as in

Table 2.11: Comparison of frequencies $\nu\pm$, dipole strengths D$\pm$ and rotational strengths R$\pm$ for ΛS and ΔS-Me-Campy calculated by the vibrational exciton model and by full DFT computations.

	ΛS-Me-Campy		ΔS-Me-Campy	
	model	DFT	model	DFT
$\nu+^a$	1512.3	1514.0	1512.3	1514.0
$\nu-^a$	1511.7	1512.0	1511.7	1511.0
D+^{b}	267.2	253.0	249.7	308.0
D-^{b}	724.8	695.0	742.3	677.0
R+^{c}	483.1	572.0	-463.3	-585.0
R-^{c}	-482.9	-714.0	463.1	739.0
Parameter obtained from DFT calculation on *ppy*-model				
D(10^{-40} esu^{2}cm^2)	496		496	
ν(cm^{-1})	1512		1512	
φ(°)	-108		110	
d(Å)	5.53		5.47	
α_1(°)	62		61	
α_2(°)	62		61	

^{a} cm^{-1}, ^{b} 10^{-40} esu^{2}cm^2, ^{c} 10^{-44} esu^{2}cm^2

refs.[156] and [165].

Using VCD spectroscopy we were able to highlighted the spectroscopic signatures for both types of chiralities, a good sensitivity of this chiroptical method to discriminate the diastereomers was found. The strong VCD doublet observed at ca. 1475 cm^{-1} turns out to be the signature for chirality at the metal. It can be correctly interpreted as vibrational exciton doublet and it is generated by the two phenyl pyridine groups directly coordinated to the metal: when the two ppy-groups form a positive helicity moiety, as in Δ-complexes, a positive vibrational exciton (+,- from low to high frequencies) is generated and observed; otherwise when the two ppy-groups form a negative helicity moiety, as in Λ-complexes,

a negative vibrational exciton is generated and observed. Such a strong and simple picture is not emerging from ECD data, due to the overlay of many electronic transitions; furthermore no specific signature for central C^* chirality is evident in ECD spectra. The latter one instead is manifested in the VCD spectra, around 1380 cm^{-1}, with features associated to C^*H bending.

Luminescence properties

Once obtained and fully characterized the whole set of complexes in their enantiomeric pure form, we tested their luminescence profiles. All the considered compounds were dissolved in spectroscopic grade solvent, dichloromethane for the chloride complexes or water for the acetate ones. The absorption bands are reported in table 2.12.

However, relevant differences were not detected among the studied complexes, except a slight shift of the higher energy band which position can be related to the ligand substituents, solvent and counterion, but not to the isomerism. In figure 2.35a are reported the absorption profiles of complexes Δ*S*-[Ir(ppy)$_2$(Me-Campy)]Cl, Δ*S*-[Ir(ppy)$_2$(H-Campy)]Cl and Δ*S*-[Ir(ppy)$_2$(Me-Campy)]AcO^-, representative of each of the three series according to the substituents and the counterion: the sharp and intense band at 264 (or 261 or 259) nm (with a series of shoulders below 350 nm) is attributed to spin-allowed π,$\pi*$ transitions of the ppy ligands [135].

At higher wavelengths (from 350 to 500 nm), weaker bands are observed. The assignment of these bands is not straightforward, as reported by various authors [23], because their low intensity rules out spin-allowed π,$\pi*$ transitions, and on the other hand, pure MLCT transitions are unlikely because of their solvent insensitivity and their structured features: in our case, it seems reasonable to attribute to these bands a mixed (MLCT-LC) character [166].

It is known that cyclometalated octahedral Ir(III) complex in solution often display aggregation phenomena which strongly affect their photophysical properties [146, 167]. For this reason, luminescence spectra have

Table 2.12: Photophysical data in air-equilibrated solution at room temperature. Solvent: dichloromethane for the chloride complexes or water for the acetate ones

			Absorption: λ/nm(ε/M^{-1}cm^{-1})	Emission: λ/nm	τ/ns
Cl^-	Me-Campy	ΔR	264(35160), 293(s), 312(s), 346(6109), 390(3424), 423(2585), 476(s)	495, 518	58.6
		ΔS	264(34474), 293(s), 312(s), 346(5990), 390(3357), 423(2535), 476(s)	495, 518	52.5
		ΛR	264(34627), 293(s), 312(s), 346(6016), 390(3372), 423(2546), 476(s)	495, 518	51.9
		ΛS	264(33798), 293(s), 312(s), 346(5872), 390(3292), 423(2485), 476(s)	495, 518	60.6
	H-Campy	ΔR	261(24413), 293(s), 312(s), 346(4378), 390(2751), 423(2086), 476(s)	495, 515	90.7
		ΔS	261(24053), 293(s), 312(s), 346(4313), 390(2710), 423(2056), 476(s)	495, 515	94.4
		ΛR	261(23767), 293(s), 312(s), 346(4262), 390(2678), 423(2031), 476(s)	495, 515	95.6
		ΛS	261(23604), 293(s), 312(s), 346(4233), 390(2659), 423(2017), 476(s)	495, 515	89.2
AcO^-	H-Campy	ΔR	259(34254), 288(s), 306(s), 342(5778), 386(3933), 418(2879), 471(s)	490, 510	433
		ΔS	259(33549), 288(s), 306(s), 342(5659), 386(3852), 418(2819), 471(s)	490, 510	435
		ΛR	259(34556), 288(s), 306(s), 342(5829), 386(3968), 418(2904), 471(s)	490, 510	422
		ΛS	259(34052), 288(s), 306(s), 342(5744), 386(3910), 418(2862), 471(s)	490, 510	413

been recorded from 1.0 E-5 M solutions, and, in order to probe possible aggregation phenomena, results were compared with the emission from 1.0 E-6 M solutions.

For all complexes except ΔR-[Ir(ppy)$_2$(Me-Campy)]Cl and its enantiomer,

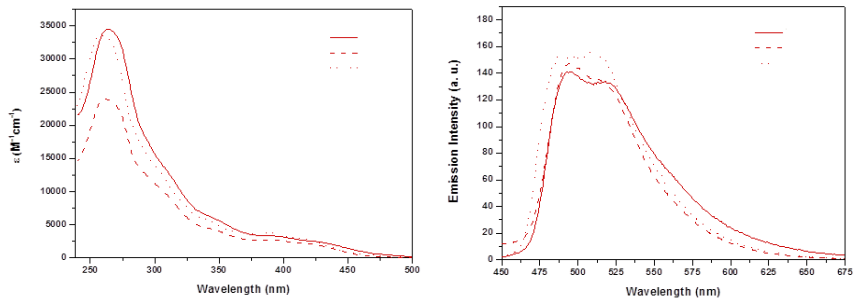

(a) **(b)**

Figure 2.35: (a) Absorption spectra of the complexes Δ*S*-[Ir(ppy)$_2$(Me-Campy)]Cl (—), Δ*S*-[Ir(ppy)$_2$(H-Campy)]Cl (- -)in CH_2Cl_2 and Δ*S*-[Ir(ppy)$_2$(Me-Campy)]AcO^- (··) in water solution at room temperature (b) and their emission spectra in air-equilibrated dichloromethane solvents at room temperature.

dilution does not modify spectral shape: the low concentrated solutions of all the complexes show two vibronic peaks emission, the first in the 490-495 nm range, and the second in the 510-518 nm range, depending of the substituent and of the counterion (see tablle 2.12).

Nevertheless, no difference in emission as well as in absorption were found that could be directly connected to the distereomeric nature of the complexes (see figure 2.35b). The luminescence profiles of the spectrum exhibit a vibronic resolution which is typical for Ir(III)-ppy complexes [168, 23, 169]; the emission is assigned to a mixed ^{3}(MLCT-LC) state; as previous observed for similar compounds, acetate complexes in water solution show considerably high lifetime values.

We observed that a different solubility of the complexes due to their stereoisomerism might be reflected on a different emission spectrum shape in solution; to investigate possible effects of chirality on the luminescence, a photophysical study on solid samples was also performed [148].

As evidenced, there is a growth of the lifetime values on moving toward the lower energy bands, this behavior can be due to the presence of

Table 2.13: Emission bands in solid sample

			Spectral range			
			470-510	510-530	530-570	570-620
Cl^-	Me-Campy	ΔR	490 (s)	w	546 (p)	563 (s)
		ΔS	493 (s)	w	540 (p)	563 (s)
		ΛR	494 (s)	w	543 (p)	565 (p)
		ΛS	484 (s)	w	554 (p)	600 (s)
	H-Campy	ΔR	486 (s)	w	524 (p)	553 (p)
		ΔS	504 (s)	533 (s)	574 (p)	603 (p)
		ΛR	-	-	548 (p)	570 (s)
		ΛS	490 (s)	515 (s)	568 (p)	597 (p)
AcO^-	H-Campy	ΔR	498 (s)	516 (p)	554 (s)	603 (s)
		ΔS	500 (s)	533 (p)	570 (s)	598 (p)
		ΛR	508 (s)	530 (p)	560 (s)	w
		ΛS	500 (s)	521 (p)	w	610 (p)

value in cm^{-1}, p:principal; s:shoulder; w:weak or undetectable

'aggregation-induced phosphorescent emission' (AIPE), which was claimed to be related to an intermolecular excimer formation in the solid state [170, 171]: in fact, this could cause a lifetime lengthening and a red-shifted emission, so the three-exponential decays could be attributed to the simultaneous presence of single molecule with aggregate ones. More interesting is the wide lifetime variation for molecules with the same substituent and the same counterion, such influence could reasonably awaited to a different packing of the enantiomers and stereoisomers that produces aggregates with different emitting properties.

The next step will be to study the photophysical properties in chiral environments or in presence of biomolecules, in order to verify if a difference in emission can be recorded and thus if they can be used in bimolecular recognition.

Chapter 3

Conclusions

Transition metals are characterized by an exterminate chemistry, several geometries and coordination numbers, making the stereochemistry of the transition metal complexes an interesting challenge. The scope of this thesis was to investigate some aspects related to chiral metal complexes, in particular when one of the stereogenic centre was the metal itself.

The first step was the synthesis, the isolation and purification of optically pure metal complexes so that these could be fully characterized by several spectroscopic techniques. The final goal was to evaluate the influence of enatiopure metal complexes in different fields such as: asymmetric catalysis, emission or interaction with chiral environment.

The great part of the catalytic systems deals with 8^{th} groups transition metal complexes; several ruthenium, platinum and iridium based emitters are known. For example in medicine *cis*-platin, a platinum (II) complex, is the progenitor of metal complexes applied in medicine and add on recently octahedral ruthenium complexes were also tested. Then we focus our investigation on octahedral complexes of the eight group.

In the first year we attempted to synthetize and use as catalyst in asymmetric catalysis, complexes chiral at the metal centre in order to evaluate

its impact in asymmetric reactions. In particular the investigated reaction was the asymmetric transfer hydrogenation of ketones, because its reaction mechanism is known and the chirality of the metal should plays a central role in it.

We were able to obtain ruthenium(II) complexes of general formula [Ru(NN)(PP)Cl_2] in optically pure form, where NN was a chiral diamine and PP was a chelating phosphine or two mono phosphines. The thermodynamic *cis* complexes were obtained from the kinetically favourite *trans* complexes via a complete stereoselective isomerization, as pointed out by the presence of the two isodichroic point in ECD spectra. The absolute configuration were determined by NMR. These complexes, after the activation into the hydride species, reduced acetophenone to 1-phenylethanol in good e.e. (up to 90 %). The configuration of the product was correctly predicted by the matching of the chirality of the product itself with that of the catalyst. With the aim of investigate the stereochemistry of the conversion from Ru-Cl bond to Ru-H, we synthesised in almost enantiomeric pure form the related [RuH(NN)P_2Cl], attempts to substitute the monophosphine or to generate the di-hydride species failed. The structure and the configuration were elucidated by NMR.

another approach was based on the stereoselectivity synthesis of complexes of the types [η^6-arene-Ru(NN)Cl] with other arene baring chiral groups, however in the most cases intractable complex mixture of stereoisomers were obtained.

When complexes enantiopure at the metal were obtained, their impact in catalysis was pointed out, confirming the key role of the metal chirality. Despite optically pure ligands were used, when low d.e. in the complexes were achieved only low e.e. were obtained in catalytic applications. Results that we also confirmed in ref. [172]. A poor distereoselection in the formation of the chiral metal centre considerably lowed the chiral induction.

The results obtained in the synthesis of η^6-arene ruthenium complexes and η^5-cyclopentadienyl iron complexes pointed out the need of a tech-

nique able to describe complex mixtures of regioisomers, preferably in solution. In diastereomeric couple NMR spectroscopy represents the technique of choice but not always it is possible to obtain meaningful informations, as reported in this case. This fact prompted us to study vibrational circular dichroism as a possible alternative solution.

VCD in tandem with DFT calculation is powerful technique for the determination of the absolute configuration and conformational analysis; despite new results concerning transition metal complexes are coming out, their applications in the study of metallorganic compounds are very few. The strength of IR and VCD spectroscopy lies in the fact that the spectra of a chiral molecule contain sufficient stereochemical details to be consistent with only a single absolute configuration and an unique solution-state conformation, or distribution of conformations, for a molecule; moreover compared with ECD the DFT calculation is more reliable.

For our purpose we selected three common motifs in organometallic chemistry never investigated by VCD spectroscopy.

We decided to investigate the carbon monoxide as the first chromophore. Carbon monoxide is one on the most common ligand for transition metal complexes; the carbonyl complexes find application as catalysts, precatalysts or stoichiometric reagents in many different reactions. The attraction of this ligand is its infra-red stretching frequency that, in mononuclear carbonyl complexes, lies in the range 2125-1850 cm^{-1}, a region of the IR spectrum devoid of other signals; therefore VCD signal of the stretching vibration was expected to be a probe of the metal centre chirality. We chose to study a series of heteroleptic ruthenium(II) complexes , strictly related with those reported before, of general formula [η^5-(menthyl)-$C_5H_4Ru(CO)(PPh_3)X$] where X could be Cl,Br,I, and the cation complex [η^5-menthyl-$C_5H_4Ru(CO)(PPh_3)(NCMe)]^+$ $BF_4{}^-$.

The complexes were synthesised and resolved in optically pure form. The structure in solution were also investigated by NMR spectroscopy. In these complexes three different chiral portions can be distinguished: the chirality on the metal centre, the chirality of the menthyl group and

the helical shape chirality on the PPh_3 ligand. Using VCD spectroscopy associated with DFT calculation we were able to recognize all the characteristic features associated with the different chiralities.

The experimental data allowed us to find a correlation between the spatial arrangement of the ligands around the metals and the VCD sign. As results the CO VCD band can be used as probe of the metal chirality in this class of complexes. Looking in the contribution of the atomic tensor involved in normal modes underneath the CO band, we speculated on the origin of the IR intensity and of the VCD sign. Although a better investigation should be performed, we argued that the VCD sign could be interpreted on the base of the ring current model.

The second chromophore was a metal-hydrogen bond, which has important role in catalytic reduction. Metal hydrides are generally very reactive species, often characterized by pronounced kinetic and thermodynamic instabilities and generally occupy one coordination site acting as a linearly coordinated ligand. The ν-M-H stretching vibration usually lies in the range 2200-1700 cm^{-1} with the corresponding absorption bands medium to weak in intensity, so it could be a valuable probe as well as the carbonyl in VCD. We studied the complex [RuH(NN)P_2Cl] and in order to avoid any possible decomposition in solution we "rediscovered" the nujol mulls technique. By VCD and ECD the complexes demonstrated to be stable in the sample condition. The ECD spectra showed a good shape and even in VCD spectroscopy we were able to recognize some bands, indeed the M-H band was found to inverted in the couple of enantiomers.

The third class of compounds was the cyclometallated iridium(III) complexes that due to their photophysical properties have been extensively studied in the last years, founding application in several fields. Here the chromophore was constituted by two orthometalled phenylpyridine coordinated at the metal in helical shape. Our approach to achieve chiral iridium(III) complexes enantiopure at the metal was the introduction of a chiral diamine as ligand followed by co-crystallization with a common chiral counter anion.

The complexes were fully characterized with three chiroptical technique: VCD, ECD, CPL, morover the crystallography structures of two complexes were resolved. VCD confirmed to be the technique that gave more chiral informations, the characteristic features of the helix chirality and of the chiral diamine were recognized. Moreover the most intense doublet at 1470 cm^{-1} is indeed a vibrational exciton, thus we builded a model based on the dipole intensity of a single ligand and the geometry in the complexes.

The results obtained with our model were in excellent agreement with the full calculation; these results confirmed that the observed doubles was actually a vibrational exitone: when the two ppy-groups form a positive helicity moiety, as in Δ-complexes, a positive vibrational exciton (+,- from low to high frequencies) is generated and observed; otherwise when the two ppy-groups form a negative helicity moiety, as in Λ-complexes, a negative vibrational exciton is observed.

In here described the carbonyl complexes and Ir(III) coordination compounds we found correlation between the VCD spectra and the chirality at the metal centre that can be used to predict the chirality in related compounds. Also whit the M-H chromophore we found a correlation between chirality at the metal and VCD sign but in this case more experimental and computational work is necessary to assert the correctness of the preview statement.

In this latter case, our interest was also adressed to study the photophysical properties of the different diastereomers and in order to verify if the emission could be influenced by the diastereomeric nature of the complexes. Despite the different stereochemistry, all the investigated compounds display similar photophysical properties in solution. Differences in emitting properties were found by exploring photophysics in solid state that can be related to a different packing of the enantiomers and stereoisomers that originates different aggregates.

Chapter 4

Experimental Section

4.1 Material and methods

All commercially available compounds were purified by distillation or crystallization before use. ^{1}H, ^{13}C, and ^{31}P NMR spectra were recorded in $CDCl_3$, CD_3OD or benzene-d_6 on Bruker DRX Advance 300 MHz equipped with a non-reverse probe or Bruker DRX Avance 400 MHz. Chemical shifts (in ppm) were referenced to residual solvent proton/carbon peak or using external standard 85% H3PO4 for ^{31}P NMR. Fast Atom Bombardment Spectra (FAB) were acquired on a VG Autospec M246 spectrometer using p-nitrobenzyl alcohol as the matrix. Elemental analyses were recorded in the analytical laboratories of Milan University on Perkin Elmer Series II CHNS/O Analyzer 2400. IR and VCD spectra were taken on a Jasco FVS6000 apparatus, by professor Abbate group at Univerità di Brescia, while photophysical studies were conducted by professor Ghedini groups at Univeristà della Calabria.

Unless otherwise stated, all synthesis involving transition metal complexes were carried out under nitrogen atmosphere using standard Schlenk techniques.

The enantiomerically pure 8-amino-5,6,7,8-tetrahydroquinolines (H-campy)

and 2-methyl-5,6,7,8-tetrahydroquinolin-8-amine (Me-Cam-py) were synthesised as we reported in the literature [172, 58].

General procedure for hydrogen transfer reaction

In a Schlenk tube sealed with a rubber septum under argon atmosphere the base (potassium tert-butoxide, 0.04 mmol) was added to a solution of precatalyst 4e7 (0.8 mmol) in 4 ml of 2- propanol and the system thermostated at 40 °C or 82 °C; then the ketone (0.8 mmol in 1 ml of 2-propanol) was added in one portion ([sub] = 0.16 M). GC analysis was performed taking 0.3 ml of reaction mixture, the sample was treated with ammonium chloride.

4.2 Ruthenium(II) diamine-diphosphine complexes

Complexes synthesis

In order to simplify the comprehension of 1H NMR spectra the following labels were used: the phosphorous *trans* to the pyridine nitrogen is defined as P^{α}, the *cis* one as P^{β}; in chelating diphosphine ligands the labels were split in P^{α} and P^{β} considering the symmetry plane of the molecule perpendicular to the P-Ru-P plane; all the protons belonging to the diamine ligand were labelled with a superscripted N.

trans-[RuCl2((S)-CAMPY)(PPh3)2], 2-Ru_{ATH}

$[RuCl_2(PPh_3)_3]$ (640 mg, 0.67 mmol) was dissolved in CH_2Cl_2 (10 ml), and to the solution was added (S)-H-CAMPY (100 mg, 0.67 mmol) dissolved in CH_2Cl_2 (5 ml), the colour change immediately to orange. The solution was stirred at room temperature for 30 min. Solvent was partially evaporate to about 5 ml than dilution with 20 ml of degassed hexane give the product as a orange powder (yield 401 mg; 71%). ^{31}P-NMR ($CDCl_3$, 298K): δ ppm 43.1 (d, J = 31.5 Hz,1P^{α}), 39.2 (d, J = 32.0 Hz,1P^{β}); ^{1}H NMR (CDCl3, 298K): δ ppm 8.46 (dd, J = 3.4 Hz, 1H, H^{2N}), 7.58 (t, J = 8.5 Hz,

6H, $Ph^{P\beta}$), 7.47 (t, J = 8.5 Hz, 6H, $Ph^{P\alpha}$), 7.35-7.08 (m, 20 H,$Ph^{P\alpha/\beta}$,H^{4N}), 6.57 (dd, J = 7.4 Hz, 1H, H^{3N}), 5.12 (m, 1H, H^{8N}), 3.38 (m, 1H, NH_2), 3.10 (m, 1H, NH_2), 2.76 (d, J = 6.7 Hz, 2H, $CH_2{}^N$), 1.88 (m, 4H, $CH_2{}^N$). ^{13}C NMR (CDCl3, 298K): δ ppm 155.9, 136-127 (aromatic carbon), 56.5, 33.2, 27.7, 21.2. $C_{45}H_{42}Cl_2N_2P_2Ru$, PM 844, calc. C 63.98 H 5.01 N 3.32; found C 64.09 H 5.32 N 3.15.

cis-[RuCl2((S)-CAMPY)(PPh3)2], (*S*)-3-Ru_{ATH}

To complex 3 (50 mg, 0.059 mmol) was added dichloromethane (10 ml), the solution was sealed in a vial purged with nitrogen and stirred at room temperature for 5-7 days. Solvent was partially evaporated to reduced pressure to 2 ml and hexane (10 ml) was added to obtain an yellow solid (yield 43.3 mg; 87%). ^{31}P-NMR ($CDCl_3$, 298K): δ ppm 50.1 (d, J = 33.0 Hz, $1P^{\beta}$), 42.9 (d, J = 33.4 Hz, $1P^{\alpha}$); ^1H NMR ($CDCl_3$, 298K): δ ppm 9.19 (m, 1H, H^{2N}), 7.98 (s, 1H, $Ph^{P\alpha}$), 7.66 (t, J =8.4 Hz, 5H, $Ph^{P\alpha}$), 7.36 (m, 6H,$Ph^{P\beta}$,H^{4N}), 7.21 (m, 15H, $Ph^{P\alpha/\beta}$), 7.04 (m, 5H, $Ph^{P\beta}$), 6.93 (m, 1H, H^{3N}), 3.32 (m, 1H, NH_2), 2.92 (m, 1H, H^{8N}), 2.67 (m, 2H, $CH_2{}^N$), 1.82 (m, 1H, $CH_2{}^N$), 1.62 (m, 2H,$CH_2{}^N$, NH_2), 1.28 (m, 1H, $CH_2{}^N$), 0.92 (m, 1H, $CH_2{}^N$); ^{13}C NMR ($CDCl_3$, 298K): δ ppm 149.3 , 135.9-128.1 (aromatic carbon), 59.0, 32.7, 27.2, 21.7. $C_{45}H_{42}Cl_2N_2P_2Ru$, PM 844, calc. C 63.98 H 5.01 N 3.32; found C 63.51 H 5.40 N 3.01.

t,c-[RuHCl((S)-CAMPY)(PPh3)2], *S*-RuH

[$RuHCl(PPh_3)_3$] (57.8 mg, 0.062 mmol) was dissolved in benzene-d_6 (2 ml), and (S)-CAMPY (10 mg, 0.067 mmol) dissolved in benzene-d^6 (1 ml) was added into the solution, the colour change immediately to orange. The solution was stirred at room temperature for 1 h before NMR analysis. ^{31}P-$\{^1H\}$ NMR (121.5 MHz, CDCl3,298 K): δ ppm 74.3 (d, J = 37.0 Hz, 1P, P^{α}), 69.6 (d, J = 37.0 Hz, 1P,P^{β});^1H NMR (400.1 MHz, CDCl3, 298 K): δ ppm 8.62 (d, J = 5.5 Hz, 1H,H^{2N}), 8.24e8.08 (m, 10H, $Ph^{P\alpha/\beta}$), 7.11e7.03 (m, 10H, $Ph^{P\alpha}$), 7.02e6.93 (m, 10H, $Ph^{P\beta}$), 6.41 (d, J = 7.7 Hz, 1H, H^{4N}), 6.05 (dd,J = 7.7, 5.5 Hz, 1H, H^{3N}), 4.03 (m, 1H, H^{8N}), 3.11 (m, 1H, NH_2),2.38

(m, 1H, NH_2), 2.01e1.91 (m, 2H, $CH_2{}^N$), 1.17e1.07 (m, 2H, $CH_2{}^N$),1.02-0.9 (m, 2H, $CH_2{}^N$), -16.7 (dd, J (H,P) = 29.6, 23.1 Hz, iH).

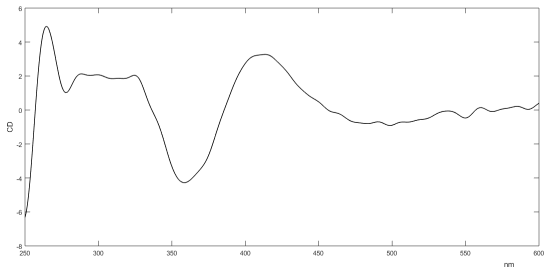

Figure 4.1: ECD spectra of ***S*-RuH** in isopropanol at root temperature.

4.3 η^6-arene ruthenium complexes

Levopimaric acid was isolated following the reported procedure [64], pure dehydroabietic acid was the obtained [173]. Menthylanisole was synthesis as reported [73], also [Ru(0)(COD)(COT)] and [Ru(0)(COD) (naphatlene)] complex were synthesised according to literature [71, 72].

Synthesis of menthoxybenzene

In a stainless steel autoclave (50 mL), equipped with temperature control and a magnetic stirrer, purged five times with hydrogen, a solution of *p*-Nitro-2-isopropyl(5-methylcyclohexyloxy)benzene (1.5 gr, 5.2 mmol), synthesized as reported [174], in methanol with 1% of Pd/C was transferred. The autoclave was pressurised at 10 atm and kept under stirring at room temperature for four hours. The mixture was then filtered on Celite and the solvent was evaporated in vacuo to give the product as yellowish oil. To a stirred solution of the obteined oil, in 2ml of H_2O/MeOH, 10 ml of H_3PO_3 2M were added and subsequently a solution $NaNO_2$. After 15 minutes the reaction was completed, The organic product were excrated

with CH_2Cl_2 and the solvent was evaporated in vacuo to give the product as yellowish oil. The product was then purify by distillation under reduced pressure (70 °C, 10^{-2} atm) and obtained as white solid in 42% yield. ^{1}H-NMR (300 MHz, $CDCl_3$) δ 7.35 – 7.24 (m), 6.98 – 6.89 (m), 4.06 (td, J = 10.5, 4.1 Hz), 2.34 – 2.13 (m), 1.82 – 1.68 (m), 1.63 – 1.42 (m), 1.21 – 0.99 (m), 0.99 – 0.90 (m), 0.84 – 0.76 (m).

General procedure for diene reaction with $RuCl_3$ and exchange with Ru(II) complexes

The reactions were conducted according with the reported procedure [66].

All the obtained products in the reaction with LPA were mixture of products, thus the assignment of the ^{1}H-NMR spectra were not possible. Elemental analysis: $C_{40}H_{56}O_4Ru_2Cl_4$ calculated: C 50.85 H 5.97 founded C 37.12 H 4.73

General procedure for complex synthesis via [Ru(0)(COD)(COT)]

In a solution of [Ru(0)(COD)(COT)] (0.2 mmol) in distilled eptane (5ml) adds ten equivalents of the arene, the shlenck tube was the put under 1 atm of H_2 and stirred for 8 hours. The solvent of the obtained brown suspension was evaporated in vacuo and then it was chromatographed under nitrogen atmosphere on neutral alumina with pentane/toluene (8/2) mixture. To the obtained pale yellow solution are added drops of HCl (12M) until the color turned red. The solvent was evaporated in vacuo, the products were dissolved in CH_2Cl_2, dried on Na_2SO_4 anhydrous, the solvent was evaporated and the obtained orange solid was washed 3 times with pentane.

[η^6-(m-methyl-anisole)-$RuCl_2$]$_2$

Brown/orange solid, yield 42%. Slightly soluble in $CHCl_3$. ^{1}H-NMR (300 MHz, DMSO-d_6) δ 6.10 (t, J = 5.7 Hz, 1H, H5), 5.61 (s, 1H, H2), 5.32 (dd, 1H, J = 6.1, 1.9 Hz), 5.14 (d, 1H, J = 5.5 Hz), 3.89 (s, 3H, OMe), 2.15 (s,

3H, Me), Elemental analysis: $C_{16}H_{20}O_2Ru_2Cl_4$ calculated C 32.67 H 3.43, founded C 32.65 H 3.45.

[η^6-menthoxybenzene-$RuCl_2$]$_2$

Orange solid, yield 35%. Slightly soluble in $CHCl_3$. ^{1}H-NMR (300 MHz, DMSO-d_6) δ 6.09 (dd, J = 13.4, 6.6 Hz, 2H), 5.59 (d, J = 6.7 Hz, 1H), 5.51 (d, J = 5.4 Hz, 1H), 5.34 (t, J = 5.3 Hz, 1H), 4.39 (td, J = 10.2, 4.4 Hz, 1H), 2.39 – 2.06 (m,2H), 1.65 (d, J = 9.9 Hz, 1H), 1.45 (s, 2H), 1.25 (s, 2H), 1.00 (d, J = 12.0 Hz, 1H), 0.96 – 0.81 (m, 7H), 0.74 (d, J = 6.8 Hz, 3H). Elemental analysis: $C_{32}H_{48}O_2Ru_2Cl_4$ calculated C 46.22 H 5.75, founded C 47.53 H 5.98.

[η^6-menthylanisole-$RuCl_2$]$_2$

brown solid, yield 60%. Slightly soluble in $CHCl_3$. The ^{1}H-NMR was difficult to analyse, due to the broawded and overlay peaks.

[η^6-menthoxybenzene-Ru (Ts-en)Cl]

In a suspension of [η^6-menthoxybenzene-$RuCl_2$]$_2$ in isopropanol were added 2eq. of Ts-en and 4eq. of TEA. The reaction mixture was refluxed for 4 hours and than the solvent was evaporated and the obtained brown/orange solid was washed 3 times with water. The products were dissolved in CH_2Cl_2, dried on Na_2SO_4 anhydrous, the solvent was evaporated given the products in 80% yields. Brown/orange solid, ^{1}H-NMR (300 MHz, $CDCl_3$) δ 7.75 (d, J = 8.1 Hz, 2H), 7.16 (d, J = 8.0 Hz, 2H), 6.53 – 6.45 (m), 6.37 (s), 5.87 (s), 5.56 (s), 5.45 (s), 5.12 (s), 5.09 – 5.00 (m), 4.99 – 4.92 (m), 4.36 (s), 3.99 (d, J = 10.7 Hz), 3.39 (s), 3.10 (s), 2.83 (s), 2.39 (d, J = 30.6 Hz), 1.75 (d, J = 10.1 Hz), 1.66 – 1.34 (m), 1.25 – 0.98 (m), 0.96 (d, J = 6.6 Hz), 0.77 (d, J = 6.1 Hz). The obtained product was a mixture of the two possible diastereomer, with a d.e. measured by ^{1}H-NMR up to 19%.

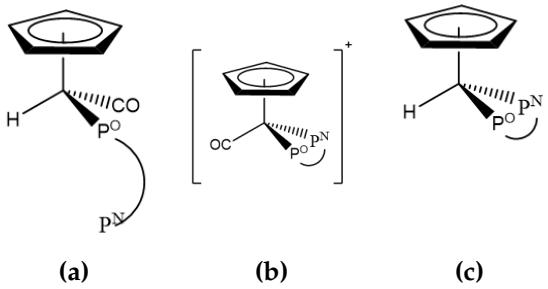

Figure 4.2: Species obteined in the reaction of Prolophos with [η^5-CpFe(CO)$_2$H]: (a) mono substitued complex, the diphosphine is coordinated via P^O phosphorous (b) Chelate cationic species (c) Chelate hydride complex.

[η^6-menthylanisole-Ru (Ts-en)Cl

It was prepared in situ (ATH) and not characterized.

4.4 η^5-cyclopentadienyl-Iron(II) hydride complex

(*S*)-Prolophos [82] and [η^5-CpFe(CO)$_2$]K [81] were synthesised according to literature.

Reaction of [η^5-CpFe(CO)$_2$H] with (*S*)-Prolophos I

0.42 mmol of [η^5-CpFe(CO)$_2$]K were dissolved in freshly distilled THF and cooled at -31 °C in water/methanol bath, under stirring, at the red solution was added 1 eq of glacial MeCOOH. The solution change colour into brown/yellow and after 5 minutes 200 mg (0.42 mmol) of (*S*)-Prolophos were added; the solution lighten and under stirring was let warmed to room temperature. After three hours the colours turned into yellow. The reaction was monitored by IR spectrometry until the carbonylic band of [η^5-CpFe(CO)$_2$H] disappeared (1925 cm^{-1}). The suspension was filtered on celite and the solvent was evaporated in vacuo providing the

products as a mixture of complexes 4.2a and 4.2b. IR: 1968, 1936 cm^{-1}. $^{31}P\{^1H\}$-NMR(121MHz, $CDCl_3$) δ 186.48 (s, 1P, P^O 4.2a), 174.15 (d, J = 61 Hz, 0.1P, P^O 4.2b), 171.75 (d, J = 77 Hz, 0.3P, P^O 4.2b), 120.34 (d, J = 61 Hz, 0.1P, P^N 4.2b), 112.74 (d, J = 77 Hz, 0.3P, P^N 4.2b), 49.84 – 46.16 (m, 1P, P^N 4.2a). ^1H-NMR (300 MHz, $CDCl_3$) δ overlay multiplets, -12.96 (d, J (H,P) = 81.8 Hz).

Thermolysis of mixture I

A sample of the obtained mixture I was dissolved in THF and heated to reflux for 16 hours, during which time no appreciable change in colour was observed. IR: 1968, 1936 cm^{-1}. $^{31}P\{^1H\}$-NMR(121MHz, $CDCl_3$) δ 186.48 (s, 1P, P^O 4.2a), 171.75 (d, J = 77 Hz, 1.1P, P^O 4.2b), 115 (s, 0.5P, P^O free ligand), 112.74 (d, J = 77 Hz, 1.1P, P^N 4.2b), 49.84 – 46.16 (m, 1.5P, P^N 4.2a + free ligand).

Conversion of I in $CHCl_3$

A sample of I was dissolved in $CHCl_3$ and stirred at RT per 16 hours. The reaction produced the only cationic complex 4.2b with a d.e. of 87%. The product can be isolated in enantiomeric pure form as reported in ref. [84]. IR: 1967. $^{31}P\{^1H\}$-NMR(121MHz, $CDCl_3$) δ 178 (d, J = 67 Hz, 0.07P, P^O 4.2b), 169 (d, J = 77 Hz, 1P, P^O 4.2b), 120 (d, J = 67 Hz, 0.07P, P^N 4.2b), 110 (d, J = 77 Hz, 1P, P^N 4.2b).

Reaction of [η^5-CpFe(CO)$_2$H] with (*S*)-Prolophos with UV irradiation II

0.42 mmol of [η^5-CpFe(CO)$_2$]K dissolved in freshly distilled THF were placed in a quartz tube and cooled at -31 °C in water/methanol bath. Under stirring, at the red solution was added 1 eq of glacial MeCOOH. The solution change colour into brown/yellow and after 5 minutes 200 mg (0.42 mmol) of (*S*)-Prolophos were added; the solution was irradiated with a Phillips high-pressure Mercury 125-W lamp for 4 hours. The reaction was monitored by IR spectrometry. The suspension was filtered on celite and the solvent was evaporated in vacuo providing the products as

a mixture of complexes 4.2a and 4.2b. IR: 1968; $^{31}P\{^{1}H\}$-NMR(121MHz, $CDCl_3$) δ 192.45 (d, J = 100 Hz, 0.3P, P^O 4.2c), 187.08 (d, J = 87 Hz, 1P, P^O 4.2c), 185.47 (s, 1P, P^O 4.2a), 139.27 (d, J = 87 Hz, 1P, P^N 4.2c), 136.70 (d, J = 100 Hz, 0.3P, P^N 4.2c), 50.74 – 45.44 (m, 1P, P^N 4.2a); ^{1}H-NMR (300 MHz, $CDCl_3$) δ overlay multiplets, -12.96 (d, J (H,P) = 81.8 Hz, 1H, 4.2a), -14.32 (dd, J (H,P) = 72, 72 Hz, 0.3H, 4.2c), -14.62 (dd, J (H,P) = 68, 72 Hz, 1H, 4.2c).

4.5 Ruthenium carbonyl complexes

Complexes synthesis

The complexes were synthesized as reported in references [91, 89, 90] with freshly distilled n-heptane as reaction solvents and separated by flash chromatography (silica gel; cyclohexane/ethylacetate, 9/1, 1psi), while cationic complexes were synthesized starting from the enatiopure chloride complexes. As general consideration, in chromatography the first eluted complex has $\bar{S}$ configuration in menthyl-Cp complexes, whereas has $\bar{R}$ configuration in the neomenthyl-Cp ones. For neomenthyl-Cp complexes the full NMR characterization were not done, since they were conformed to literature, their ^{1}H-NMR and $^{31}P\{^{1}H\}$-NMR here are not reported.

T-4-S_{Ru}-η^5-[(1*R*,2*S*,5*R*)-menthyl)-C_5H_4)Ru(CO)(P(C_6H_5)$_3$)Cl] ($\bar{S}$-RuCl)

Yellow powder. ^{1}H-NMR (300 MHz, $CDCl_3$) δ 7.65-7.52 (m, 6H, oPh), 7.46-7.34 (m, 9H, mPh/pPh), 5.15 (s, 1H, H1), 4.72 (s, 1H, H4), 4.68 (s, 1H, H2), 3.78 (s, 1H, H3), 2.34-2.18 (m, 2H, H7/H5), 1.94-1.62 (m, 3H, H17/ H12/ H15), 1.56-1.41 (m, 1H, H8), 1.16-0.97 (m, 2H, H14/ H16), 0.95 (d, J = 6.5 Hz, 3H, C10), 0.90 (m, 2H, H6/H13), 0.86 (d, J = 6.9 Hz, 3H, C16), 0.82 (d, J = 6.8 Hz, 3H, C15); $^{31}P\{^{1}H\}$-NMR(121MHz, $CDCl_3$) δ 49.08 (s,1P); $^{13}C\{^{1}H\}$-NMR (75 MHz, $CDCl_3$) δ 204.78 (d, J (C,P)= 21.1 Hz, CO), 135.47 (dd, J (C,P)= 47.3 Hz, CP), 134.03 (d, J (C,P)= 10.8 Hz, oPh), 130.54 (s, J

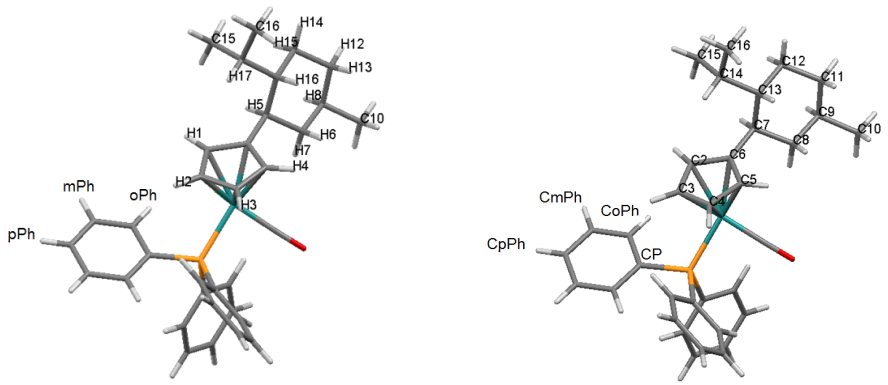

(a) **(b)**

Figure 4.3: Proton (left) and carbon (right) labels used in NMR assignations. For ($\bar{R}$)Ru configuration were retained the same labels

(C,P)= 2.1 Hz, pPh), 128.62 (d, J (C,P)= 10.2 Hz, mPh), 114.27 (d, J (C,P)= 8.0 Hz, C6), 94.79 (s,C2), 89.86 (s,C3), 79.82 (d, J (C,P)= 2.3 Hz, C5), 75.14 (s,C4), 50.89 (s, C13), 43.53 (s, C8), 38.42 (s, C7), 35.64 (s, C11), 33.34 (s, C9), 27.84 (s, C14), 25.15 (s, C12), 22.85 (s, C10), 22.07 (s, C16), 16.04 (s, C15); IR 1957 cm^{-1} vs(CO stretching),1482,1457,1436 cm^{-1} m (aromatics and HCH bendings),1386,1370, 1349, 1261, cm^{-1} w (methyl and aromatic deformations) 1187,1095 cm^{-1} s (PPh_3 CC stretchings); EA $C_{34}H_{38}ClOPRu$ calculated C: 64.81%, H: 6.04% found: C: 65.12%, H: 6.11%.

T-4-R_{Ru}-η^5-[(1*R*,2*S*,5*R*)-menthyl)-C_5H_4)Ru(CO)(P(C_6H_5)$_3$)Cl] ($\bar{R}$-RuCl)

Yellow powder. ^{1}H-NMR (300 MHz, $CDCl_3$) δ 7.68-7.47 (m, 6H, oPh), 7.42 (m, 9H, mPh/pPh), 5.23 (s, 1H, H4), 4.80 (s, 1H, H3), 4.50 (s, 1H, H2), 4.22 (s, 1H, H1), 2.14 (m, 1H, H7), 1.93-1.75 (m, 1H, H5), 1.73-1.53 (m, 3H, H17/ H12/ H15), 1.49-1.34 (m, 1H, H8), 1.19-0.98 (m, 1H, H6), 0.94 (d, J = 6.4 Hz, 3H, C10), 0.98-0.86 (m, 3H, H14/H16/H13), 0.83 (d, J = 6.8 Hz, 3H, C16), 0.69 (d, J = 6.7 Hz, 3H, C15).; ^{31}P{^{1}H}-NMR(121MHz, $CDCl_3$)

δ 49.18 (s,1P); $^{13}C\{^1H\}$-NMR (75 MHz, $CDCl_3$) δ 204.80 (d, J (C,P)= 21.3 Hz, CO), 135.60 (d, J (C,P)= 47.4 Hz, CP), 134.00 (d, J (C,P)= 10.8 Hz, oPh), 130.55 (s, J (C,P)= 2.26 Hz, pPh), 128.64 (d, J (C,P)= 10.2 Hz, mPh), 113.83 (d, J (C,P)= 4.2 Hz, C6), 91.01 (d, J (C,P)= 4.9 Hz, C5), 86.95 (s, C4), 84.80 (s, C3), 78.89 (s, C2), 51.12 (s, C13), 43.32 (s, C8), 39.31 (s, C7), 35.55 (s,C11), 33.38(s, C9), 33.18(s, C14), 27.48 (s, C12), 22.74 (s, C10), 21.93(s, C16), 15.92 (s, C15); IR 1957 cm^{-1} vs(CO stretching),1482,1457,1436 cm^{-1} m (aromatics and HCH bendings),1386,1370, 1349, 1261, cm^{-1} w (methyl and aromatic deformations) 1187,1095 cm^{-1} s (PPh_3 CC stretchings); EA $C_{34}H_{38}ClOPRu$ calculated C: 64.81%, H: 6.04% found: C:65.08%, H: 5.93%.

T-4-R_{Ru}-η^5-[(1*R*,2*S*,5*R*)-menthyl)-C_5H_4)Ru(CO)($P(C_6H_5)_3$)Br] ($\bar{S}$-RuBr)

Yellow powder. ^{1}H-NMR (300 MHz, $CDCl_3$) δ 7.62-7.50 (m, 6H, oPh), 7.45-7.34 (m, 9H, mPh/pPh), 5.28 (s, 1H, H1), 4.74 (s, 1H, H4), 4.61 (s, 1H, H2), 3.78 (s, 1H, H3), 2.40-2.20 (m, 2H, H7/H5), 1.90-1.63 (m, 3H, H17/ H12/ H15), 1.56-1.41 (m, 1H, H8), 1.16-0.97 (m, 2H, H14/ H16), 0.95 (d, J = 6.5 Hz, 3H, C10), 0.90 (m, 2H, H6/H13), 0.86 (d, J = 6.9 Hz, 3H, C16), 0.82 (d, J = 6.8 Hz, 3H, C15); $^{31}P\{^1H\}$-NMR(121MHz, $CDCl_3$) δ 48.50 (s,1P); $^{13}C\{^1H\}$-NMR (75 MHz, $CDCl_3$) δ 204.50 (d, J (C,P)= 21.6 Hz, CO), 135.89 (d, J (C,P)= 47.36 Hz, CP), 134.11 (d, J (C,P)= 10.5 Hz, oPh), 130.51 (d,J (C,P)= 2 Hz, pPh), 128.57 (d, J (C,P)= 9.95 Hz, mPh), 112.45 (d, J (C,P)= 8.41 Hz, C6), 95.57 (s, C2), 89.64 (s, C3), 80.37 (s, C5), 76.30 (s, C4), 50.95 (s, C13), 44.05 (s, C8), 38.42 (s, C7), 35.58 (s,C11), 33.34(s, C9), 27.86(s, C14), 25.03 (s, C12), 22.90 (s, C10), 22.04(s, C16), 15.99 (s, C15); IR 1957 cm^{-1} vs(CO stretching); EA $C_{34}H_{38}BrOPRu$ calculated C: 60.53%, H: 5.68% found: C:60.85%, H: 5.72%.

T-4-S_{Ru}-η^5-[(1*R*,2*S*,5*R*)-menthyl)-C_5H_4)Ru(CO)($P(C_6H_5)_3$)Br] ($\bar{R}$-RuBr)

Yellow powder. ^{1}H-NMR (300 MHz, $CDCl_3$) δ 7.64-7.51 (m, 6H,-oPh), 7.46-7.34 (m, 9H, mPh/pPh), 5.24 (s, 1H, H4), 4.78 (s, 1H, H3), 4.50 (s, 1H, H2),

4.25 (s, 1H, H1), 2.15 (m, 1H ,H7), 1.93-1.75(m, 1H, H5), 1.73-1.53 (m, 3H, H17/ H12/ H15), 1.49-1.34 (m, 1H, H8), 1.19-0.98 (m, 1H, H6), 0.95 (d, J = 6.5 Hz, 3H, C10), 0.98-0.86 (m, 3H, H14/ H16/ H13), 0.83 (d, J = 6.9 Hz, 3H, C16), 0.70 (d, J = 6.8 Hz, 3H, C15).; $^{31}P\{^{1}H\}$-NMR(121MHz, $CDCl_3$) δ 49.19 (s,1P); $^{13}C\{^{1}H\}$-NMR (75 MHz, $CDCl_3$) δ 204.30 (d, J (C,P)= 21.88 Hz, CO), 135.70 (d, J (C,P)= 47.5 Hz, CP), 134.05 (d, J (C,P)= 10.5 Hz, oPh), 130.53 (d,J (C,P)= 2.04 Hz, pPh), 128.59 (d, J (C,P)= 9.95 Hz, mPh), 113.44 (s, C6), 90.83 (d, J (C,P)= 5.53 Hz, C5), 86.76 (s, C4), 85.67 (s, C3), 79.34 (s, C2), 51.15 (s, C13), 43.78 (s, C8), 39.35 (s, C7), 35.42 (s,C11), 33.45(s, C9), 27.81(s, C14), 25.04 (s, C12), 22.82 (s, C10), 21.96(s, C16), 15.87 (s, C15); IR 1959 cm^{-1} vs(CO stretching); EA $C_{34}H_{38}BrOPRu$ calculated C: 60.53%, H: 5.68% found: C:60.62%, H: 5.70%.

T-4-R_{Ru}-η^5-[(1*R*,2*S*,5*R*)-menthyl)-C_5H_4)Ru(CO)(P(C_6H_5)$_3$)I] ($\bar{S}$-RuI)

Yellow powder. ^{1}H-NMR (300 MHz, $CDCl_3$) δ 7.62-7.48 (m, 6H, oPh), 7.46-7.36 (m, 9H, mPh/pPh), 5.35 (s, 1H, H1), 4.79 (s, 1H, H4), 4.46 (s, 1H, H2), 3.98 (s, 1H, H3), 2.34 (t,J = 9.93 Hz, 1H, H5), 2.23 (m, J = 12.46 Hz, 1H, H7), 1.83-1.73 (m, 2H, H17/H12), 1.72-1.65 (m, 1H,H15), 1.56-1.41 (m, 1H, H8), 1.16-0.97 (m, 2H, H14/H16), 0.95 (d, J = 6.4 Hz, 3H, C10), 0.90 (m, 2H, H6/H13), 0.84 (d, J = 6.8 Hz, 3H, C16), 0.80 (d, J = 6.78 Hz, 3H, C15); $^{31}P\{^{1}H\}$-NMR(121MHz, $CDCl_3$) δ 48.78 (s,1P); $^{13}C\{^{1}H\}$-NMR (75 MHz, $CDCl_3$) δ 204.01 (d, J (C,P)= 20.26 Hz, CO), 136.08 (d, J (C,P)= 47.66 Hz, CP), 133.86 (d, J (C,P)= 10.0 Hz, oPh), 130.10 (s, pPh), 128.11 (d, J (C,P)= 9.40 Hz, mPh), 110.53 (d, J (C,P)= 6.97 Hz, C6), 94.50 (s, C2), 88.03 (s, C3), 80.81 (s, C5), 79.01 (s, C4), 50.60 (s, C13), 44.72 (s, C8), 38.33 (s, C7), 35.14 (s,C11), 32.96(s, C9), 27.50(s, C14), 24.57 (s, C12), 22.50 (s, C10), 21.63(s, C16), 15.56 (s, C15); IR 1957 cm^{-1} vs(CO stretching); EA $C_{34}H_{38}IOPRu$ calculated C: 56.59%, H: 5.31% found: C:56.76%, H: 5.38%.

T-4-S_{Ru}-η^5-[(1*R*,2*S*,5*R*)-menthyl)-C_5H_4)Ru(CO)($P(C_6H_5)_3$)I] ($\bar{R}$-RuI)

Yellow powder. ^{1}H-NMR (300 MHz, $CDCl_3$) δ 7.59–7.48 (m, 6H,oPh), 7.46-7.35 (m, 9H, mPh/pPh), 5.29 (s, 1H, H4), 4.77 (s, 1H, H3), 4.46 (s, 1H, H2), 4.40 (s, 1H, H1), 2.15 (d, J = 12.97 Hz, 1H, H7), 1.96(t, J = 9.51 Hz, 1H, H5), 1.73-1.53 (m, 3H, H17/ H12/ H15), 1.49-1.34 (m, 1H, H8), 1.19 – 0.98 (m, 1H, H6), 0.95 (d, J = 6.3 Hz, 3H, C10), 0.98-0.86 (m, 3H, H14/ H16/ H13), 0.83 (d, J = 7.3 Hz, 3H, C16), 0.71 (d, J = 6.7 Hz, 3H, C15).; ^{31}P{^{1}H}-NMR(121MHz, $CDCl_3$) δ 49.66(s,1P); ^{13}C{^{1}H}-NMR (75 MHz, $CDCl_3$) δ 203.77 (d, J (C,P)= 21.11 Hz, CO), 136.03 (d, J (C,P)= 48.02 Hz, CP), 133.75 (d, J (C,P)= 10.3 Hz, oPh), 130.13 (s, pPh), 128.14 (d, J (C,P)= 9.0 Hz, mPh), 112.77 (s, C6), 88.83 (s, C5), 86.08 (s, C4), 85.64 (s, C3), 80.95 (s, C2), 50.82 (s, C13), 43.92 (s, C8), 39.03 (s, C7), 34.99 (s,C11), 33.15(s, C9), 27.41(s, C14), 24.63 (s, C12), 22.41 (s, C10), 21.57(s, C16), 15.49 (s, C15); IR 1959 cm-1 vs(CO stretching); IR 1957 cm^{-1} vs(CO stretching); EA $C_{34}H_{38}IOPRu$ calculated C: 56.59%, H: 5.31% found: C:56.81%, H: 5.43%.

T-4-R_{Ru}-η^5-[(1*R*,2*S*,5*R*)-menthyl)-C_5H_4)Ru(CO)($P(C_6H_5)_3$) (CH_3CN]BF_4 ($\bar{S}$-Ru^+)

Yellow powder. ^{1}H-NMR (300 MHz, $CDCl_3$) δ 7.57–7.47 (m, 6H,oPh), 7.43-7.32 (m, 9H, mPh/ pPh), 5.54 (s, 1H, H1), 4.92 (s, 1H, H4), 4.71 (s, 1H, H2), 4.40 (s, 1H, H3), 2.34-2.18 (m, 2H, H7/H5), 2.24 (s, 3H, CH_3CN), 1.94–1.62 (m, 3H, H17/ H12/ H15), 1.56-1.41 (m, 1H, H8), 1.16-0.97 (m, 2H, H14/H16), 0.93 (d, J = 6.4 Hz, 3H, C10), 0.90 (m, 2H, H6/H13), 0.84 (d, J = 6.8 Hz, 3H, C16), 0.83 (d, J = 6.7 Hz, 3H, C15); ^{31}P{^{1}H}-NMR(121MHz, $CDCl_3$) δ 50.07 (s,1P); ^{13}C{^{1}H}-NMR (75 MHz, $CDCl_3$) δ 201.71 (d, J (C,P)= 20.26 Hz, CO), 133.68 (d, J (C,P)= 11.1 Hz, oPh), 132.74 (d, J (C,P)= 50.3 Hz, CP), 131.63 (d, J (C,P)= 2.2 Hz, pPh), 130.03 (s,CH_3CN), 129.48 (d, J (C,P)= 11.1 Hz, mPh), 118.16 (d, J (C,P)= 6.1 Hz, C6), 94.02(s, C2), 90.29 (s, C3), 79.31 (s, C5), 77.77 (s, C4), 50.92 (s, C13), 45.06 (s, C8), 38.55 (s, C7), 35.25 (s,C11), 33.26(s, C9), 27.99(s, C14), 24.83 (s, C12), 22.88 (s, C10), 22.01(s, C16), 15.79 (s, C15), 2.57 (s,CH_3CN) ; IR 1984 cm^{-1} vs(CO stretch-

ing); EA $C_{34}H_{38}IOPRu$ calculated C: 59.84%, H: 5.72% found: C:59.15%, H: 5.74%.

T-4-S_{Ru}-η^5-[(1*R*,2*S*,5*R*)-menthyl)-C_5H_4)Ru(CO)(P(C_6H_5)$_3$) (CH_3CN]BF_4 ($\bar{R}$-RuBF$_4$)

Yellow powder. ^{1}H-NMR (300 MHz, $CDCl_3$) δ 7.58-7.48 (m, 6H, oPh), 7.44-7.31 (m, 9H, mPh/pPh), 5.83 (s, 1H, H4), 5.14 (s, 1H, H3), 4.50 (s, 2H, H2/H1), 2.22 (s, 3H, CH_3CN), 2.14-1.90(m, 1H, H5), 1.87-1.68 (m, 3H, H7/ H12/ H15), 1.62 (m, 1H, H17), 1.49-1.34 (m, 1H, H8), 1.26 (m, 1H, H6), 0.96 (d, J = 6.4 Hz, 3H, C10), 1.12 (m, 1H, H16),1.03 (m, 1H, H14), 0.93 (m, 1H, H13), 0.85 (d, J = 6.9 Hz, 3H, C16), 0.75 (d, J = 6.9 Hz, 3H, C15).; ^{31}P{^{1}H}-NMR(121MHz, $CDCl_3$) δ 50.38 (s,1P); ^{13}C{^{1}H}-NMR (75 MHz, $CDCl_3$) δ 201.91 (d, J (C,P)= 18.8 Hz, CO), 133.66 (d, J (C,P)= 11.1 Hz, oPh), 132.79 (d, J (C,P)= 50.3 Hz, CP), 131.60 (d, J (C,P)= 2.8 Hz, pPh), 130.20 (s,CH_3CN), 129.45 (d, J (C,P)= 10.5 Hz, mPh), 115.00 (d, J (C,P)= 6.1 Hz, C6), 94.5 (d, J (C,P)= 3.9 Hz, C5), 87.66 (s, C4), 86.46 (s, C3), 78.11 (s, C2), 50.92 (s, C13), 44.92 (s, C8), 39.38 (s, C7), 34.98 (s,C11), 33.55(s, C9), 28.01(s, C14), 24.91 (s, C12), 22.75 (s, C10), 21.82(s, C16), 15.88 (s, C15);IR 1981 cm^{-1} vs(CO stretching); EA $C_{34}H_{38}IOPRu$ calculated C: 59.84%, H: 5.72% found: C:59.78%, H: 5.72%.

VCD Experimental data

VCD spectra have been taken for CCl_4 solutions in the range 2100-850 cm-1. In the range 2100-1800 cm^{-1} we set 8 cm^{-1} resolution (concentration 0.036M), while in the range 1700-850 cm-1 we set 4 cm-1 resolution with concentrations 0.09M for (*R*)-RuCl and 0.073 (*S*)-RuCl. In both frequency regions 2000 scans were accumulated and averaged, a 200 µm pathlength BaF2 cell was employed. The region between 1800 and 2400 cm-1 has been calibrated by running the spectra of (3*R*)-methylcyclopentanone-d_4 [175].

Matrices of peak intensities

In tables 4.1 and 4.2 we reported the matrices A of the two diastereomers S_{Ru}-RuCl and R_{Ru}-RuCl. The integration of the peaks intensity of the NOESY spectra recorded with (τm) = 1.3 s provided the matrices of peaks I; A are given by $I_{ij} \div M_j^0$ where M^0 is the matrix of equilibrium magnetization (the intensity of diagonal peaks at τ_m = 0).

DFT calculations

DFT calculations were conducted with G09; the complex was treated in vacuo with a choice of functional and basis functions analogous to ref. [101]: B97D/SVP. The conformational search was carried out by first starting from the conformer of (*S*)-RuCl determined by x-ray, introducing a pseudo atom PSu at the center of the cyclopentadienyl ring, and drawing a line PSu-Ru around which the ring was rotated in five successive steps. For each one of the five positions thus reached, the menthyl moiety was allowed to rotate to avoid steric hindrance and the two orientations 0° and 180°of the menthyl moiety (referring to dihedral angle Ru-PSu-menthyl-isopropyl) have been tested. The lowest energy four conformers optimized at B97D/SVP level for both (*R*)-RuCl and (*S*)-RuCl, are shown in Figure 4SI and most representative distances are reported in table 2.2.

4.6 Iridium complexes

In the following section, when the counter-anion is omitted it is meant to be Cl^-.

Complexes synthesis

Synthesis of diastereoisomeric mixture

To a solution of $[(ppy)_2Ir(\mu-Cl)]_2$ (100 mg, 0.093 mmol) in CH_2Cl_2/ MeOH (20 mL, 3:1 v/v) was added an enatiomerically pure diamine, Me-campy or H-campy, (1.1 eq) and heated to reflux for 6 h [145]. The solution was

Table 4.1: A matrix of (*S*)-RuCl

	oPh	mPh	H1	H4	H2	H3	H5	H7	H17	H12	H8	C10	H6	H13	C15
oPh	107.11	9.72	0.58	0.13	0.77	0.75	0	0.04	0	0	0	0	0	0	0
mPh	3.77	159.89	0	0	0	0	0	0	0	0	0	0	0	0	0
H1	0.67	0	17.45	0	0.84	0	0.5	0	0.55	0	0	0	0	0	0,5
H4	0.16	0	0	15.81	0	0.82	0	0.04	0.06	0	0	0	0.97	0	0
H2	0.96	0	0.83	0	16.88	0.81	0	0	0.03	0	0	0	0	0	0
H3	0.75	0	0	0.83	0.81	16.57	0	0	0	0	0	0	0	0	0
H5	0	0	0.51	0	0	0	8.53	0	0	0	0	0	0	0	0,45
H7	0.04	0	0	0.05	0	0	0	8.53	0	0	1.47	0	3.44	0	0
H17	0	0	0.53	0.09	0.03	0	0	0	9.43	0	0	0	0	0	1,14
H12	0	0	0	0	0	0	0	0	0	9.43	0.22	0	0	3.23	0
H8	0	0	0	0	0	0	0	1.08	0	0.43	12.14	0.53	0	0	0
C10	0	0	0	0	0	0	0	0	0	0	0.47	19.44	0	0	0
H6	0	0	0	0.89	0	0	0	3.5	0	0	0	0	7.85	0	0
H13	0	0	0	0	0	0	0	0	0	3.66	0	0	0	7.85	0
C15	0	0	0.57	0	0	0	0.45	0	1.47	0	0	0	0	0	23,55

Table 4.2: A matrix of (*R*)-RuCl

	oPh	mPh	H1	H2	H3	H4	H7	H5	H17	H8	H6	C15
oPh	130.09	5.26	0.22	0.81	0.9	0.67	0.16	0	0	0	0	0
mPh	4.79	163.94	0.01	0.08	0.08	0.04	0	0	0	0	0	0
H1	0.22	0.02	16.1	0.78	0	0	0	0	0	0	1.01	0
H2	0.81	0.07	0.75	17.69	0.68	0	0	0	0	0	0	0
H3	0.86	0.1	0	0.68	16.32	0.67	0	0	0	0	0	0
H4	0.61	0.06	0	0	0.67	14.71	0	0.62	0.78	0	0	0,53
H7	0.16	0	0	0	0	0	8.54	0.59	0	0.8	2.91	0
H5	0	0	0	0	0	0.65	0.61	19.21	0	0.8	0	0,75
H17	0	0	0	0	0	0.78	0	0	15.04	0	0	0,82
H8	0	0	0	0	0	0	0.84	0.8	0	21.03	0	0
H6	0	0	0.95	0	0	0	2.88	0	0	0	11.79	0
C15	0	0	0	0	0	0.52	0	0.8	0.085	0	0	22,95

Table 4.3: For each diastomers, S_{Ru}-RuCl and R_{Ru}-RuCl, the four structure relative to table 4.4 are reported.

S_{Ru}-RuCl			
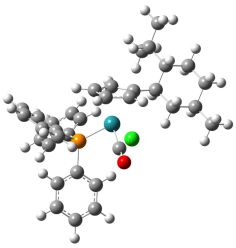	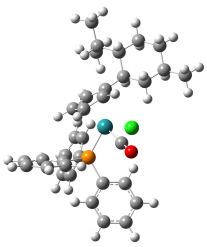	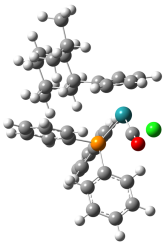	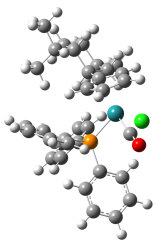
a	b	c	d
R_{Ru}-RuCl			
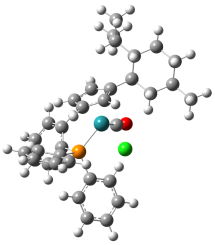	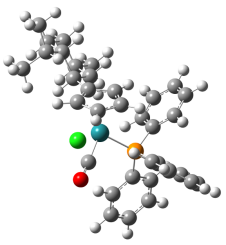	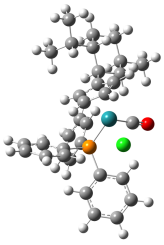	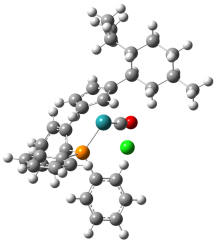
a	b	c	d

allowed to cool to room temperature and the solvent evaporated. The yellow residue was dissolved in 10 mL of CH_2Cl_2 and filtered. Solvent was partially evaporated up to 2 mL then 5 mL of diethyl ether were added to obtain the products as yellow powder (yield up to 90

NMR measurement of Δ,Λ*S*-Ir-Me-Campy mixture

^{1}1H-NMR (400 MHz, $CDCl_3$) δ: 10.02 (d, J = 5.7 Hz, 1H), 9.90 (d, J = 5.6 Hz, 1H), 8.04 (d, J = 5.8 Hz, 1H), 7.97 (d, J = 8.2 Hz, 2H), 7.94–7.75 (m, 6H), 7.62 (d, J = 7.6 Hz, 1H), 7.58–7.52 (m, 3H), 7.50–7.41 (m, 3H), 7.39

Table 4.4: Atom-atom distances in (*S*)-RuCl and (*R*)-RuCl as evaluated from NOE spectra; X-Ray diffraction data; DFT calculated data of the lowest energy structures.

S-RuCl	XRD	NOE	a	b	c	d	*R*-RuCl	NOE	a	b	c	d
H1 - H5	2.69	2.8	2.7	2.6	2.8	2.8	H1 - H5	2.8	2.7	2.8	2.6	2.9
H1 -H17	2.92	2.8	2.6	3.1	2.6	2.5	H1 -H17	2.7	2.9	2.4	3.0	2.2
H1 - C15	2.77	2.9	2.3	2.6	2.4	2.3	H1 - C15	2.8	2.5	2.3	2.5	2.4
H4 - H6	2.41	2.5	2.3	2.4	2.2	2.3	H4 - H6	2.4	2.3	2.3	2.5	2.3
H4 - H7	3.21	3.7	2.9	3.3	3	2.7	H4 - H7	n.d.	3.1	2.6	3.4	2.5
H1 - oPh	3.18	3.1	2.2	2.4	2.6	3	H1 - oPh	2.9	2.6	4.9	3.0	4.5
H4- oPh	5.85	4.0	5	4.4	2.7	4.2	H4- oPh	3.7	4.2	3.5	4.5	2.3
H2 - oPh	2.8	2.9	3.1	2.8	4.5	3.2	H2 - oPh	2.8	2.6	2.8	3.0	3.0
H3 - oPh	2.78	3.0	3.1	3.1	4.3	5.2	H3 - oPh	2.9	3.1	2.4	4.4	2.8
H7- oPh	4.3	4.6	4.6	4.3	2.5	2.1	H7- oPh	4.2	4.5	2.3	2.1	4.7

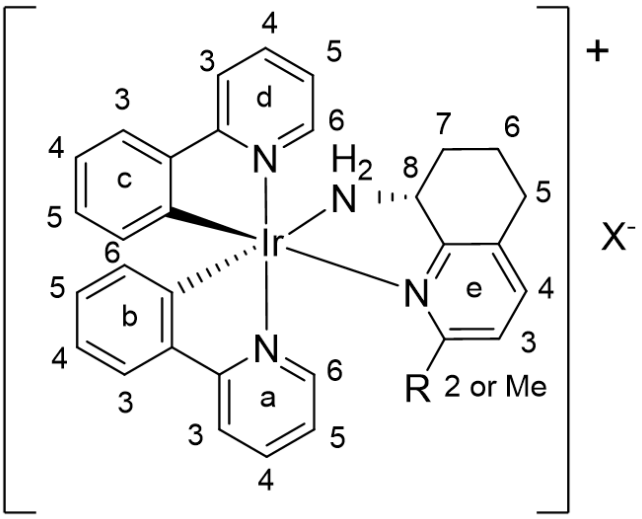

Figure 4.4: Labels used in ^{1}H-NMR assignments

(t, J = 6.2 Hz, 1H), 7.27–7.23 (m, 1H), 7.14 (t, J = 6.5 Hz, 1H), 7.05–6.99 (m, 2H), 6.96–6.83 (m, 6H), 6.81–6.60 (m, 5H), 6.26 (d, J = 7.8 Hz, 1H), 6.13 (d, J = 7.4 Hz, 2H), 6.01 (d, J = 7.8 Hz, 1H), 4.94 (m, 1H), 3.79 (s, 1H), 3.33–3.18 (m, 2H), 3.18–2.62 (m, 4H), 2.27–2.16 (m, 1H), 2.16–1.90 (m, 4H), 1.87 (s, 3H), 1.71 (s, 3H), 1.70–1.51 (m, 5H). MS (FAB): m/z 663 [M]+, 501 $[Ir(ppy)_2]^+$. CHN calculated: C 54.82%, H 4.33%, N 7.97% found: C 55.04%, H 4.33%, N 8.02%.

NMR measurement of Δ,Λ*S*-Ir-H-Campy mixture

^{1}1H-NMR (400 MHz, $CDCl_3$) δ: 10.37–9.94 (m, 2H), 8.02 (d, J = 7.8 Hz, 1H), 7.97–7.84 (m, 4H), 7.84–7.71 (m, 4H), 7.68 (d, J = 7.7 Hz, 1H), 7.66–7.60 (m, 2H), 7.60–7.54 (m, 2H), 7.51 (d, J = 7.6 Hz, 2H), 7.44 (d, J = 4.9 Hz, 1H), 7.40–7.33 (m, 1H), 7.15–7.07 (m, 3H), 7.07–6.94 (m, 5H), 6.94–6.83 (m, 3H), 6.83–6.68 (m, 5H), 6.48 (d, J = 7.4 Hz, 1H), 6.30 (d, J = 7.5 Hz, 1H), 6.19 (d, J = 7.6 Hz, 2H), 4.74 (s, 1H), 3.93 (s, 1H), 3.48–3.38 (m, 1H), 3.38–3.23 (m, 1H), 3.08–2.90 (m, 2H), 2.90–2.67 (m, 4H), 2.12–1.99 (m,

2H), 1.97–1.78 (m, 2H), 1.73–1.62 (m, 2H). MS (FAB): m/z 649 [M]+, 501 $[Ir(ppy)_2]^+$. CHN calculated: C 54.41%, H 4.12%, N 8.1% found: C 54.1%, H 4.12%, N 8.12%.

General procedure for diastereomers separation with potassium (+)-10-camphorsulfonate

In a solution of Δ, Λ $[(ppy)_2Ir(R\text{-campy})]Cl$ (50mg) in CH_2Cl_2/MeOH (10 mL, 3:1 v/v) were added 3 eq of potassium (+)-10-camphorsulfonate and heated to reflux for 1 h. The solution was allowed to cool to room temperature and the solvent evaporated. The light yellow residue was suspended in 10 mL of acetone. The yellow precipitate constituted by the first camphorsulfonate diastereomer was filtered off and washed three times with acetone. The resulting acetone solutions were combined, solvent was evaporated and the thus obtained yellow residue was redissolved in 3 mL of acetone and filtered. Once the solvent evaporated, the second counterpart camphorsulfonate diastereomer was obtained. Finally, both camphorsulfonate salts were stirred in a biphasic mixture of H_2O/CH_2Cl_2 (20 mL,1:1 v/v) with 10 eq. of NH_4Cl. The organic phase was dried over anhydrous Na_2SO_4, the solvent was partially evaporated up to 1 mL and 5 mL of diethyl ether were added to obtain the corresponding chloride product as yellow powder. The diastereomeric ratios were determined by ^{1}H-NMR spectroscopy in $CDCl_3/CD_3OD$ (3:1 v/v).

NMR measurement of ΔS-Ir-Me-Campy

Obtained from the soluble camphorsulfonate derivative. Yellow solid, yield 22 mg (44%). ^{1}H-NMR (300 MHz, $CDCl_3$) δ: 9.91 (d, J = 6.4 Hz, 1H, a6), 8.03 (d, J = 5.8 Hz, 1H, d6), 7.99–7.75 (m, 4H, d3/a3/d4/a4), 7.60 (d, J = 7.1 Hz, 1H, b3), 7.53 (d, J = 6.8 Hz, 1H, c3), 7.45 (d, J = 7.8 Hz, 1H, e4), 7.38 (t, J = 5.9 Hz, 1H, a5), 7.14 (t, J = 6.6 Hz, 1H, d5), 6.92 (d, J = 7.9 Hz, 1H, e3), 6.84 (t, J = 7.5 Hz, 2H, b4/c4), 6.70 (m, 2H, b5/c5), 6.49 (t, J = 12.1 Hz, 1H, NH), 6.11 (d, J = 7.7 Hz, 1H, b6), 6.00 (d, J = 7.8 Hz, 1H, c6), 3.77 (m, 1H, e8), 3.22 (d, J = 12.1 Hz, NH), 3.02 (m, 2H, e5/e7), 2.72 (d, J = 16.7 Hz, H, e5'), 2.17 – 2.10 (m, 1H, e7'), 1.99 (m, 1H, e6), 1.71 (s, 3H, Me), 1.58

(m, 1H, e6′).^{13}C-NMR (75 MHz, $CDCl_3$) δ: 169.22, 168.23, 160.99, 160.20, 154.33, 153.76, 149.51, 144.71, 144.49, 143.10, 139.71, 138.19, 137.81, 134.31, 132.62, 131.04, 130.82, 129.95, 125.48, 124.93, 124.57, 123.63, 123.27, 122.61, 121.26, 120.33, 118.84, 58.69, 32.78, 28.82, 26.52, 22.18. CHN calculated: C 55.04%, H 4.33%, N 8.02% found: C 54.8%, H 4.33%, N 7.98%.

NMR measurement of Λ*S*-Ir-Me-Campy

Obtained from the precipitated camphorsulfonate derivative. Yellow solid, yield 23 mg (46%). 1H NMR (300 MHz, $CDCl_3/CD_3OD$, 3:1 v/v) δ 9.26 (d, J = 5.2 Hz, 1H, a6) [in $CDCl_3$ at 9.77 ppm], 7.93 (d, J = 8.1 Hz, 1H, d3), 7.88–7.71 (m, 3H, a3/d4/a4), 7.58–7.47 (m, 2H, c3/b3), 7.46–7.35 (m, 2H, d6/a5), 7.26 (m, 1H, e4), 7.07–6.94 (m, 2H, d4/e2), 6.81 (d, J = 2.8 Hz, 2H, b4/c4), 6.67 (dd, J = 7.9, 7.4 Hz, 2H, b5/c5), 6.11 (d, J = 7.8 Hz, 1H, b6), 6.07 (d, J = 7.4 Hz, 1H, d6), 5.98 (s, 1H, NH), 4.75 (s, 1H, e8), 3.05(m, 1H, NH), 2.77 (s, 2H, e7/e5), 2.68 (m, 1H, e5), 1.93 (s, 2H, e5/e6), 1.82 (s, 3H, Me) [in CDCl3 at 1.87 ppm], 1.59 (s, 1H, e5). ^{13}C-NMR (75 MHz, $CDCl_3$) δ 169.30, 169.24, 161.72, 160.31, 155.27, 153.03, 148.18, 144.06, 143.98, 143.05, 139.69, 138.22, 137.93, 133.69, 132.44, 131.75, 130.58, 130.13, 126.23, 124.61, 124.41, 123.64, 123.11, 122.38, 121.51, 120.11, 119.25, 58.66, 33.67, 28.45, 28.21, 21.64. CHN calculated: C 55.04%, H 4.33%, N 8.02% found: C 54.92%, H 4.33%, N 8.00%.

NMR measurement of Δ*S*-Ir-H-Campy

Obtained from soluble camphorsulfonate derivative. Yellow solid, yield 22 mg (44%). ^{1}H-NMR (300 MHz, $CDCl_3$) δ 10.08 (d, J = 4.8Hz, 1H, a6), 7.99 (d, J = 8.0 Hz, 1H, d3), 7.88 (m, 3H, a3/d6/d4), 7.78 (t, J = 7.5 Hz, 1H, a4), 7.69 (d, J = 7.6 Hz, 1H, b3), 7.62 (d, J = 7.7 Hz, 1H, c3), 7.51 (d, J = 7.6 Hz, 1H, e4), 7.45 (d, J = 5.1 Hz, 1H, e2), 7.39 (m, 1H, a5), 7.10 (t, J = 6.2 Hz, 1H, d5), 7.03 – 6.93 (m, 2H, e3/b4), 6.89 (t, J = 7.2 Hz, 1H, c4), 6.78 (t+m, J = 7.4 Hz, 3H, b5/c5/NH), 6.31 (d, J = 7.5 Hz, 1H, c6), 6.18 (d, J = 7.5 Hz, 1H, b6), 3.92 (m, 1H, e8), 3.30 (m, 1H, NH), 3.00 (m, 2H, e7/e5), 2.75 (m, 1H, e5′), 2.30 (m, 1H, e7′), 2.06 (m, 1H, e6), 1.64 (m,1H, e6′). ^{13}C-NMR (75 MHz, $CDCl_3$) δ 170.12, 167.20, 160.54, 154.04, 151.97, 148.97, 148.32, 147.23, 144.57, 143.57, 138.43, 138.21, 137.79, 137.68, 133.92,

131.78, 130.80, 129.98, 124.96, 124.73, 124.12, 122.72, 122.35, 122.09, 120.13, 119.03, 58.38, 31.84, 28.42, 22.55. CHN calculated: C 54.41%, H 4.12%, N 8.19% found: C 53.96%, H 4.22%, N 8.07%.

NMR measurement of ΛS-Ir-H-Campy

Obtained from the precipitated camphorsulfonate derivative. Yellow solid, yield 23 mg (46%). ^{1}H-NMR (300 MHz, $CDCl_3$) δ: 10.13 (d, J = 5.5 Hz, 1H, a6) [in $CDCl_3/CD_3OD$ 3:1 9.16 ppm], 7.92 (d, J = 8.3 Hz, 1H, d3), 7.78 (m, 3H, a3/d4/a4), 7.58 (m, 3H,c3/b3/e2), 7.46 (m, 2H, a5/e4), 7.09 (m, 2H, e3/d6), 7.04–6.90 (m, d5/c4/NH) [NH in $CDCl_3/CD_3OD$ 3:1 5.82 ppm], 6.90–6.74 (m, 3H, b4/b5/c5), 6.51 (d, J = 6.7 Hz, 1H, c6), 6.18 (d, J = 7.2 Hz, 1H, b6), 4.65 (m, 1H, e8), 3.50 (m, 1H, NH), 2.77 (m, 3H, e5/e5′/e7), 2.04–1.6 (m, 3H, e7′, e6, e6′). ^{13}C-NMR (75 MHz, $CDCl_3$) δ 168.49, 162.52, 154.96, 153.66, 148.20, 148.04, 147.53, 144.81, 143.57, 138.12, 138.00, 137.57, 136.90, 133.03, 132.04, 130.60, 130.52, 125.20, 124.45, 124.45, 124.32, 122.71, 122.01, 121.94, 119.86, 118.99, 58.96, 32.51, 28.26, 22.47. CHN calculated: C 54.41%, H 4.12%, N 8.19% found: C 54.7%, H 4.18%, N 8.22%.

Synthesis of Δ, ΛS-Ir-H-Campy acetate derivatives

In a solution of optically pure [(ppy)2Ir(H-campy)]Cl (25 mg, 3.7 E-2 mmol) in methanol (5mL) 1.1 eq of silver acetate were added, the reaction mixture, protected from light, was further stirred for 2 hours. Then the solvent was evaporated, CH2Cl2 was added and the AgCl formed was filtered out. The pure products were obtained by subsequent recrystallizations from CH2Cl2/n-Hexane.

NMR measurement of ΔS-Ir-H-Campy CH_3COO^-

^{1}H-NMR (300 MHz, $CDCl_3$) δ: 10.03 (d, J = 5.4 Hz, 1H, a6), 7.99 (d, J = 6.7 Hz, 1H, d3), 7.94–7.75 (m, 5H, a3/d6/d4/a4/NH), 7.71–7.57 (m, 2H, b3/c3), 7.51 (d, J = 4.0 Hz, 1H, e4), 7.47–7.34 (m, 2H, e2/a5), 7.16–7.04 (m, 1H d5), 7.04–6.83 (m, 3H, e3/b4/c4), 6.83–6.72 (m, 2H, b5/c5), 6.29 (d, J = 6.6 Hz, 1H, c6), 6.16 (d, J = 7.6 Hz, 1H, b6), 3.99–3.81 (m, 1H, e8), 3.10–2.88 (m, 3H, NH/e7/e5), 2.84–2.61 (m, 1H, e5′), 2.30 (m, 1H, e7′), 2.08 (s, 3H,

CH_3COO^-), 2.07 (s, 1H, e6), 1.66 (m, 1H, e6′). CHN calculated: C 55.99%, H 4.41%, N 7.91% found: C 55.88%, H 4.41%, N 7.89%.

NMR measurement of Δ,Λ*S*-Ir-H-Campy CH_3COO^-

^{1}H-NMR (400 MHz, $CDCl_3$) δ: 9.80 (d, J = 5.4 Hz, 1H, a6), 7.94 (d, J = 8.2 Hz, 1H, d3), 7.81 (t, J = 8.5 Hz, 1H, a3), 7.76 (dd, J = 14.5, 7.3 Hz, 2H, d4/a4), 7.71–7.55 (m, 5H, NH/e2/d4/b3/c3), 7.51 (d, J = 7.9 Hz, 1H, e4), 7.44 (t, J = 6.0 Hz, 1H, a5), 7.17–7.07 (m, 2H, e3/d6), 7.03–6.92 (m, 2H,d5/c4), 6.92–6.76 (m, 3H,c5/b5/b4), 6.47 (d, J = 7.2 Hz, 1H, c6), 6.23 (d, J = 7.7 Hz, 1H, b6), 4.79 (s, 1H, e8), 3.04 (t, J = 12.0 Hz, 1H, NH), 2.96–2.67 (m, 3H, e5/e5′/e7), 2.08–1.90 (m, 3H,CH_3COO^-), 1.83 (s, 2H, e7′, e6), 1.74–1.53 (m, 1H, e6′); CHN calculated: C 55.99%, H 4.41%, N 7.91% found: C 55.87%, H 4.42%, N 7.89%.

X-ray crystallographic analysis

Single crystal data of were collected at room temperature with a Bruker-Nonius X8APEXII CCD area detector system equipped with a graphite monochromator with radiation Mo Kα (λ = 0.71073 Å). The data were processed through the SAINT[176] reduction and SADABS[177] absorption software. The structure was solved by direct methods through the SHELXTL-NT[178] structure determination package and refined by full-matrix least-squares based on F^2. All non-hydrogen atoms were refined anisotropically and hydrogen atoms were included as idealized riding atoms. In the structure of Ir-Me-Campy, hydrogen atoms of the co-crystallized water molecules have been included in calculated positions and restrained bond distances and angles have been used. The final geometrical calculations and the graphical manipulations were performed using the XP utility of the SHELXTL system. The details of the resolved structure are reported in appendix A in CIF.

VCD and IR (Vibrational Absorption = VA) Spectra

All spectra were taken with a Jasco FVS6000 VCD spectrometer with liquid N_2-cooled MCT detector. The spectra were taken for CD_2Cl_2 solutions

in the range 0.027-0.037 M concentration, in 200 μm BaF_2 cells. In some cases a drop of CD_3OD was added to the solution, to facilitate dissolving the sample. Repeated sets of 2000 scans were taken for each sample and spectra were co-added, when needed; subtraction of VA and VCD spectra of the solvent were performed.

ECD and UV Spectra

The spectra were recorded at room temperature on a Jasco J500 Spectrophotometer or a Jasco 815SE spectrometer and 2 mm quartz cells were employed; with CD_2Cl_2 solutions in concentration range from 0.00023 M to 0.00026 M.

Photophysical studies

Spectrofluorimetric grade solvents were used for the photophysical investigations in solution, at room temperature. A Perkin Elmer Lambda 900 spectrophotometer was used to obtain the absorption spectra. Steady-state emission spectra were recorded on a HORIBA Jobin-Yvon Fluorolog-3 FL3-211 spectrometer equipped with a 450 W xenon arc lamp, double-grating excitation and single-grating emission monochromators (2.1 nm/mm dispersion; 1200 grooves/mm), and a Hamamatsu R928 photomultiplier tube. Emission and excitation spectra were corrected for source intensity (lamp and grating) and emission spectral response (detector and grating) by standard correction curves. To prevent that second order diffraction light from the source could reach detector, cut/off filters were used, if necessary. Time-resolved measurements were performed using the time-correlated single-photon counting (TCSPC) option on the Fluorolog 3. NanoLED at 379 nm, fwhm <200 ps with repetition rate at 1 MHz, was used to excite the sample. Excitation source was mounted directly on the sample chamber at 90°to a single-grating emission monochromator (2.1 nm/mm dispersion; 1200 grooves/mm) and the emission was collected with a TBX-04-D single-photon-counting detector. The photons collected at the detector were correlated by a time-to-amplitude converter

(TAC) to the excitation pulse. Signals were collected using an IBH Data Station Hub photon counting module, and data analysis was performed using the commercially available DAS6 software (HORIBA Jobin Yvon IBH). The quality of the fit was assessed by minimizing the reduced $\chi 2$ function and visual inspection of the weighted residuals. With regard to the solid state measurements, the samples were prepared by placing a given amount of powder between two quartz slides and standardizing the layer.

CPL Spectra

The spectra were taken with a home-built apparatus described in ref. [179, 180, 181] with excitation radiation brought in through an optical fibre from a Jasco FP8200 fluorimeter. The same solution used for the ECD spectra was employed for CPL measurements. 5 scans were accumulated for each spectrum. The excitation wavelength has been 380 nm. The Fluorescence spectra reported in this work are those simultaneously taken with the same non-commercial apparatus.

Density Functional Theory (DFT) Calculations

DFT calculations were conducted with the module of Gaussian09 [182], which was run at the B3LYP/6-31+G(d,p) level of theory; the LANL2DZ pseudopotential was used for the Ir atom. We are aware that B3LYP is an old functional with issues, however it is still used with good results in simulation of VCD spectra [87, 85, 86]. The input geometry was taken from X-ray diffractions data and then optimized with due allowance of solvent in the PCM polarizable continuum approximation [183]. Calculation of Dipole and Rotational Strengths through the field-response approach [111] was carried out; VA and VCD spectra were generated by assigning 8 cm^{-1} bandwidth Lorentzian bandshape to each vibrational transition. In all cases we also allowed for the presence of one Cl^- counterion. The scaling factor 0.975 was applied to the calculated frequencies. Time-Dependent DFT (TDDFT) calculations have been employed, within

the same Gaussian package, to obtain ECD spectra: the same level of theory was adopted and 40 excited states were admitted. Spectra were then plotted by associating Gaussian bands to each transition with 0.15 eV bandwidth. Absolute shieldings σ were calculated using the GIAO [184, 185] method, on the optimized geometries at the B3LYP level using the same basis on all the atoms, these small basis set allow short CPU times with satisfy results [186]. In order to achieve a better comparison between the theoretical and experimental data, ^{1}H σ computed by GIAO method were converted in chemical shifts δ by a regression analysis [187, 188].

Table 4.5: Energy values and population factors for the three reported conformers. Electronic energy, zero-point energy, energy-evaluated populations, free energy and free energy populations.

ΛS-Ir-Me-Campy					
	Eelec[a]	ΔE^{0b}	pop-ΔE^0	ΔG^b	pop-ΔG
half-chair (C24)	-2021.636857	0.0	0.903769	0.0	0.804877
half-chair (C25)	-2021.632337	2.710213	0.009321	2.619225	0.009679
boat	-2021.634325	1.38742	0.08691	0.869728	0.185445
ΔS-Ir-Me-Campy					
	Eelec	ΔE^0	pop-ΔE^0	ΔG	pop-ΔG
half-chair (C24)	-2021.637237	0.0	0.975609	0.0	0.95687
half-chair (C25)	-2021.633955	2.205068	0.023602	2.591614	0.012056
boat	-2021.630397	4.21875	0.000789	2.030621	0.031074

[a] E_h, [b] kcal/mol

Normal Mode assignments

Here we reported our normal modes assignments of the two diastereomers Δ*S*-Ir-Me-Campy and Λ*S*-Ir-Me-Campy, similar results were obtained

Table 4.6: Calculated structures of the three conformers lower in energy of Λ*S*-Ir-Me-Campy (top) and Δ*S*-Ir-Me-Campy (bottom).

Λ*S*-Ir-Me-Campy		
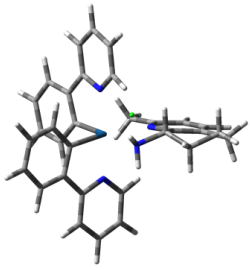	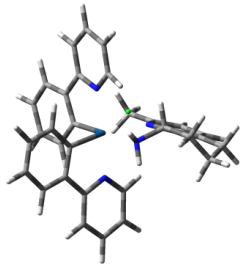	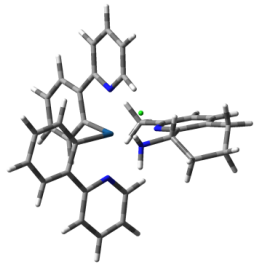
half-chair on (C24)	half-chair on (C25)	boat
Δ*S*-Ir-Me-Campy		
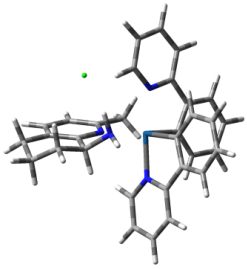	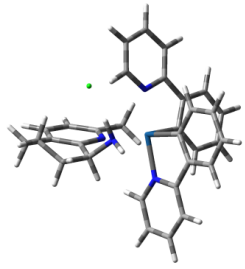	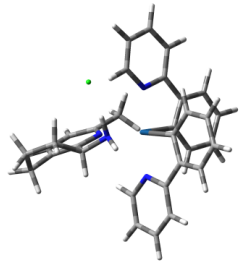
half-chair on (C24)	half-chair on (C25)	boat

with H-Campy complexes.

Table 4.7: Normal Mode assignments for Δ*S*-Ir-Me-Campy. In brackets is specified the ring involved in the normal mode (see figure 4.4). Units for dipole strength and rotatory strength are 10^{-40} esu^{2}cm^2 and 10^{-44} esu^{2}cm^2 respectively.

#	ν	D	R	Normal Mode Descriptions
120	1200	11	-12	CC stretching (e), CH2 e5/e6/e7 twisting, CC/CN stretching (e)
121	1221	6	9	CC stretching (e), C*H bending out of HCN plane, NH2/CH2 e5/e6/e7 twisting, CC/CN stretching (e7 ring)
122	1240	15	-14	CC stretching (e), C*H bending out of HCN plane, NH2/CH2 e5/e6/e7 twisting, CC/CN stretching (e)
123	1262	67	20	Symmetric CC stretching (c/d), NH2 wagging, CH2 e5/e6/e7 twisting
124	1264	12	6	C*H bending in-plane HCN, NH2 wagging, CH e5/e6/e7 twisting
125	1268	142	-32	C*H bending in-plane HCN, NH2 wagging, CH e5/e6/e7 twisting
126	1281	10	-4	C*H bending out of HCN plane, CC stretching (e), CH2 e5/e6/e7 twisting
127	1290	133	1	CC stretching (e), CH e5/e7 twisting
128	1300	63	-7	CC stretching (d), CN stretching (e), N-Ir-C (c/d) rocking
129	1301	15	15	Symmetric CC stretching (e/a), NH/bending in-plane HCN, C*H bending out of HCN plane, CH2 e6 twisting, in-plane aromatic CH bending (a)
130	1304	48	97	Anti-symmetric CC stretching (a/b and c/d), NH/ C*H bending out of HCN plane, in-plane aromatic CH bending (b)
131	1308	28	-94	Symmetric CC stretching (c/d)
132	1309	121	57	Symmetric CC stretching (a/b), NH/ C*H bending in-plane HCN, in-plane aromatic CH bending (a)
133	1334	56	-83	Symmetric CC stretching (a/b/c/d), in-plane aromatic CH bending (c)
134	1335	149	100	Symmetric CC stretching (a/b/c/d), in-plane aromatic CH bending (b)
135	1346	31	-3	Anti-symmetric CC stretching (c/d), in-plane aromatic CH bending (d)

Table 4.7:continued on next page

Table 4.7:continued from previous page

#	ν	D	R	Normal Mode Descriptions
136	1350	23	8	Anti-symmetric CC stretching (a/b/e ring), C*H bending orthogonal to HCN plane in-plane aromatic CH bending (a)
137	1351	40	-21	CH2 e5 rocking, CH2 e6 twisting, C*H bending orthogonal to HCN plane
138	1371	8	13	NH/CH e5/e7 bending, CH2 e6 rocking, CH e8 bending (in-plane HCN)
139	1384	26	17	C*H bending orthogonal to HCN plane, NH2/CH2 e5/6 rocking, CH2 e7 twisting
140	1393	26	-44	NH/CH e7/CH e6 bending
141	1414	60	29	C*H bending orthogonal to HCN plane, NH2 rocking, CH3 wagging, CC stretching (e), CH2 e5 wagging
142	1421	4	-9	C*H bending in-plane HCN, NH2 twisting, CH3 wagging, CC stretching (e), CH2 e5 wagging
143	1429	46	-33	CH e8 bending in-plane HCN, NH2 twisting, CH3 wagging
144	1456	182	-24	Symmetric CC stretching ppy (c/d), in-plane aromatic CH bending (d/c)
145	1462	97	-3	Symmetric CC stretching ppy (a/b), CH CH3 bending, in-plane aromatic CH bending (b/a)
146	1472	33	11	Anti-Symmetric CC stretching ppy (a/b), CH3 asymmetrical bending, in-plane aromatic CH bending (b/a)
147	1473	62	-11	CH3 asymmetrical bending, CH2 e5 scissoring, Symmetric CC stretching ppy (a/b), in-plane aromatic CH bending (b)
148	1474	27	-13	Symmetric CC stretching ppy (c/d), IrC-IrN rocking, in-plane aromatic CH bending (c)
149	1475	29	-7	CHe5 scissoring
150	1488	138	-37	CH3 asymmetrical bending
151	1489	43	36	CH3 asymmetrical bending, anti-symmetric CC stretching ppy (c/d)
152	1494	28	-62	CH2 e6 scissoring, anti-symmetric CC stretching ppy (a/b)
153	1494	42	45	CH2 e6 scissoring
154	1504	174	-68	CH2 e7/e5 scissoring, CC stretching (e)
155	1507	87	4	CH2 e7 scissoring
156	1511	677	739	Anti-symmetric rings stretching (d/a)

Table 4.7:continued on next page

Table 4.7:continued from previous page

#	ν	D	R	Normal Mode Descriptions
157	1514	308	-585	Symmetric rings stretching (a/d)
158	1591	63	5	Symmetric ring stretching (c/d)
159	1593	31	-6	Symmetric ring stretching (b/a)
160	1607	96	-5	Anti-symmetric ring stretching (d/c)

Table 4.7:ended

Table 4.8: Normal Mode assignments for ΛS-Ir-Me-Campy. In brackets is specified the ring involved in the normal mode (see figure 4.4). Units for dipole strength and rotatory strength are 10^{-40} esu^{2}cm^2 and 10^{-44} esu^{2}cm^2 respectively.

#	ν	D	R	Normal Mode Descriptions
120	1207	156	-37	C*H bending in-plane HCN, NH2 wagging, CH2 e6/e5 twisting, CC stretching (e)
121	1235	29	51	C*H bending out of HCN plane, NH2 twisting, CH2 e6 twisting, CC stretching (e)
122	1249	19	6	C*H bending out of HCN plane, NH2 twisting, CH2 e6 twisting, CC stretching (e)
123	1254	144	91	C*H bending out of HCN plane, NH2 wagging, CH2 e6 twisting, CC stretching (e)
124	1264	71	-29	CC stretching (c/d/b/a), in-plane CH stretching (c)
125	1267	61	46	CC stretching (c/d/b/a), in-plane CH stretching (b)
126	1282	5	7	C*H bending out of HCN plane, CH2 e5/e7 twisting
127	1289	184	-45	CC stretching (e), NH2/CH2 e7/e5 twisting
128	1296	11	18	C*H bending out of HCN plane, NH2/CH2 e7/e6/e5 twisting, CC stretching (e)
129	1302	42	-4	CCN anti-symmetric stretching a6, CN stretching a2, in-plane aromatic CH bending (a)
130	1304	56	-23	CN anti-symmetric stretching (a), CC stretching (c), in-plane aromatic CH bending (d)
131	1307	97	39	Symmetric rings stretching (b/a), in-plane aromatic CH bending (a)
132	1308	45	-79	CN anti-symmetric stretching (d), CC stretching (d)
133	1335	45	154	Symmetric rings stretching (b/c)
134	1336	195	-153	Symmetric rings stretching (b/c)

Table 4.8:continued on next page

Table 4.8:continued from previous page

#	ν	D	R	Normal Mode Descriptions
135	1348	37	45	Anti-symmetric rings stretching (d/c), C*H bending out of HCN plane, CH2 e7 twisting, in-plane aromatic CH bending (d ring)
136	1348	34	-18	Anti-symmetric rings stretching (a/b), C*H bending out of HCN plane, CH2 e7 twisting, in-plane aromatic CH bending (a)
137	1349	8	-31	C*H bending out of HCN plane, CH2 e7 twisting, CH2 e5, CC stretching (e)
138	1370	1	-2	C*H bending in-plane HCN, NH2/CH2 e5 twisting, CH2 e7/e6 wagging, CC e7/e6 stretching
139	1376	8	14	C*H bending (out of HCN plane), CH2 e7/e6 twisting, NH2/CH2 e5 wagging
140	1385	15	-8	CC e6/e7 stretching, CH2 e6/e7 wagging
141	1414	84	-11	CH3 wagging, CH2 e5 wagging, C*H bending out of HCN plane, CC stretching (e)
142	1425	48	-88	C*H bending in-plane HCN, NH2 twisting, CH3 wagging, CH2 e5 wagging
143	1435	63	-51	C*H bending in-plane HCN, NH2 twisting, CH3 wagging
144	1457	207	44	Symmetric rings stretching (c/d), in-plane aromatic CH bending (d/c)
145	1460	98	-40	Symmetric rings stretching (b/a), in-plane aromatic CH bending (a/b)
146	1472	25	14	CH2 e5 scissoring
147	1473	31	-3	Anti-symmetric rings stretching (b/a), in-plane aromatic CH bending (b)
148	1474	24	16	Anti-symmetric rings stretching (c/d), in-plane aromatic CH bending (c)
149	1480	59	4	CH3 asymmetrical bending
150	1489	83	75	CH3 asymmetrical bending Anti-symmetric rings stretching (d/c)
151	1490	118	-72	CH3 asymmetrical bending, Anti-symmetric rings stretching (d/c)
152	1493	34	33	CH2 e6/e7 scissoring, CC stretching (a/b)
153	1493	9	-46	CH2 >e7/e6 scissoring
154	1499	128	99	CH2 e5/e6/e7 scissoring, CC stretching (e)
155	1502	114	57	CH2 >e6/e7 scissoring

Table 4.8:continued on next page

Table 4.8:continued from previous page

#	ν	D	R	Normal Mode Descriptions
156	1512	695	-714	Anti-symmetric rings stretching (d/a)
157	1514	253	572	Symmetric rings stretching (a/d)
158	1591	60	-66	Symmetric rings stretching (b/a)
159	1592	37	75	Symmetric rings stretching (c/d)
160	1607	100	33	Anti-symmetric rings stretching (d/c)
161	1609	102	-37	Anti-symmetric rings stretching (a/b-ring)
162	1616	69	12	Ring stretching (e)
163	1626	232	-54	Symmetric ring stretching (b/c)
164	1630	211	43	Anti-symmetric rings stretching (c/b)
165	1640	52	0	Ring stretching (e)
166	1651	162	25	Ring stretching (d)
167	1651	246	-71	Ring stretching (a)
168	1666	84	36	NH2 scissoring

Table 4.8:ended

Appendix A

Metal complexes nomenclature

In this chapter we provided some notions of stereochemistry nomenclature of the metal complexes; they are limited to which geometries treated in this thesis. The milestone in this field is *Stereochemistry Of Coordination Compounds* [17] to which we address the interested reader.

A.1 Pseudo tetrahedral geometry

In complexes where the three *fac* positions are occupied by the η^5-cp ring, the absolute configuration of a stereogenic metal center is specified following the well-known Cahn–Ingold–Prelog (CIP) priority rules. The issue consist on the assignment of the priority to the polyhapto ligands, such as η^5-Cyclopentadienyl or η^6-arene ligands, were all the atoms are equally coordinated to the metal.

In these cases, the priority for the polihapto ligands is based on the sum of the atomic weights of the atoms coordinated to the metal center. Thus a η^5-Cyclopentadienyl is considered as a pseudo-atom of molecular weight of 60 amu, whereas a η^6-arene has a molecular weight of 72 amu. As a consequence, the priority sequence is the following: I > Br > η^6-arene > η^5-Cyclopentadienyl > η^3-allyl > Cl > P (such as in PPh3) > O > N > η^1-C

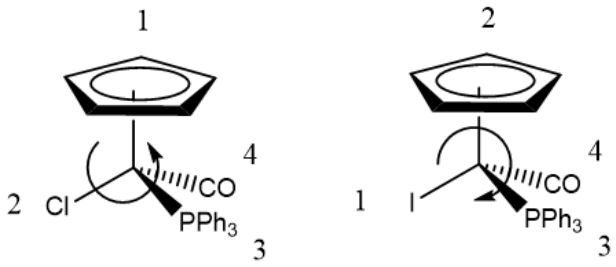

(a) S_{Ru} **(b)** R_{Ru}

Figure A.1: Example of absolute configuration in pseudo tetrahedral geometry.

After that, the determination of R or S configuration takes place in the ordinary CIP rules. Typically the configuration of the metal center is listed first followed by that of the ligand and subscripts are applied for clarification.

A.2 Octahedral geometry: C/A convention

The absolute configurations of some octahedral complexes can be described using either the skew-line reference system (*vide infra*) or the C/A system. The C/A system has the advantage that is more general and may be used for most complexes [189].

In an octahedral geometry the reference axis is that axis containing the ligating atom of highest CIP priority and the trans ligating atom of lowest possible priority. In order to assign the chiral descriptor, the atoms in the coordination plane perpendicular to the reference axis are viewed from the ligands with the highest priority and then at the structure is assigned the symbol C or A, according to whether the clockwise (C) or anticlockwise (A) sequence is lower at the first point of difference.

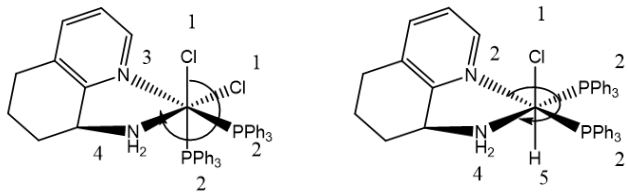

(a) OC6-42-A **(b)** OC6-54-C

Figure A.2: Example of absolute configuration in octahedral complexes assigned by C/A convention.

A.3 Skew lines

The first two methods here expose are susceptible to pseudo-inversion, instead two skew lines define uniquely a helical system in a coordination entities. Therefore in system with at least two bidentate ligands a methodology based on the skew lines was developed, that allows the definition of the chirality with a direct relation to the chiral object. This system can thus be applied at the octahedral complexes and to the distorted square planar geometry reported in this thesis.

The symbols for the helical chirality are Δ, that correspond to a right handed screw, and Λ, left handed screw, this symbols involve the whole chirality of the system, in the same way to describe the conformation of a chelate rings the δ and λ notation can be used.

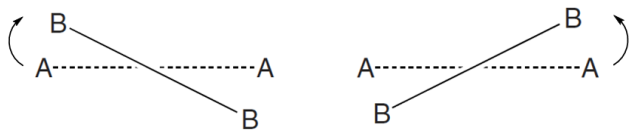

(a) $\Delta or \delta$ **(b)** $\Lambda or \lambda$

Figure A.3: Two pair of skew lines and their definition.

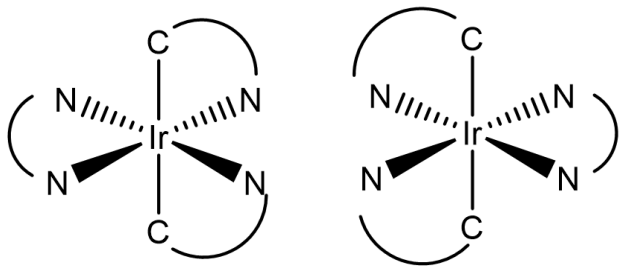

(a) Δ **(b)** Λ

Figure A.4: Example of absolute configuration in octahedral complexes assigned by skew lines.

Appendix B

Crystallographic structures

Table B.1: T-4-R_{Ru}-η^5-[(1*R*,2*S*,5*R*)-menthyl)-C_5H_4)Ru(CO)(P(C_6H_5)$_3$)Br]

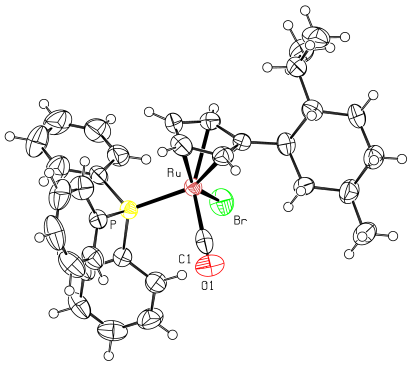

selected structure refinement parameters.	
empirical formula	$C_{34}H_{38}BrOPRu$
Crystal system	Orthorhombic
Space group	$P2_12_12_1$
Z	4
fw	674.59
a , Å	8.311(5)
b , Å	16.646(5)
c , Å	22.530(5)
α, β, γ, deg	90, 90, 90
V, Å^3	3117(2)
dc, g cm-3	1.438
μ, mm^{-1}	1.860
Independent reflections [R(int)]	9893 [0.0404]
Data/ restraints/ parameters	4532 / 0 / 343
Goodness-of-fit on F^2	0.895
Absolute structure parameter	0.047(11)
R1 [I > 2 σ (I)]	0.0567
wR2	0.0802

Table B.2: Δ-[Ir(ppy)$_2$((*R*)−Me−Campy)]Cl · H_2O

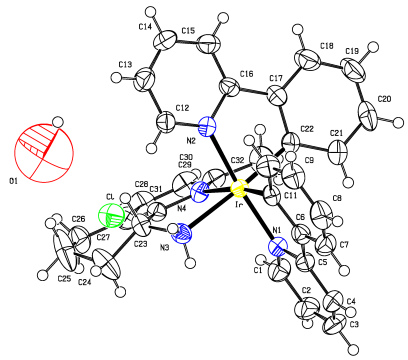

selected structure refinement parameters.	
empirical formula	$C_{23}H_{23}ClIrN_4O$
Crystal system	Orthorhombic
Space group	$P2_12_12_1$
Z	4
fw	716.27
a , Å	10.662(3)
b , Å	14.595(3)
c , Å	18.403(5)
α, β, γ, deg	90, 90, 90
V, Å^3	2863.7(12)
dc, g cm^{-3}	1.661
μ, mm^{-1}	4.788
Independent reflections [R(int)]	5716 [0.0404]
Data/ restraints/ parameters	5421 / 3 / 354
Goodness-of-fit on F^2	0.957
Absolute structure parameter	-0.003(5)
R1 [I > 2 σ (I)]	0.0183
wR2	0.0457

Table B.3: Λ-[Ir(ppy)$_2$((*S*)−H−Campy)]Cl

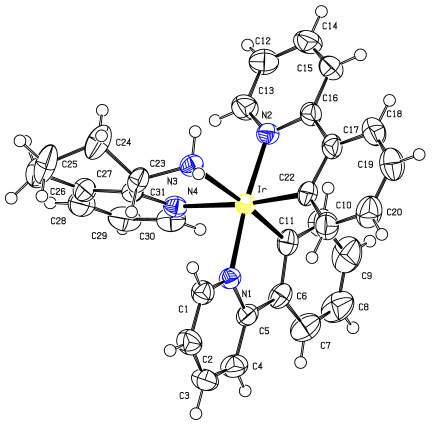

selected structure refinement parameters.

empirical formula	$C_{31}H_{28}ClIrN_4$
Crystal system	Orthorhombic
Space group	$P2_12_12_1$
Z	4
fw	684.22
a , Å	10.140(1)
b , Å	14.357(2)
c , Å	18.998(3)
α, β, γ, deg	90, 90, 90
V, Å^3	2766.0(7)
dc, g cm^{-3}	1.643
μ, mm^{-1}	4.950
Independent reflections [R(int)]	5530 [0.0296]
Data/ restraints/ parameters	5340 / 0 / 334
Goodness-of-fit on F^2	1.034
Absolute structure parameter	-0.003(5)
R1 [I > 2 σ (I)]	0.0169
wR2	0.0374

Table B.4: Λ-[Ir(ppy)$_2$((*S*)−H−Campy)]$^+$ camphorsulfonate$^-$

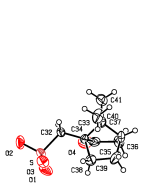

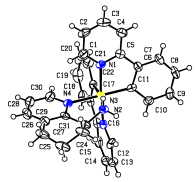

selected structure refinement parameters.

empirical formula	$C_{41}H_{43}IrN_4O_4S$
Crystal system	Orthorhombic
Space group	$P2_12_12_1$
Z	4
fw	880.05
a , Å	10.494(4)
b , Å	14.456(7)
c , Å	24.007(11)
α, β, γ, deg	90, 90, 90
V, Å^3	3642(3)
dc, g cm^{-3}	1.605
μ, mm^{-1}	3.772
Independent reflections [R(int)]	6706 [0.0788]
Data/ restraints/ parameters	5965 / 3 / 460
Goodness-of-fit on F^2	0.950
Absolute structure parameter	-0.008(7)
R1 [I > 2 σ (I)]	0.0384
wR2	0.0671

Bibliography

[1] C. S. Wu, E. Ambler, R. W. Hayward, D. D. Hoppes, and R. P. Hudson. Experimental Test of Parity Conservation in Beta Decay. *Phys. Rev.*, 105(4):1413–1415, feb 1957.

[2] Richard L. Garwin, Leon M. Lederman, and Marcel Weinrich. Observations of the Failure of Conservation of Parity and Charge Conjugation in Meson Decays: the Magnetic Moment of the Free Muon. *Phys. Rev.*, 105(4):1415–1417, feb 1957.

[3] T. D. Lee and C. N. Yang. Question of Parity Conservation in Weak Interactions. *Phys. Rev.*, 104(1):254–258, oct 1956.

[4] Benoît Darquié, Clara Stoeffler, Alexander Shelkovnikov, Christophe Daussy, Anne Amy-Klein, Christian Chardonnet, Samia Zrig, Laure Guy, Jeanne Crassous, Pascale Soulard, Pierre Asselin, Thérèse R Huet, Peter Schwerdtfeger, Radovan Bast, and Trond Saue. Progress toward the first observation of parity violation in chiral molecules by high-resolution laser spectroscopy. *Chirality*, 22(10):870–84, nov 2010.

[5] Martin Quack. How important is parity violation for molecular and biomolecular chirality? *Angew. Chem. Int. Ed. Engl.*, 41(24):4618–30, dec 2002.

[6] B. D. Vineyard, W. S. Knowles, M. J. Sabacky, G. L. Bachman, and D. J. Weinkauff. Asymmetric hydrogenation. Rhodium chiral bisphosphine catalyst. *J. Am. Chem. Soc.*, 99(18):5946–5952, aug 1977.

[7] William S. Knowles. Asymmetric Hydrogenations (Nobel Lecture) Copyright© The Nobel Foundation 2002. We thank the Nobel Foundation, Stockholm, for permission to print this lecture. *Angew. Chemie Int. Ed.*, 41(12):1998, jun 2002.

[8] Joseph S M Samec, Jan-E Bäckvall, Pher G Andersson, and Peter Brandt. Mechanistic aspects of transition metal-catalyzed hydrogen transfer reactions. *Chem. Soc. Rev.*, 35(3):237–48, mar 2006.

[9] Alfred Werner. Beitrag zur Konstitution anorganischer Verbindungen. *Zeitschrift für Anorg. Chemier Anorg. Chemie*, 3(1):267–330, 1893.

[10] R S Cahn, Christopher Ingold, and V Prelog. Specification of Molecular Chirality. *Angew. Chemie Int. Ed. English*, 5(4):385–415, 1966.

[11] Edwin C Constable. Stereogenic metal centres - from Werner to supramolecular chemistry. *Chem. Soc. Rev.*, 42(4):1637–51, feb 2013.

[12] Alfred Werner and A Vilmos. Beitrag zur Konstitution anorganischer Verbindungen. XVII. Mitteilung. Über Oxalatodiäthylendiaminkobaltisalze . *Zeitschrift für Anorg. Chemie*, 21(1):145–158, 1899.

[13] A Werner. Zur Kenntnis des asymmetrischen Kobaltatoms. I. *Berichte der Dtsch. Chem. Gesellschaft*, 44(2):1887–1898, 1911.

[14] A Werner. Zur Kenntnis des asymmetrischen Kobaltatoms XII. Über optische Aktivität bei kohlenstofffreien Verbindungen. *Berichte der Dtsch. Chem. Gesellschaft*, 47(3):3087–3094, 1914.

[15] Daryle H. Busch. The stereochemistry of complex inorganic compounds. *J. Chem. Educ.*, 41(2):77, feb 1964.

[16] Steven J Malcolmson, Simon J Meek, Elizabeth S Sattely, Richard R Schrock, and Amir H Hoveyda. Highly efficient molybdenum-based catalysts for enantioselective alkene metathesis. *Nature*, 456(7224):933–7, dec 2008.

[17] Alexander von Zelewsky. *Stereochemistry of Coordination Compounds*. John Wiley & Sons, Ltd, 1996.

[18] Murielle Chavarot, Stéphane Ménage, Olivier Hamelin, Florence Charnay, Jacques Pécaut, and Marc Fontecave. "Chiral-at-Metal" octahedral ruthenium(II) complexes with achiral ligands: a new type of enantioselective catalyst. *Inorg. Chem.*, 42(16):4810–6, aug 2003.

[19] Claudio Villani, Francesco Gasparrini, Marco Pierini, Stefano Levi Mortera, Ilaria D'Acquarica, Alessia Ciogli, and Giovanni Zappia. Dynamic HPLC of stereolabile iron(II) complexes on chiral stationary phases. *Chirality*, 21(1):97–103, jan 2009.

[20] H. Brunner. Optical Activity at an Asymmetrical Manganese Atom. *Angew. Chemie Int. Ed. English*, 8(5):382–383, may 1969.

[21] Francine Agbossou, Edward J O'Connor, Charles M Garner, N Quirós Méndez, Jesús M Fernández, Alan T Patton, James A Ramsden, J A Gladysz, Joseph M O'Connor, Tracy Tajima, and Kevin P Gable. Cyclopentadienyl Rhenium Complexes. In *Inorg. Synth.*, pages 211–225. John Wiley & Sons, Inc., 2007.

[22] J. W. Faller, Jenna Thu Nguyen, W. Ellis, and Maria R. Mazzieri. Resolution of CpMo(NO)X(.eta.3-2-methallyl) complexes and their enantioselective reactions with an aldehyde. *Organometallics*, 12(4):1434–1438, apr 1993.

[23] Melanie Helms, Zhijie Lin, Lei Gong, Klaus Harms, and Eric Meggers. Method for the Preparation of Nonracemic Bis-Cyclometalated Iridium(III) Complexes. *Eur. J. Inorg. Chem.*, 2013(24):4164–4172, 2013.

[24] Alexander P Smirnoff. Zur Stereochemie des Platinatoms; über relativ asymmetrische Synthese bei anorganischen Komplexen. *Helv. Chim. Acta*, 3(1):177–195, 1920.

[25] Dušan Drahoňovský and Alex von Zelewsky. Asymmetric Synthesis of Coordination Compounds: Back to the Roots. Diastereoselective Synthesis of Simple Platinum(IV) Complexes. *Helv. Chim. Acta*, 88(3):496–506, 2005.

[26] Jeanne Crassous. Transfer of chirality from ligands to metal centers: recent examples. *Chem. Commun.*, 48(78):9684, sep 2012.

[27] Haohua Huo, Chen Fu, Klaus Harms, and Eric Meggers. Asymmetric catalysis with substitutionally labile yet stereochemically stable chiral-at-metal iridium(III) complex. *J. Am. Chem. Soc.*, 136(8):2990–3, feb 2014.

[28] Carola Ganzmann and John A. Gladysz. Phase Transfer of Enantiopure Werner Cations into Organic Solvents: An Overlooked Family of Chiral Hydrogen Bond Donors for Enantioselective Catalysis. *Chem. - A Eur. J.*, 14(18):5397–5400, jun 2008.

[29] Zhong-Yan Cao, William D. G. Brittain, John S. Fossey, and Feng Zhou. Recent advances in the use of chiral metal complexes with achiral ligands for application in asymmetric catalysis. *Catal. Sci. Technol.*, 5(7):3441–3451, jun 2015.

[30] Hani Amouri and Michel Gruselle. Chiral Enantiopure Molecular Materials. In *Chirality Transit. Met. Chem.*, pages 179–237. John Wiley & Sons, Ltd, 2009.

[31] Peter Göbel, Florian Ritterbusch, Melanie Helms, Matthias Bischof, Klaus Harms, Manfred Jung, and Eric Meggers. Probing Chiral Recognition of Enzyme Active Sites with Octahedral Iridium(III) Propeller Complexes. *Eur. J. Inorg. Chem.*, 2015(10):1654–1659, 2015.

[32] Brian M Zeglis, Valerie C Pierre, and Jacqueline K Barton. Metallo-intercalators and metallo-insertors. *Chem. Commun. (Camb).*, (44):4565–79, nov 2007.

[33] Suzanne E Howson, Laura E N Allan, Nikola P Chmel, Guy J Clarkson, Remy van Gorkum, and Peter Scott. Self-assembling optically pure Fe(A-B)3 chelates. *Chem. Commun. (Camb).*, (13):1727–9, apr 2009.

[34] Nicholas C. Fletcher, Ciarán Martin, and Heather J. Abraham. Enantiomeric programming in tripodal transition metal scaffolds. *New J. Chem.*, 31(8):1407, jul 2007.

[35] Paul Pfeiffer and Kurt Quehl. Über einen neuen Effekt in Lösungen optisch-aktiver Substanzen (I. Mitteil.). *Berichte der Dtsch. Chem. Gesellschaft (A B Ser.*, 64(10):2667–2671, 1931.

[36] Olivier Hamelin, Jacques Pécaut, and Marc Fontecave. Crystallization-induced asymmetric transformation of chiral-at-metal ruthenium(II) complexes bearing achiral ligands. *Chemistry*, 10(10):2548–54, may 2004.

[37] Dusan Hesek, Yoshihisa Inoue, Simon R. L. Everitt, Hitoshi Ishida, Mieko Kunieda, and Michael G. B. Drew. Diastereoselective Preparation and Characterization of Ruthenium Bis(bipyridine) Sulfoxide Complexes. *Inorg. Chem.*, 39(2):317–324, jan 2000.

[38] Frédéric Pezet, Jean-Claude Daran, Isabelle Sasaki, Hassan Aït-Haddou, and Gilbert G. A. Balavoine. Highly Diastereoselective Preparation of Ruthenium Bis(diimine) Sulfoxide Complexes: New

Concept in the Preparation of Optically Active Octahedral Ruthenium Complexes. *Organometallics*, 19(20):4008–4015, oct 2000.

[39] Lei Gong, Zhijie Lin, Klaus Harms, and Eric Meggers. Isomerization-Induced Asymmetric Coordination Chemistry: From Auxiliary Control to Asymmetric Catalysis. *Angew. Chemie Int. Ed.*, 49(43):7955–7957, oct 2010.

[40] Lei Gong, Seann P Mulcahy, Deepa Devarajan, Klaus Harms, Gernot Frenking, and Eric Meggers. Chiral salicyloxazolines as auxiliaries for the asymmetric synthesis of ruthenium polypyridyl complexes. *Inorg. Chem.*, 49(17):7692–9, sep 2010.

[41] Lei Gong, Seann P Mulcahy, Klaus Harms, and Eric Meggers. Chiral-auxiliary-mediated asymmetric synthesis of tris-heteroleptic ruthenium polypyridyl complexes. *J. Am. Chem. Soc.*, 131(28):9602–3, jul 2009.

[42] Lei Gong, Christian Müller, Mehmet Ali Celik, Gernot Frenking, and Eric Meggers. 2-Diphenylphosphino-2′-hydroxy-1,1′-binaphthyl as a chiral auxiliary for asymmetric coordination chemistry. *New J. Chem.*, 35(4):788, apr 2011.

[43] Zhijie Lin, Lei Gong, Mehmet Ali Celik, Klaus Harms, Gernot Frenking, and Eric Meggers. Asymmetric Coordination Chemistry by Chiral-Auxiliary-Mediated Dynamic Resolution under Thermodynamic Control. *Chem. - An Asian J.*, 6(2):474–481, feb 2011.

[44] Hisako Sato and Akihiko Yamagishi. VCD studies on chiral characters of metal complex oligomers. *Int. J. Mol. Sci.*, 14(1):964–78, jan 2013.

[45] Valentin Paul Nicu, Attila Mándi, Tibor Kurtán, and Prasad L Polavarapu. On the complementarity of ECD and VCD techniques. *Chirality*, 26(9):525–31, sep 2014.

[46] Laurence A Nafie. *Vibrational Optical Activity*. John Wiley & Sons, Ltd, 2011.

[47] Eike B Bauer. Chiral-at-metal complexes and their catalytic applications in organic synthesis. *Chem. Soc. Rev.*, 41(8):3153–67, apr 2012.

[48] Karl-Josef Haack, Shohei Hashiguchi, Akio Fujii, Takao Ikariya, and Ryoji Noyori. The Catalyst Precursor, Catalyst, and Intermediate in the RuII-Promoted Asymmetric Hydrogen Transfer between Alcohols and Ketones. *Angew. Chemie Int. Ed. English*, 36(3):285–288, feb 1997.

[49] Ryoji Noyori and Shohei Hashiguchi. Asymmetric Transfer Hydrogenation Catalyzed by Chiral Ruthenium Complexes. *Acc. Chem. Res.*, 30(2):97–102, feb 1997.

[50] Robert H Morris. Exploiting metal-ligand bifunctional reactions in the design of iron asymmetric hydrogenation catalysts. *Acc. Chem. Res.*, 48(5):1494–502, may 2015.

[51] Walter Baratta and Pierluigi Rigo. 1-(Pyridin-2-yl)methanamine-Based Ruthenium Catalysts for Fast Transfer Hydrogenation of Carbonyl Compounds in 2-Propanol. *Eur. J. Inorg. Chem.*, 2008(26):4041–4053, sep 2008.

[52] Masashi Yamakawa, Hisashi Ito, and Ryoji Noyori. The Metal−Ligand Bifunctional Catalysis: A Theoretical Study on the Ruthenium(II)-Catalyzed Hydrogen Transfer between Alcohols and Carbonyl Compounds. *J. Am. Chem. Soc.*, 122(7):1466–1478, feb 2000.

[53] Christian A. Sandoval, Takeshi Ohkuma, Kilian Muñiz, and Ryoji Noyori. Mechanism of Asymmetric Hydrogenation of Ketones Catalyzed by BINAP/1,2-Diamine−Ruthenium(II) Complexes. *J. Am. Chem. Soc.*, 125(44):13490–13503, nov 2003.

[54] Robert Abbel, Kamaluddin Abdur-Rashid, Michael Faatz, Alen Hadzovic, Alan J Lough, and Robert H Morris. A succession of isomers of ruthenium dihydride complexes. Which one is the ketone hydrogenation catalyst? *J. Am. Chem. Soc.*, 127(6):1870–82, feb 2005.

[55] Alen Hadzovic, Datong Song, Christina M. MacLaughlin, and Robert H. Morris. A Mechanism Displaying Autocatalysis: The Hydrogenation of Acetophenone Catalyzed by RuH(S -binap)(app) Where app Is the Amido Ligand Derived from 2-Amino-2-(2-pyridyl)propane. *Organometallics*, 26(24):5987–5999, nov 2007.

[56] Jason B. Crawford, Gang Chen, David Gauthier, Trevor Wilson, Bryon Carpenter, Ian R. Baird, Ernie McEachern, Alan Kaller, Curtis Harwig, Bem Atsma, Renato T. Skerlj, and Gary J. Bridger. AMD070, a CXCR4 Chemokine Receptor Antagonist: Practical Large-Scale Laboratory Synthesis. *Org. Process Res. Dev.*, 12(5):823–830, sep 2008.

[57] John C. Sutherland. Measurement of the Circular Dichroism of Electronic Transitions. pages 35–63.

[58] Isabella Rimoldi, Giorgio Facchetti, Edoardo Cesarotti, Michela Pellizzoni, Marco Fusè, and Daniele Zerla. Enantioselective Transfer Hydrogenation of Aryl Ketones: Synthesis and 2D-NMR Characterization of New 8-amino-5,6,7,8-tetrahydroquinoline Ru(II)-complexes. *Curr. Org. Chem.*, 16(24):2982–2988, 2012.

[59] Daniele S. Zerla, Isabella Rimoldi, Edoardo Cesarotti, Giorgio Facchetti, Michela Pellizzoni, and Marco Fusè. Diastereoselectivity and catalytic activity in ruthenium complexes chiral at the metal centre. *J. Organomet. Chem.*, 771:2–8, nov 2014.

[60] Virginia M. Loeblich, Doris E. Baldwin, R. T. O'Connor, and Ray V. Lawrence. Thermal Isomerization of Levopimaric Acid. *J. Am. Chem. Soc.*, 77(23):6311–6313, dec 1955.

[61] Hiroshi Takeda, Walter H. Schuller, and Ray V. Lawrence. Thermal isomerization of abietic acid. *J. Org. Chem.*, 33(4):1683–1684, apr 1968.

[62] Maria João Brites, Ana Guerreiro, Bárbara Gigante, and M.J. Marcelo-Curto. Quantitative determination of dehydroabietic acid methyl ester in disproportionated rosin. *J. Chromatogr. A*, 641(1):199–202, jul 1993.

[63] P J Kersten, B J Kopper, K F Raffa, and B L Illman. Rapid analysis of abietanes in conifers. *J. Chem. Ecol.*, 32(12):2679–85, dec 2006.

[64] Winston D. Lloyd and Glen W. Hedrick. Levopimaric Acid. *Org. Synth.*, 45:64, 1965.

[65] R. A. Zelonka and M. C. Baird. Benzene Complexes of Ruthenium(II). *Can. J. Chem.*, 50(18):3063–3072, sep 1972.

[66] M A Bennett, T.-N. Huang, T W Matheson, A K Smith, Steven Ittel, and William Nickerson. 16. (η6-Hexamethylbenzene)Ruthenium Complexes. In *Inorg. Synth.*, pages 74–78. John Wiley & Sons, Inc., 2007.

[67] D. Rose and G. Wilkinson. The blue solutions of ruthenium(II) chloride: a cluster anion. *J. Chem. Soc. A Inorganic, Phys. Theor.*, page 1791, 1970.

[68] J. D. Gilbert, D. Rose, and G. Wilkinson. Preparative use of blue solutions of ruthenium(II): ruthenium-(II) and -(III) complexes with amines, nitriles, phosphines, etc. *J. Chem. Soc. A Inorganic, Phys. Theor.*, page 2765, 1970.

[69] John W. Hull and Wayne L. Gladfelter. .eta.4-Bonding in (arene)ruthenium complexes of octamethylnaphthalene. *Organometallics*, 3(4):605–613, apr 1984.

[70] Ray F. Severson and Walter H. Schuller. The Thermal Behavior of Some Resin Acids at 400–500 °C. *Can. J. Chem.*, 50(14):2224–2229, jul 1972.

[71] Paolo Pertici, Giovanni Vitulli, Maurizio Paci, and Lido Porri. A new synthetic method for the preparation of cyclo-olefin ruthenium complexes. *J. Chem. Soc. Dalt. Trans.*, (10):1961, jan 1980.

[72] Paolo Pertici, Giovanni Vitulli, Raffaello Lazzaroni, Piero Salvadori, and Pier Luigi Barili. A simple preparation for (?6-arene)(?4-cycloocta-1,5-diene)ruthenium-(0) complexes and their conversion into the corresponding arene?dichlororuthenium(II) complexes. *J. Chem. Soc. Dalt. Trans.*, (6):1019, jan 1982.

[73] Tobias Thaler, Benjamin Haag, Andrei Gavryushin, Katrin Schober, Evelyn Hartmann, Ruth M Gschwind, Hendrik Zipse, Peter Mayer, and Paul Knochel. Highly diastereoselective Csp_3-Csp_2 Negishi cross-coupling with 1,2-, 1,3- and 1,4-substituted cycloalkylzinc compounds. *Nat. Chem.*, 2(2):125–30, feb 2010.

[74] Kovuru Gopalaiah. Chiral iron catalysts for asymmetric synthesis. *Chem. Rev.*, 113(5):3248–96, may 2013.

[75] Dong Wang and Didier Astruc. The Golden Age of Transfer Hydrogenation. *Chem. Rev.*, jun 2015.

[76] S G Davies. The chiral auxiliary [(C5H5)Fe(CO)(PPh3)] for asymmetric synthesis. *Aldrichimica Acta*, 23(2):31–37, 1990.

[77] Stephen J Cook, James F Costello, Stephen G Davies, and Henry T Kruk. A novel one-pot synthesis of homochiral (R)-(-)- and (S)-(+)- Fe(CO)([small eta]5-C5H5)(PPh3)COCH3. *J. Chem. Soc.{,} Perkin Trans. 1*, (17):2369–2372, 1994.

[78] Edoardo Cesarotti, Laura Prati, Angelo Sironi, Gianfranco Ciani, and Colin White. Synthesis and stereochemical studies of the chiral ruthenium complexes [Ru(?-C5H5){(S)dpompyr-PP?}X][dpompyr =N-diphenylphosphino-2-(diphenylphosphinoxymethyl)pyrrolidine, X = H or Cl]. Crystal structure of [(S)Ru(?-C5H5){(S)dpompyr-PP?}Cl]. *J. Chem. Soc. Dalt. Trans.*, (5):1149, jan 1987.

[79] Thomas A. Shackleton, Stephen C. Mackie, Stuart B. Fergusson, Laura J. Johnston, and Michael C. Baird. The chemistry of (.eta.5-cyclopentadienyl)dicarbonyliron hydride revisited. *Organometallics*, 9(8):2248–2253, aug 1990.

[80] Stuart B. Fergusson, Laura J. Sanderson, Thomas A. Shackleton, and Michael C. Baird. CpFe(CO)2H: a reassessment of the literature. *Inorganica Chim. Acta*, 83(2):L45–L47, mar 1984.

[81] Jeffrey S. Plotkin and Sheldon G. Shore. Convenient preparation and isolation of pure potassium cyclopentadienyldicarbonylferrate, K[(.eta.5-C5H5)Fe(CO)2]. *Inorg. Chem.*, 20(1):284–285, jan 1981.

[82] E. Cesarotti, A. Chiesa, and G. D'Alfonso. Asymmetric hydrogenation by chiral aminophosphine-phosphinite rhodium compexes. *Tetrahedron Lett.*, 23(29):2995–2996, jan 1982.

[83] Stephen G. Devies, John Hibberd, Stephen J. Simpson, Susan E. Thomas, and Oliver Watts. Carbon monoxide reduction. [Fe(?5-C5H5)(Ph2PCH2CH2PPh2)(CO)H]: reactions and formation by reduction of the complex [Fe(?5-C5H5)(Ph2PCH2CH2PPh2)(CO)]PF6. *J. Chem. Soc. Dalt. Trans.*, (4):701, jan 1984.

[84] E. Cesarotti, M. Grassi, and L. Prati. Optically active transition metal compounds, chiral at the metal centre. Synthesis and stereochemical studies of the chiral cyclopentadienyl iron complexes

[Fe(η5-C5H5){(S)-Prolophos}(CO)]PF6. *Polyhedron*, 9(5):639–644, jan 1990.

[85] Christian Merten and Yunjie Xu. A comparative vibrational CD study of homo- and heteroleptic complexes of the type [Cu(trans-1,2-diaminocyclohexane) 2 L](ClO 4) 2. *Dalt. Trans.*, 42(29):10572–10578, may 2013.

[86] Zahra Dezhahang, Mohammad Reza Poopari, Joseph Cheramy, and Yunjie Xu. Conservation of Helicity in a Chiral Pyrrol-2-yl Schiff-Base Ligand and Its Transition Metal Complexes. *Inorg. Chem.*, 54(9):4539–49, may 2015.

[87] Gábor Szilvágyi, Balázs Brém, Gábor Báti, László Tölgyesi, Miklós Hollósi, and Elemér Vass. Dirhodium complexes: determination of absolute configuration by the exciton chirality method using VCD spectroscopy. *Dalton Trans.*, 42(36):13137–44, sep 2013.

[88] Henri Brunner. Optically Active Organometallic Compounds of Transition Elements with Chiral Metal Atoms. *Angew. Chemie Int. Ed.*, 38(9):1194–1208, 1999.

[89] Edoardo Cesarotti, Gianfranco Ciani, and Angelo Sironi. Synthesis, crystal structure and absolute configuration of the menthylcyclopentadienyl complex of ruthenium (+)578-(η5-MCp)Ru(CO)P(C6H5)3Cl. *J. Organomet. Chem.*, 216(1):87–95, 1981.

[90] Edoardo Cesarotti, Anna Chiesa, Gian Franco Ciani, Angelo Sironi, Rahmatollah Vefghi, and Colin White. Synthesis and absolute configuration of a series of chiral ruthenium complexes; crystal structure of (R)-[Ru([small eta]5-C5H4R*)(CO)(PPh3)I](R*= neomenthyl). *J. Chem. Soc., Dalt. Trans.*, (4):653–661, 1984.

[91] Edoardo Cesarotti, Maria Angoletta, Nigel P C Walker, Michael B Hursthouse, Rahmatollah Vefghi, Peter A Schofield, and Colin

White. Stereochemistry of substitution reactions at a chiral ruthenium atom: The crystal structure of (R)-[Ru(η5-C5H4R*)(CO)(PPh3)NCCH3]PF6 (R* = neomenthyl). *J. Organomet. Chem.*, 286(3):343–360, 1985.

[92] I.A. Khodov, S.V. Efimov, V.V. Klochkov, G.A. Alper, and L.A.E. Batista de Carvalho. Determination of preferred conformations of ibuprofen in chloroform by 2D NOE spectroscopy. *Eur. J. Pharm. Sci.*, 65:65–73, dec 2014.

[93] Leroy Cronin, Catherine L Higgitt, and Robin N Perutz. Structure and Dynamic Exchange in Rhodium η2-Naphthalene and Rhodium η2-Phenanthrene Complexes: Quantitative NOESY and EXSY Studies. *Organometallics*, 19(4):672–683, feb 2000.

[94] David Neuhaus and Micheal P. Williamson. *The Nuclear Overhauser Effect in Structural and Conformational Analysis*. Wiley-vch, 2000.

[95] Cristiano Zuccaccia, Gianfranco Bellachioma, Giuseppe Cardaci, and Alceo Macchioni. Solution Structure Investigation of Ru(II) Complex Ion Pairs: Quantitative NOE Measurements and Determination of Average Interionic Distances. *J. Am. Chem. Soc.*, 123(44):11020–11028, nov 2001.

[96] Albert Moscowitz. Theoretical Aspects of Optical Activity Part One: Small Molecules. In *Adv. Chem. Phys.*, pages 67–112. John Wiley & Sons, Inc., 2007.

[97] Kohzo Konno, Isamu Shiina, and Hiroharu Yui. Fine structures in vibrational circular dichroism spectra of chiral molecules with rotatable hydroxyl groups and their application in the analysis of local intermolecular interactions. *J. Mol. Struct.*, 1035(0):260–266, 2013.

[98] Sergio Abbate, Alessia Ciogli, Stefania Fioravanti, Francesco Gasparrini, Giovanna Longhi, Lucio Pellacani, Egon Rizzato, Domenico

Spinelli, and Paolo A Tardella. Solving the Puzzling Absolute Configuration Determination of a Flexible Molecule by Vibrational and Electronic Circular Dichroism Spectroscopies and DFT Calculations: The Case Study of a Chiral 2,2′-Dinitro-2,2′-biaziridine. *European J. Org. Chem.*, 2010(32):6193–6199, 2010.

[99] Sergio Abbate, Franca Castiglione, France Lebon, Giovanna Longhi, Alessandro Longo, Andrea Mele, Walter Panzeri, Angela Ruggirello, and Vincenzo Turco Liveri. Spectroscopic and Structural Investigation of the Confinement of d and l Dimethyl Tartrate in Lecithin Reverse Micelles. *J. Phys. Chem. B*, 113(10):3024–3033, 2009.

[100] 2009. M. J. Frisch, G. W. Trucks, H. B. Schlegel, G. E. Scuseria, M. A. Robb, J. R. Cheeseman, G. Scalmani, V. Barone, B. Mennucci, G. A. Petersson, H. Nakatsuji, M. Caricato, X. Li, H. P. Hratchian, A. F. Izmaylov, J. Bloino, G. Zheng, J. L. Sonnenberg, M. Had. Gaussian 09, Revision D.01.

[101] Renzo Ruzziconi, Gianfranco Bellachioma, Gianluca Ciancaleoni, Susan Lepri, Stefano Superchi, Riccardo Zanasi, and Guglielmo Monaco. Cationic half-sandwich quinolinophaneoxazoline-based ([small eta]6-p-cymene)ruthenium(ii) complexes exhibiting different chirality types: synthesis and structural determination by complementary spectroscopic methods. *Dalt. Trans.*, 43(4):1636–1650, 2014.

[102] Stefan Grimme. Semiempirical GGA-type density functional constructed with a long-range dispersion correction. *J. Comput. Chem.*, 27(15):1787–1799, 2006.

[103] Stefan Grimme, Jens Antony, Stephan Ehrlich, and Helge Krieg. A consistent and accurate ab initio parametrization of density functional dispersion correction (DFT-D) for the 94 elements H-Pu. *J. Chem. Phys.*, 132(15):–, 2010.

[104] Ansgar Schäfer, Hans Horn, and Reinhart Ahlrichs. Fully optimized contracted Gaussian basis sets for atoms Li to Kr. *J. Chem. Phys.*, 97(4):2571–2577, 1992.

[105] Giovanna Longhi, Sergio Abbate, Patrizia Scafato, and Carlo Rosini. A vibrational circular dichroism approach to the determination of the absolute configuration of flexible and transparent molecules: fluorenone ketals of 1,n-diols. *Phys. Chem. Chem. Phys.*, 12(18):4725–4732, 2010.

[106] Marco Passarello, Sergio Abbate, Giovanna Longhi, Susan Lepri, Renzo Ruzziconi, and Valentin Paul Nicu. Importance of C*–H Based Modes and Large Amplitude Motion Effects in Vibrational Circular Dichroism Spectra: The Case of the Chiral Adduct of Dimethyl Fumarate and Anthracene. *J. Phys. Chem. A*, 118(24):4339–4350, 2014.

[107] Valentin Paul Nicu, Elke Debie, Wouter Herrebout, Benjamin Van der Veken, Patrick Bultinck, and Evert Jan Baerends. A VCD robust mode analysis of induced chirality: The case of pulegone in chloroform. *Chirality*, 21(1E):E287–E297, 2009.

[108] Cody L. Covington and Prasad L. Polavarapu. Similarity in Dissymmetry Factor Spectra: A Quantitative Measure of Comparison between Experimental and Predicted Vibrational Circular Dichroism. *J. Phys. Chem. A*, 117(16):3377–3386, apr 2013.

[109] Sándor Góbi and Gábor Magyarfalvi. Reliability of computed signs and intensities for vibrational circular dichroism spectra. *Phys. Chem. Chem. Phys.*, 13(36):16130–3, sep 2011.

[110] Giovanna Longhi, Matteo Tommasini, Sergio Abbate, and Prasad L. Polavarapu. The Connection Between Robustness Angles and Dissymmetry Factors in Vibrational Circular Dichroism Spectra. *Chem. Phys. Lett.*, oct 2015.

[111] Philip J Stephens. Theory of vibrational circular dichroism. *J. Phys. Chem.*, 89(5):748–752, 1985.

[112] Valentin Paul Nicu, Mojgan Heshmat, and Evert Jan Baerends. Signatures of counter-ion association and hydrogen bonding in vibrational circular dichroism spectra. *Phys. Chem. Chem. Phys.*, 13(19):8811–25, may 2011.

[113] Valentin Paul Nicu, Jochen Autschbach, and Evert Jan Baerends. Enhancement of IR and VCD intensities due to charge transfer. *Phys. Chem. Chem. Phys.*, 11(10):1526–38, mar 2009.

[114] Piero Macchi and Anna Krawczuk. The polarizability of organometallic bonds. *Comput. Theor. Chem.*, 1053:165–172, feb 2015.

[115] Francesco Neve and Alessandra Crispini. C−H···Br-M Interactions at Work: Tetrabromometalates of the Bolaamphiphilic N , N '-Dodecamethylenedipyridinium Cation. *Cryst. Growth Des.*, 1(5):387–393, sep 2001.

[116] R. F. W. Bader. Atoms in molecules. *Acc. Chem. Res.*, 18(1):9–15, jan 1985.

[117] M Nishio, M Hirota, and Y Umezawa. *The CH/π Interaction: Evidence, Nature, and Consequences*. Methods in Stereochemical Analysis. Wiley, 1998.

[118] Osamu Takahashi, Yuji Kohno, and Motohiro Nishio. Relevance of weak hydrogen bonds in the conformation of organic compounds and bioconjugates: evidence from recent experimental data and high-level ab initio MO calculations. *Chem. Rev.*, 110(10):6049–76, oct 2010.

[119] Laurence A. Nafie and Teresa B. Freedman. Ring current mechanism of vibrational circular dichroism. *J. Phys. Chem.*, 90(5):763–767, feb 1986.

[120] Daryl A. Young, Teresa B. Freedman, Elmer D. Lipp, and Laurence A. Nafie. Vibrational circular dichroism in transition-metal complexes. 2. Ion association, ring conformation, and ring currents of ethylenediamine ligands. *J. Am. Chem. Soc.*, 108(23):7255–7263, nov 1986.

[121] Teresa B. Freedman, Daryl A. Young, M. Reza Oboodi, and Laurence A. Nafie. Vibrational circular dichroism in transition-metal complexes. 3. Ring currents and ring conformations of amino acid ligands. *J. Am. Chem. Soc.*, 109(5):1551–1559, mar 1987.

[122] Christian Merten, Kaitlynd Hiller, and Yunjie Xu. Effects of electron configuration and coordination number on the vibrational circular dichroism spectra of metal complexes of trans-1{,}2-diaminocyclohexane. *Phys. Chem. Chem. Phys.*, 14(37):12884–12891, 2012.

[123] Henri B. Kagan. Asymmetric catalytic reduction with transition metal complexes. I. Catalytic system of rhodium(I) with (-)-2,3-0-isopropylidene-2,3-dihydroxy-1,4-bis(diphenylphosphino)butane, a new chiral diphosphine. *J. Am. Chem. Soc.*, 94(18):6429–6433, sep 1972.

[124] J Halpern. Mechanism and stereoselectivity of asymmetric hydrogenation. *Science*, 217(4558):401–7, jul 1982.

[125] John M. Brown. Tilden Lecture. Selectivity and mechanism in catalytic asymmetric synthesis. *Chem. Soc. Rev.*, 22(1):25, jan 1993.

[126] Max Diem, Euphemia Photos, Hani Khouri, and Laurence A. Nafie. Vibrational circular dichroism in amino acids and peptides. 3. Solution- and solid-phase spectra of alanine and serine. *J. Am. Chem. Soc.*, 101(23):6829–6837, nov 1979.

[127] Juan Ramón Avilés Moreno, Francisco Partal Ureña, and Juan Jesús López González. Chiral terpenes in different phases: R-(−)-

camphorquinone studied by IR–Raman–VCD spectroscopies and theoretical calculations. *Struct. Chem.*, 22(1):67–76, nov 2010.

[128] Pavlína Novotná and Marie Urbanová. A Solid Phase Vibrational Circular Dichroism Study of Polypeptide-Surfactant Interaction. *Chirality*, sep 2015.

[129] Ettore Castiglioni, Paolo Biscarini, and Sergio Abbate. Experimental aspects of solid state circular dichroism. *Chirality*, 21 Suppl 1:E28–36, jan 2009.

[130] Kamaluddin Abdur-Rashid, Sean E. Clapham, Alen Hadzovic, Jeremy N. Harvey, Alan J. Lough, and Robert H. Morris. Mechanism of the Hydrogenation of Ketones Catalyzed by trans- Dihydrido(diamine)ruthenium(II) Complexes †. *J. Am. Chem. Soc.*, 124(50):15104–15118, dec 2002.

[131] Mohammad K Nazeeruddin, Cedric Klein, Michael Grätzel, Libero Zuppiroli, and Detlef Berner. Molecular Engineering of Iridium Complexes and their Application in Organic Light Emitting Devices. In *Highly Effic. OLEDs with Phosphorescent Mater.*, pages 363–390. Wiley-VCH Verlag GmbH & Co. KGaA, 2008.

[132] Zhu-qi Chen, Zu-qiang Bian, and Chun-hui Huang. Functional IrIII complexes and their applications. *Adv. Mater.*, 22(13):1534–9, apr 2010.

[133] Christoph Ulbricht, Beatrice Beyer, Christian Friebe, Andreas Winter, and Ulrich S. Schubert. Recent Developments in the Application of Phosphorescent Iridium(III) Complex Systems. *Adv. Mater.*, 21(44):4418–4441, nov 2009.

[134] Audrey Auffrant, Andrea Barbieri, Francesco Barigelletti, Jérôme Lacour, Pierre Mobian, Jean-Paul Collin, Jean-Pierre Sauvage, and Barbara Ventura. Bimetallic Iridium(III) Complexes Consisting of

Ir(ppy)2 Units (ppy = 2-Phenylpyridine) and Two Laterally Connected N∧N Chelates as Bridge: Synthesis, Separation, and Photophysical Properties. *Inorg. Chem.*, 46(17):6911–6919, 2007.

[135] Enrico Marchi, Riccardo Sinisi, Giacomo Bergamini, Michele Tragni, Magda Monari, Marco Bandini, and Paola Ceroni. Easy Separation of Δ and Λ Isomers of Highly Luminescent [IrIII]-Cyclometalated Complexes Based on Chiral Phenol-Oxazoline Ancillary Ligands. *Chem. – A Eur. J.*, 18(28):8765–8773, 2012.

[136] Misa Ashizawa, Lifen Yang, Katsuaki Kobayashi, Hisako Sato, Akihiko Yamagishi, Fumio Okuda, Takunori Harada, Reiko Kuroda, and Masa-aki Haga. Syntheses and photophysical properties of optical-active blue-phosphorescent iridium complexes bearing asymmetric tridentate ligands. *Dalt. Trans.*, (10):1700–1702, 2009.

[137] Jiajia Ma, Xiaobing Ding, Ying Hu, Yong Huang, Lei Gong, and Eric Meggers. Metal-templated chiral Brønsted base organocatalysis. *Nat. Commun.*, 5:4531, jan 2014.

[138] Lei Gong, Liang-An Chen, and Eric Meggers. Asymmetric catalysis mediated by the ligand sphere of octahedral chiral-at-metal complexes. *Angew. Chem. Int. Ed. Engl.*, 53(41):10868–74, oct 2014.

[139] Toshitada Yoshihara, Masahiro Hosaka, Motoki Terata, Kazuki Ichikawa, Saori Murayama, Asami Tanaka, Masanobu Mori, Hideyuki Itabashi, Toshiyuki Takeuchi, and Seiji Tobita. Intracellular and in Vivo Oxygen Sensing Using Phosphorescent Ir(III) Complexes with a Modified Acetylacetonato Ligand. *Anal. Chem.*, 87(5):2710–2717, 2015.

[140] Youngmin You. Phosphorescence bioimaging using cyclometalated Ir(III) complexes. *Curr. Opin. Chem. Biol.*, 17(4):699–707, aug 2013.

[141] Qiang Zhao, Chunhui Huang, and Fuyou Li. Phosphorescent heavy-metal complexes for bioimaging. *Chem. Soc. Rev.*, 40(5):2508–2524, 2011.

[142] Kenneth Kam-Wing Lo, Man-Wai Louie, and Kenneth Yin Zhang. Design of luminescent iridium(III) and rhenium(I) polypyridine complexes as in vitro and in vivo ion, molecular and biological probes. *Coord. Chem. Rev.*, 254(21-22):2603–2622, nov 2010.

[143] Kenneth Kam-Wing Lo and Kenneth Yin Zhang. Iridium(iii) complexes as therapeutic and bioimaging reagents for cellular applications. *RSC Adv.*, 2(32):12069–12083, 2012.

[144] Li Feng, Yann Geisselbrecht, Sebastian Blanck, Alexander Wilbuer, G Ekin Atilla-Gokcumen, Panagis Filippakopoulos, Katja Kräling, Mehmet Ali Celik, Klaus Harms, Jasna Maksimoska, Ronen Marmorstein, Gernot Frenking, Stefan Knapp, Lars-Oliver Essen, and Eric Meggers. Structurally sophisticated octahedral metal complexes as highly selective protein kinase inhibitors. *J. Am. Chem. Soc.*, 133(15):5976–86, apr 2011.

[145] Teresa F. Mastropietro, Yogesh J. Yadav, Elisabeta I. Szerb, Anna Maria Talarico, Mauro Ghedini, and Alessandra Crispini. Luminescence mechanochromism in cyclometallated Ir(iii) complexes containing picolylamine. *Dalt. Trans.*, 41:8899, 2012.

[146] Yogesh Jivajirao Yadav, Benoît Heinrich, Giuseppina De Luca, Anna Maria Talarico, Teresa Fina Mastropietro, Mauro Ghedini, Bertrand Donnio, and Elisabeta Ildyko Szerb. Chromonic-Like Physical Luminescent Gels Formed by Ionic Octahedral Iridium(III) Complexes in Diluted Water Solutions. *Adv. Opt. Mater.*, 1(Iii):844–854, 2013.

[147] Peter J Spellane, Richard J Watts, and Calvin J Curtis. Analysis of the proton and carbon-13 NMR spectra of [Ir(Hbpy-C3,N')(bpy-

N,N')2]3+: evidence for a carbon-bonded structure. *Inorg. Chem.*, 22(26):4060–4062, 1983.

[148] Loredana Ricciardi, Massimo La Deda, Andreea Ionescu, Nicolas Godbert, Iolinda Aiello, Mauro Ghedini, Marco Fusè, Isabella Rimoldi, and Edoardo Cesarotti. Luminescent chiral ionic Ir(III) complexes: Synthesis and photophysical properties. *J. Lumin.*, page LUMIND1500684, aug 2015.

[149] Anna Maria Talarico, Iolinda Aiello, Anna Bellusci, Alessandra Crispini, Mauro Ghedini, Nicolas Godbert, Teresa Pugliese, and Elisabeta Szerb. Highly luminescent bis-cyclometalated iridium(iii) ethylenediamine complex: synthesis and correlation between the solid state polymorphism and the photophysical properties. *Dalt. Trans.*, 39(7):1709–1712, 2010.

[150] Anna Maria Talarico, Elisabeta Ildyko Szerb, Teresa F. Mastropietro, Iolinda Aiello, Alessandra Crispini, and Mauro Ghedini. Tuning solid state luminescent properties in a hydrogen bonding-directed supramolecular assembly of bis-cyclometalated iridium(iii) ethylenediamine complexes. *Dalt. Trans.*, 41:4919, 2012.

[151] Utrecht University, Utrecht, The Netherlands and A. L. Spek. PLATON, A Multipurpose Crystallographic Tool, 1998.

[152] D G Evans and J C A Boeyens. Conformational analysis of ring pucker. *Acta Crystallogr. Sect. B*, 45(6):581–590, 1989.

[153] Arijit Mukherjee, Srinu Tothadi, and Gautam R Desiraju. Halogen Bonds in Crystal Engineering: Like Hydrogen Bonds yet Different. *Acc. Chem. Res.*, 47(8):2514–2524, 2014.

[154] Frederick J Coughlin, Michael S Westrol, Karl D Oyler, Neal Byrne, Christina Kraml, Eli Zysman-Colman, Michael S Lowry, and Stefan

Bernhard. Synthesis, Separation, and Circularly Polarized Luminescence Studies of Enantiomers of Iridium(III) Luminophores. *Inorg. Chem.*, 47(6):2039–2048, 2008.

[155] Christine Schaffner-Hamann, Alexander von Zelewsky, Andrea Barbieri, Francesco Barigelletti, Gilles Muller, James P Riehl, and Antonia Neels. Diastereoselective Formation of Chiral Tris-Cyclometalated Iridium (III) Complexes: Characterization and Photophysical Properties. *J. Am. Chem. Soc.*, 126(30):9339–9348, 2004.

[156] Sergio Abbate, France Lebon, Susan Lepri, Giovanna Longhi, Roberto Gangemi, Sara Spizzichino, Gianfranco Bellachioma, and Renzo Ruzziconi. Vibrational Circular Dichroism: A Valuable Tool for Conformational Analysis and Absolute Configuration Assignment of Chiral 1-Aryl-2,2,2-Trifluoroethanols. *ChemPhysChem*, 12(18):3519–3523, 2011.

[157] Nobuyuki Harada, Koji Nakanishi, and Nina Berova. Electronic CD Exciton Chirality Method: Principles and Applications. In *Compr. Chiroptical Spectrosc.*, pages 115–166. John Wiley & Sons, Inc., 2012.

[158] Tohru Taniguchi and Kenji Monde. Exciton Chirality Method in Vibrational Circular Dichroism. *J. Am. Chem. Soc.*, 134(8):3695–3698, 2012.

[159] Sergio Abbate, Giuseppe Mazzeo, Silvia Meneghini, Giovanna Longhi, Stefan E Boiadjiev, and David A Lightner. Bicamphor: A Prototypic Molecular System to Investigate Vibrational Excitons. *J. Phys. Chem. A*, 119(18):4261–4267, 2015.

[160] Sergio; Abbate, Giovanna; Longhi, Giuseppe; Mazzeo, Ettore; Castiglioni, Stefan E; Boiadjiev, and David A Lightner. Combined Use of Electronic and Vibrational Circular Dichroism and of Circularly Polarized Luminescence on pH Sensitive Chiral Molecules. In *Chirality 2014 Conf.*, pages Note SC–28, Prague, 2014.

[161] Teresa B Freedman and Laurence A Nafie. Stereochemical Aspects of Vibrational Optical Activity. *Top. Stereochem.*, 17:113–206, 1987.

[162] John David Jackson. *Classical electrodynamics; 3rd ed.* Wiley, New York, NY, 1999.

[163] G. Holzwarth. Optical Activity of Vibrational Transitions: A Coupled Oscillator Model. *J. Chem. Phys.*, 57(4):1632, sep 1972.

[164] M Ziegler and Alexander von Zelewsky. Charge-transfer excited state properties of chiral transition metal coordination compounds studied by chiroptical spectroscopy. *Coord. Chem. Rev.*, 177(1):257–300, oct 1998.

[165] Giuseppe Mazzeo, Giovanna Longhi, Sergio Abbate, Federica Buonerba, and Renzo Ruzziconi. Chiroptical Signatures of Planar and Central Chirality in [2]Paracyclo[2](5,8)quinolinophane Derivatives. *European J. Org. Chem.*, 2014(33):7353–7363, 2014.

[166] Arnold B Tamayo, Bert D Alleyne, Peter I Djurovich, Sergey Lamansky, Irina Tsyba, Nam N Ho, Robert Bau, and Mark E Thompson. Synthesis and Characterization of Facial and Meridional Tris-cyclometalated Iridium(III) Complexes. *J. Am. Chem. Soc.*, 125(24):7377–7387, 2003.

[167] Sergey Lamansky, Peter Djurovich, Drew Murphy, Feras Abdel-Razzaq, Hae-Eun Lee, Chihaya Adachi, Paul E. Burrows, Stephen R. Forrest, and Mark E. Thompson. Highly Phosphorescent Bis-Cyclometalated Iridium Complexes: Synthesis, Photophysical Characterization, and Use in Organic Light Emitting Diodes. *J. Am. Chem. Soc.*, 123(18):4304–4312, may 2001.

[168] Loredana Ricciardi, Teresa Fina Mastropietro, Mauro Ghedini, Massimo La Deda, and Elisabeta Ildyko Szerb. Ionic-pair effect on the phosphorescence of ionic iridium(III) complexes. *J. Organomet. Chem.*, 772-773:307–313, 2014.

[169] Rubén D Costa, Enrique Ortí, Henk J Bolink, Filippo Monti, Gianluca Accorsi, and Nicola Armaroli. Luminescent ionic transition-metal complexes for light-emitting electrochemical cells. *Angew. Chem. Int. Ed. Engl.*, 51(33):8178–211, aug 2012.

[170] Qiang Zhao, Lei Li, Fuyou Li, Mengxiao Yu, Zhipan Liu, Tao Yi, and Chunhui Huang. Aggregation-induced phosphorescent emission (AIPE) of iridium(iii) complexes. *Chem. Commun.*, (6):685–687, jan 2008.

[171] Guo-Gang Shan, Ling-Yu Zhang, Hai-Bin Li, Shuang Wang, Dong-Xia Zhu, Peng Li, Chun-Gang Wang, Zhong-Min Su, and Yi Liao. A cationic iridium(III) complex showing aggregation-induced phosphorescent emission (AIPE) in the solid state: synthesis, characterization and properties. *Dalton Trans.*, 41(2):523–30, jan 2012.

[172] Daniele Zerla, Giorgio Facchetti, Marco Fusè, Michela Pellizzoni, Carlo Castellano, Edoardo Cesarotti, Raffaella Gandolfi, and Isabella Rimoldi. 8-Amino-5,6,7,8-tetrahydroquinolines as ligands in iridium(III) catalysts for the reduction of aryl ketones by asymmetric transfer hydrogenation (ATH). *Tetrahedron: Asymmetry*, 25(13-14):1031–1037, jul 2014.

[173] Noah J. Halbrook and Ray V. Lawrence. The Isolation of Dehydroabietic Acid from Disproportionated Rosin. *J. Org. Chem.*, 31(12):4246–4247, dec 1966.

[174] Mauro Ghedini, Daniela Pucci, Edoardo Cesarotti, Patrizia Antogniazza, Oriano Francescangeli, and Roberto Bartolino. Transition metals complexed to ordered mesophases. Synthesis, characterization, and mesomorphic properties of new potentially ferroelectric liquid crystals: chiral p,p'-dialkoxyazobenzenes and their cyclopalladated dinuclear complexes. *Chem. Mater.*, 5(6):883–890, jun 1993.

[175] Patrizia Scafato, Francesca Caprioli, Laura Pisani, Daniele Padula, Fabrizio Santoro, Giuseppe Mazzeo, Sergio Abbate, France Lebon,

and Giovanna Longhi. Combined use of three forms of chiroptical spectroscopies in the study of the absolute configuration and conformational properties of 3-phenylcyclopentanone, 3-phenylcyclohexanone, and 3-phenylcycloheptanone. *Tetrahedron*, 69(50):10752–10762, 2013.

[176] Bruker Analytical X-ray Systems Inc. SAINT, Version 6.45 Copyright (c), 2003.

[177] G.M. Sheldrick and 2003 Bruker AXS Inc., Madison, WI, USA. SADABS. Version 2.10.

[178] Bruker Analytical X-ray Systems Inc. SHELXTL-NT, Version 5.1 Copyright (c), 1999.

[179] Ettore Castiglioni, Sergio Abbate, and Giovanna Longhi. Revisiting with Updated Hardware an Old Spectroscopic Technique: Circularly Polarized Luminescence. *Appl. Spectrosc.*, 64(12):1416–1419, 2010.

[180] Giovanna Longhi, Ettore Castiglioni, Sergio Abbate, France Lebon, and David A Lightner. Experimental and Calculated CPL Spectra and Related Spectroscopic Data of Camphor and Other Simple Chiral Bicyclic Ketones. *Chirality*, 25(10):589–599, 2013.

[181] Sergio Abbate, Giovanna Longhi, France Lebon, Ettore Castiglioni, Stefano Superchi, Laura Pisani, Francesca Fontana, Franck Torricelli, Tullio Caronna, Claudio Villani, Rocchina Sabia, Matteo Tommasini, Andrea Lucotti, Daniele Mendola, Andrea Mele, and David A Lightner. Helical Sense-Responsive and Substituent-Sensitive Features in Vibrational and Electronic Circular Dichroism, in Circularly Polarized Luminescence, and in Raman Spectra of Some Simple Optically Active Hexahelicenes. *J. Phys. Chem. C*, 118(3):1682–1695, 2014.

[182] M J Frisch, G W Trucks, H B Schlegel, G E Scuseria, M A Robb, J R Cheeseman, G Scalmani, V Barone, B Mennucci, G A Peters-

son, H Nakatsuji, M Caricato, X Li, H P Hratchian, A F Izmaylov, J Bloino, G Zheng, J L Sonnenberg, M Hada, M Ehara, K Toyota, R Fukuda, J Hasegawa, M Ishida, T Nakajima, Y Honda, O Kitao, H Nakai, T Vreven, J A Montgomery Jr., J E Peralta, F Ogliaro, M Bearpark, J J Heyd, E Brothers, K N Kudin, V N Staroverov, R Kobayashi, J Normand, K Raghavachari, A Rendell, J C Burant, S S Iyengar, J Tomasi, M Cossi, N Rega, J M Millam, M Klene, J E Knox, J B Cross, V Bakken, C Adamo, J Jaramillo, R Gomperts, R E Stratmann, O Yazyev, A J Austin, R Cammi, C Pomelli, J W Ochterski, R L Martin, K Morokuma, V G Zakrzewski, G A Voth, P Salvador, J J Dannenberg, S Dapprich, A D Daniels, Ö Farkas, J B Foresman, J V Ortiz, J Cioslowski, and D J Fox. Gaussian∼09 Revision D.01.

[183] Jacopo Tomasi, Benedetta Mennucci, and Roberto Cammi. Quantum Mechanical Continuum Solvation Models. *Chem. Rev.*, 105(8):2999–3094, 2005.

[184] R Ditchfield. Molecular Orbital Theory of Magnetic Shielding and Magnetic Susceptibility. *J. Chem. Phys.*, 56(11), 1972.

[185] Krzysztof Wolinski, James F Hinton, and Peter Pulay. Efficient implementation of the gauge-independent atomic orbital method for NMR chemical shift calculations. *J. Am. Chem. Soc.*, 112(23):8251–8260, 1990.

[186] David E. Hill, Neil Vasdev, and Jason P. Holland. Evaluating the accuracy of density functional theory for calculating 1H and 13C NMR chemical shifts in drug molecules. *Comput. Theor. Chem.*, 1051:161–172, jan 2015.

[187] David A Forsyth and Albert B Sebag. Computed 13C NMR Chemical Shifts via Empirically Scaled GIAO Shieldings and Molecular Mechanics Geometries. Conformation and Configuration from 13C Shifts. *J. Am. Chem. Soc.*, 119(40):9483–9494, 1997.

[188] Alessandro Contini, Donatella Nava, and Pasqualina Trimarco. Tautomeric Equilibria of [1]Benzopyrano[3,4-d]imidazol-4(3H)-ones, a Theoretical and NMR Study. *J. Org. Chem.*, 71(1):159–166, 2006.

[189] N G Connelly, Royal Society of Chemistry (Great Britain), International Union of Pure, and Applied Chemistry. *IUPAC Recommendations 2005*. Royal Society of Chemistry Publishing/IUPAC,., 2005.

[190] Santiago Herrero and Miguel Angel Usón. A Straightforward Method for Assigning Stereochemical Λ/Δ Descriptors to Octahedral Coordination Compounds. *J. Chem. Educ.*, 72(12):1065, dec 1995.

Publications

- **Enantioselective Transfer Hydrogenation of Aryl Ketones: Synthesis and 2D-NMR Characterization of New 8-amino-5,6,7,8-tetrahydroquinoline Ru(II)-complexes** I. Rimoldi, G. Facchetti, E. Cesarotti, M. Pellizzoni, M. Fusè, D. Zerla, Curr. Org. Chem. **2012**, 16, 2982–2988.

- **Diastereoselectivity and catalytic activity in ruthenium complexes chiral at the metal centre** D. S. Zerla, I. Rimoldi, E. Cesarotti, G. Facchetti, M. Pellizzoni, M. Fusè*, J. Organomet. Chem. **2014**, 771, 2–8.

- **8-Amino-5,6,7,8-tetrahydroquinolines as ligands in iridium(III) catalysts for the reduction of aryl ketones by asymmetric transfer hydrogenation (ATH)** D. Zerla, G. Facchetti, M. Fusè, M. Pellizzoni, C. Castellano, E. Cesarotti, R. Gandolfi, I. Rimoldi, Tetrahedron: Asymmetry **2014**, 25, 1031–1037.

- **VCD spectroscopy as an excellent probe of chiral metal complexes containing a carbon monoxide vibrational chromophore** M. Fusè, G. Mazzeo, G. Longhi, S. Abbate, D. Zerla, I. Rimoldi, A. Contini, E. Cesarotti, Chem. Commun. **2015**, 51, 9385–9387.

- **Luminescent chiral ionic Ir(III) complexes: Synthesis and photophysical properties** L. Ricciardi, M. La Deda, A. Ionescu, N. Godbert, I. Aiello, M. Ghedini, M. Fusè*, I. Rimoldi, E. Cesarotti, J. Lumin. **2015**, LUMIND1500684.
- **Simple 1,3-diamines and their application as ligands in ruthenium(ii) catalysts for asymmetric transfer hydrogenation of aryl ketones** G. Facchetti, R. Gandolfi, M. Fusè, D. Zerla, E. Cesarotti, M. Pellizzoni, I. Rimoldi, New J. Chem. **2015**, DOI 10.1039/c5nj00110b.
- **Vibrational circular dichroism and chiroptical properties of chiral Ir(III) luminescent complexes** Giuseppe Mazzeo, Marco Fusè, Giovanna Longhi, Isabella Rimoldi, Edoardo Cesarotti, Alessandra Crispini, Sergio Abbate *submitted manuscript*
- **Evaluation of chemical diversity of biotinylated chiral 1,3 diamines as a catalytic moiety in artificial imine reductase** Michela Pellizzoni, Raffaella Gandolfi, Giorgio Facchetti, Marco Fusè, Alessandro Contini and Isabella Rimoldi *submitted manuscript*